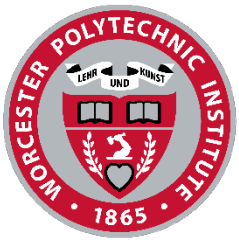

WPI

Effects of Low Voltage Testing on PEM Fuel Cell with Current Control by Hydrogen Flow

A Major Qualifying Project Report
Submitted to the faculty of
WORCESTER POLYTECHNIC INSTITUTE
In partial fulfillment of the requirements for the
Degree of Bachelor of Science

Submitted to:
Stephen Kmiotek

By:
Veronica Goldsmith
Lindsay Mitchel

March 28th 2014

Co-Advised by:
Caroline Bonnet (ENSIC)
Francois Lapique (ENSIC)

Abstract

This project conducted at ENSIC in Nancy, France studied the operation of a PEMFC at low voltages and tests were done to determine if current control with hydrogen flow was possible and the degradation effects on the MEA. Varying length CA and CP tests were conducted. Performance and degradation of the fuel cell were analyzed using GEIS, LSV, and CV. It was determined that the current of a FC could be directly controlled by hydrogen flow within 3% of the target value. Operating at a low voltage of 0.2 V presents a potential application of FCs with supercapacitors and minimal degradation effects. Additionally running a FC with dry inlet gases or at OCV for an extended time was found to rapidly "kill" the MEA.

Acknowledgements

We would like to thank ENSIC for their partnership and collaboration in completing this project. We would like to particularly thank the members of LRGP for warmly welcoming us into their laboratory. A special acknowledgement and gracious thank you to Fracois Lapique and Caroline Bonnet for their invaluable knowledge, support, and friendship. Finally, we would like to thank WPI for the opportunity to complete our project abroad and Professor Stephen Kmiotek for his kind encouragement and guidance.

Table of Contents

Table of Figures

Table of Tables

Introduction

With the world relying more and more on fossil fuels including coal, oil, and natural gas, which produce harmful carbon dioxide when combusted, the need for viable alternative energy sources is in high demand. Fuel cells are one alternative energy source that is growing more common. They are electrochemical devices that produce electrical energy directly from the chemical energy of fuels and an oxidant. Unlike traditional heat engines their process is not limited by Carnot efficiency and with a byproduct of water vapor they are much more environmentally conscious.

For a long time fuel cells were not a viable option for alternative power due to their high cost. However, with advances in membrane technology and continued research the price is going down. Major car companies are even beginning to develop and release fuel cell powered cars in areas with hydrogen infrastructure.

As fuel cell technology grows, researchers are finding new uses for the cells. Recently Hinaje et al. ran experiments with a fuel cell connected to a discharged supercapacitor for a brief moment at a specified hydrogen flow rate. During the experiments the fuel cell was short circuited in different stoichiometric ratios to allow operation as a current source controlled by hydrogen. The study concluded that additional tests should be conducted to determine the severity of any membrane degradation. Researchers at Ecole Nationale Supérieure des Industries Chimiques (ENSIC) in Nancy, France were interested to see if similar results could be duplicated without the need to short circuit the fuel cell.

In the Major Qualifying Project (MQP) report the performance and degradation of a 100 cm2 proton exchange membrane (PEM) fuel cell was analyzed through various tests. Experiments were designed to create polarization curves, understand the resistances, determine the active surface area, and explore the hydrogen crossover in the membrane. Different inlet gas humidifications were utilized in early testing to determine ideal conditions for tests run at low voltages. Chronoamperometry testing was done at varying lengths at low voltages to see if Hinaje and coworkers' results of current controlled by hydrogen flow could be duplicated.

This report will discuss some additional background information including the history of fuel cells, various types of fuel cell, the components, and mathematical concepts. Section 3 is devoted to explaining the fuel cell bench as well as the procedures for all of the testing that was conducted. Section 4 highlights the results obtained and analyzes the results. Supporting documents including data tables can be found in the Appendices.

2.0 Background

2.1 Principles of Fuel Cells

Electrochemistry is a field that studies the relationships between chemical reactions and electricity. In electrochemistry if electric current is used to drive a reaction then the reactant compound is split in a process known as electrolysis. If a reaction is spontaneous then an electrical current is generated and is equivalent to "inverse electrolysis." This process is the basis for voltaic cells, such as batteries and fuel cells.

Fuel cells are electrochemical devices that produce electrical energy directly from the chemical energy of fuels and an oxidant. If there is a continuous supply of fuel and oxidant then a fuel cell is a constant

source of electricity. The basic chemical reaction of a hydrogen fuel cell utilizes gases for the inverse electrolysis of water. It involves the “combustion” of hydrogen with oxygen to produce water and heat.

$$2H_2 + O_2 \rightarrow 2H_2O$$

The overall reaction is based on redox or half reactions that occur at each of the cell electrodes or electron conductors. The hydrogen is oxidized at the anode electrode and the oxygen is reduced at the cathode electrode. Electrons flow from the anode, through an external wire, to the cathode, producing a current or “load.” Gas ions are conducted via the electrolyte medium. The difference in charge between the electrode and the electrolyte is the potential or cell voltage. If the oxidation and reduction reactions are occurring at the same rate or in equilibrium then there is no difference in charge and there is no cell voltage. However, these reactions do not occur in equilibrium and when no load is demanded the cell voltage or potential is known as its open circuit voltage (OCV).

Fuel cells are attractive devices for potential power sources because unlike traditional heat engines their process in not limited by Carnot efficiency. The achievable efficiency of a power cycle is known as the Carnot efficiency and is limited by the outlet temperature of a heat engine. In theory if the inverse electrolysis reaction was carried out in an ideal situation a fuel cell could have 100% efficiency and have a maximum potential of 1.3V. However, the reaction is not ideal and is impeded by charge transfer and ohmic resistances, mass transport, and the electrode capacitance. Therefore, 1.3V is unobtainable in reality. In order to increase the potential available multiple fuel cells can be stacked for additive voltage or power.

2.2 History of Hydrogen Fuel Cells

The inverse electrolysis of water was first discovered by Christian F. Schoenbein a German-Swiss scientist in 1838. Schoenbein’s work involved platinum electrodes and dilute sulfuric acid for the electrolyte. In 1839 Welsh scientist, William R. Grove practically demonstrated Schoenbein’s discovery

through the “gas battery” experiments shown in Figure 1 below. Grove deducted that the three phase interface between the gas, the electrolyte, and the electrode is vital for the reaction. Grove used platinum electrodes with platinum particles deposited on the surface in order to increase surface area and the area available for the three phase contact.

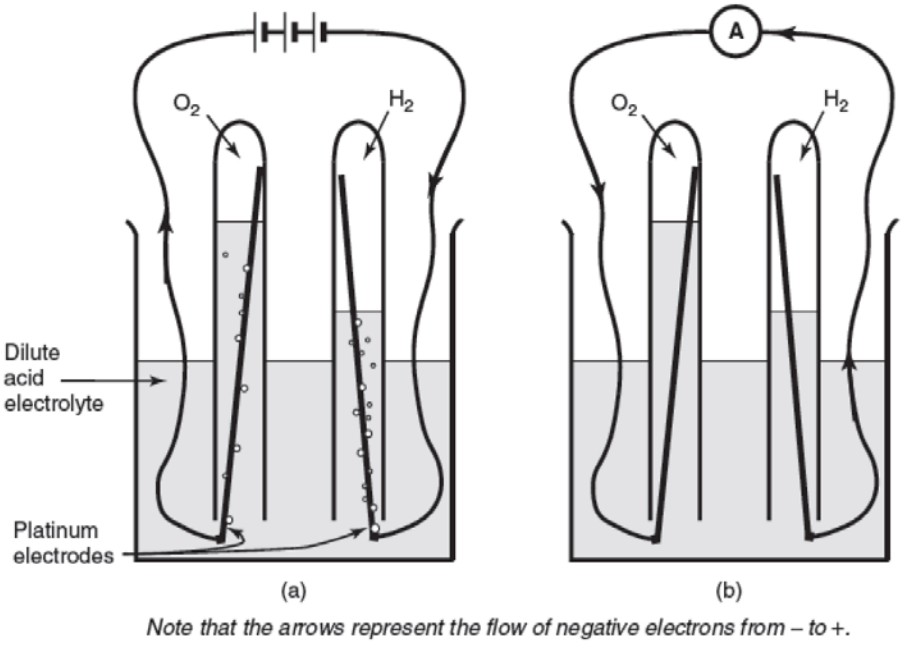

Figure 1 Beginning fuel cell experiments. (a) Electrolysis of water due to an applied current. (b) Reverse electrolysis or fuel cell chemistry. Small current induced.

The second half of the twentieth century saw a reinvention of the fuel cell as United States industrial companies and national laboratories increased research and development efforts. There were several advancements as different types of cells were discovered and individual components such as the catalyst layer and bipolar plates were improved. Also fuel cell technology gained recognition as it was applied in space exploration and at the end of the century as automotive companies, such as General Motors (GM), began investing in fuel cell vehicles. Of particular relevance is the creation of the first proton-exchange membrane (PEM) or solid electrolyte by General Electric (GE) in the late 1950-1960s.

GE and DuPont advanced the PEM in the mid-1960s with the innovation of the Nafion® membrane. Success of this membrane gave birth to the proton-exchange membrane fuel cell (PEMFC). The progression of fuel cell development is shown in Figure 2 below.

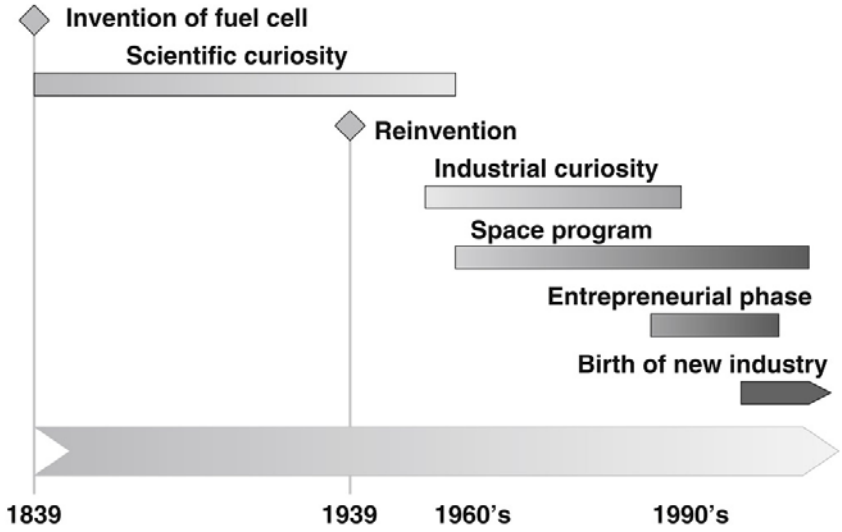

Figure 2 Invention and progression of fuel cell technology within the scientific community and industry.

At the beginning of the twenty-first century fuel cell company stock in the United States peak signifying the interest within the industry. Since then stock prices have decreased, however, the number of patents in fuel cell technology has continued to increase and in 2009 reached 6,000 patents in the United States. Therefore the growth of the fuel cell industry successfully continues today.

2.3 Types of Fuel Cells

The electrolyte characterizes the type of fuel cell and currently there are five main types of fuel cells shown in Table 1. All of the fuel cells use hydrogen as a reactant gas but have varying applications and different advantages in comparison.

Table 1 Various types of hydrogen fuel cells and their characteristics and applications.

Type	Electrolyte	Fuel	Temperature	Applications	Advantages

Proton-exchange Membrane Fuel Cell (PEMFC)	Solid organic polyperfluorosulfonic acid polymer	H_2	50-100	-Backup power -Portable power -Small distributed generation -Transportation -Specialty vehicles	-Less electrolyte corrosion & management problems -Low temperature -Quick start-up
Alkaline Fuel Cell (AFC)	Matric soaked in an aqueous solution of potassium hydroxide	H_2	65-220	-Military -Space	-Fast cathode reaction and high temperatures -Variety of catalysts
Phosphoric Acid Fuel Cell (PAFC)	Matrix soaked in liquid phosphoric	H_2	150-200	-Distributed generation	-High tolerance to hydrogen impurities
Molten Carbonate Fuel Cell (MCFC)	Matrix soaked in lithium, sodium, and/or potassium carbonate solution	H_2 CO CH_4	600-700	-Electric utility -Large distributed generation	-High efficiency -Fuel flexibility -Variety of catalysts
Solid Oxide Fuel Cell (SOFC)	Yttria stabilized zirconia	H_2 CO CH_4	600-1000	-Auxiliary power -Electric utility -Large distributed generation	-High efficiency -Fuel flexibility -Variety of catalysts -Less electrolyte management problems

PEMFCs operate at lower temperatures ranging from 50-100C which is advantageous for quick start-up and easy operation and application. However, at lower temperatures the reaction rate of the inverse electrolysis is slower. An advantage of PEMFCs is that the solid polymer membrane undergoes less corrosion and is easily managed.

2.4 PEMFC

A PEMFC consists of several components each serving a unique purpose in the overall operation of the cell. The main parts are the cell plates and the membrane electrode assembly (MEA). The characteristics

and assembly of these parts facilitate reverse electrolysis and the flows of reactants, products, and current. Figure 3 shows the layered structure of a single fuel cell similar to a “sandwich.”

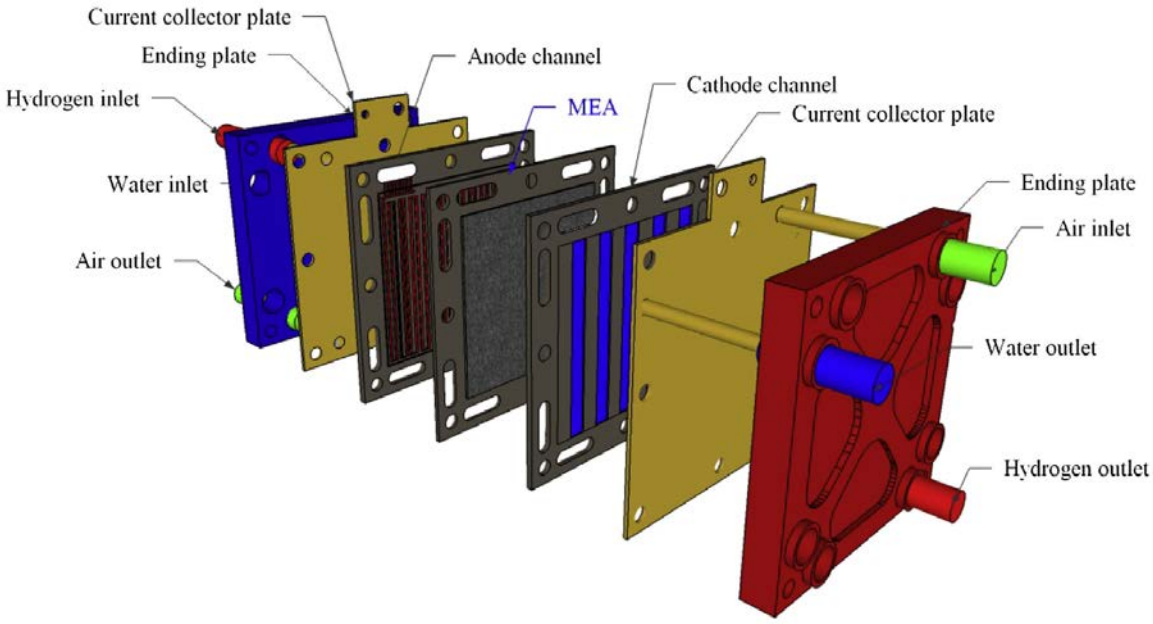

Figure 3 Layered components of a single PEMFC.

The FC plates include end plates, current collecting plates, and flow plates. The MEA contains various layers including the gas diffusion layers (GDLs), the electrodes, and the electrolyte membrane.

2.4.1 Plates

Several layers of the fuel cell are plates with different functions. On the outermost sides of the cell there are end plates with holes for inlet and outlet streams of gases and water. Following the end plate on either side of the cell is a current collecting plate which serves to collect and conduct the electron flow from the electrodes. The current collecting plate has a contact lead for the establishment of an external circuit. Following the current collecting plates are channel plates. Channel plates are commonly made from carbon and polymer based materials which ensure strength and support as well as conductivity.

Channel plates have inscribed patterns of conduits or channels through which water or gases flow. The plates can either be double sided with a gas flow pattern on one side and water on the other or single sided. If single sided two channel plates are needed one for the gas and one for the water. The gases flow through the channels and are distributed to the MEA while water flows through the channels to regulate the cell temperature. In a fuel cell stack it is necessary to have a double sided channel plate with flow patterns for gases on either side. This is to facilitate the flow of hydrogen to the anode of one cell and the flow of oxygen to the cathode of an adjacent cell in the stack. These plates are in contact with both electrodes of opposite charge and are known as bipolar plates.

2.4.2 Membrane Electrode Assembly (MEA)

The MEA is the site of the three phase interface necessary for reverse electrolysis. There are two main methods by which the MEA is made. In the separate electrode method each electrode is fixed to a GDL and then those layers are hot pressed on either side of the PEM. In the direct method the electrodes are painted, sprayed, or printed on either side of the PEM and after the GDLs are fixed on either side.

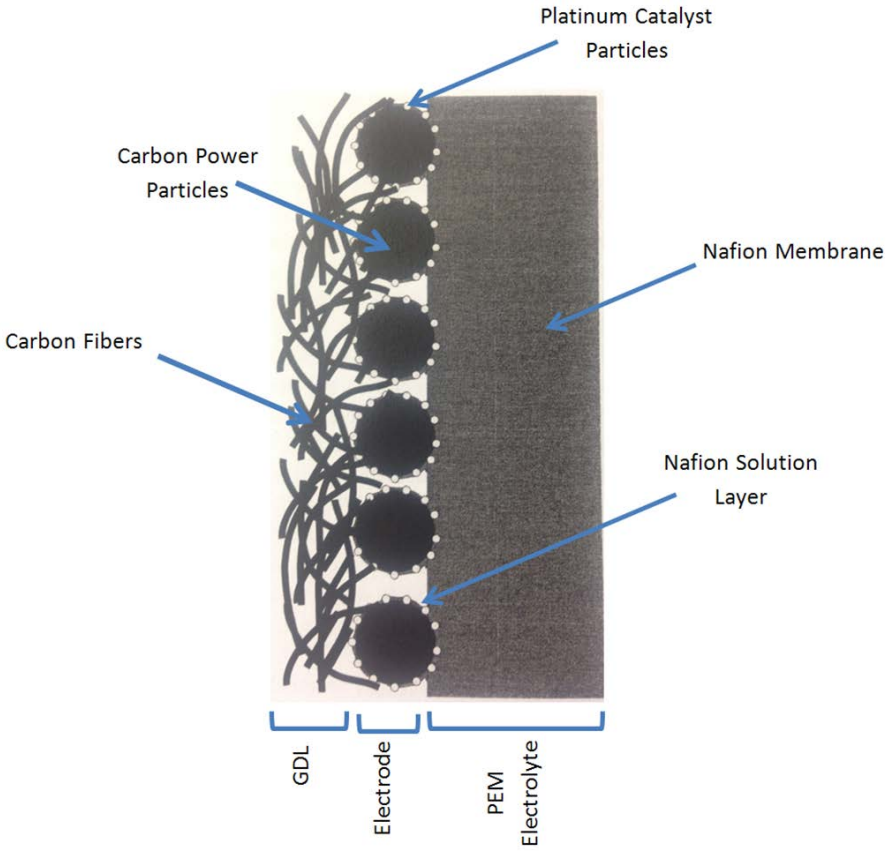

Figure 4 MEA structure containing the carbon fiber GDL, carbon and platinum electrode, and Nafion PEM electrolyte. Representation of the ideal three phase contact.

Regardless of the production method Figure 4 shows the ideal structure of an MEA. It is shown that a MEA is made to allow for maximum contact of the electrolyte and the electrode catalyst particles.

2.4.2.1 Electrolyte Membrane

The membrane is known as a proton-exchange membrane or polymer electrolyte membrane (PEM) and is the defining part of a PEMFC. The membrane serves to separate the oxidation and reduction reactions of the reverse electrolysis reaction. The membrane is ideally impermeable to electrons and porous for the transport of water and protons. A PEM is made of a polytetrafluoroethylene (PTFE) polymer with sulphonated side chains known as a perfluorosulfonic acid (PFSA) polymer. The side chains are acidic ionomers and terminate with SO_3^- and H^+ ions. The PFSA PTFE copolymer can have many different side

chain structures depending on the manufacturer, but the most common type is Nafion. Nafion typically has a perfluorovinyl side chain as shown in Figure 5. The PTFE backbone is highly hydrophobic and the sulphonic acid groups on the ends of the side chains are highly hydrophilic.

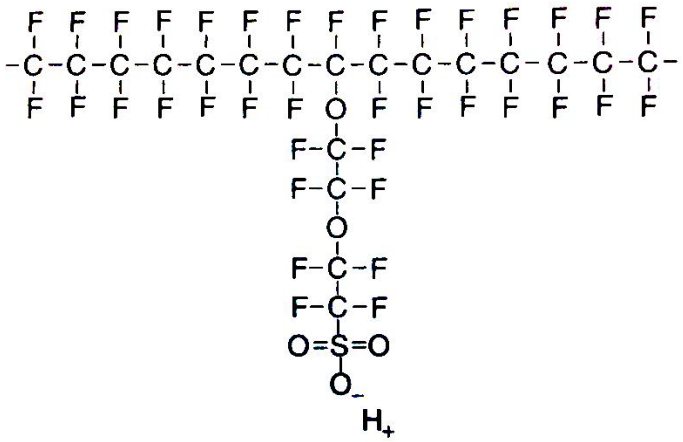

Figure 5 Perfluorosulfonic acid (PFSA) polytetrafluoroethylene (PTFE) polymer with perfluorovinyl side chain. The polymer is known as Nafion and is the most common material used to make PEMs.

The hydrophobic backbone provides mechanical structure and strength to the membrane. The hydrophilic regions or pores of the membrane fill with water and dissociate the acid groups creating a dilute acidic medium that is ideal for proton conductivity. Protons diffuse from the anode to cathode across the electrical field of the cell while transporting water in a movement known as electro-osmotic drag. In contrast water can also move by back diffusion from the cathode to the anode due to a pressure gradient.

Hydration of the PEM is necessary for adequate conductivity; however, it is possible for the pores to become too saturated with water. This is known as flooding and can occur at either the anode or the cathode. Flooding can be detrimental to the performance of the cell by limiting the flow of the gaseous hydrogen protons through the membrane. Therefore, analysis and management of the cell water balance is necessary in PEMFCs.

In the ideal fuel cell the reverse electrolysis reaction would produce enough water to hydrate the membrane. In reality, it is often necessary to humidify the air or both air and hydrogen inlet gases in order to introduce more water to the cell and membrane for sufficient proton conductivity. As a result the cell operating conditions greatly affect the water balance and affectivity of the membrane.

2.4.2.2 Electrode

The electrode connects the current gas diffusion layer and the electrolyte. The anode and cathode are located on either side of the electrolyte membrane and are the sites of oxidation and reduction half reactions, respectively, shown in Figure 6.

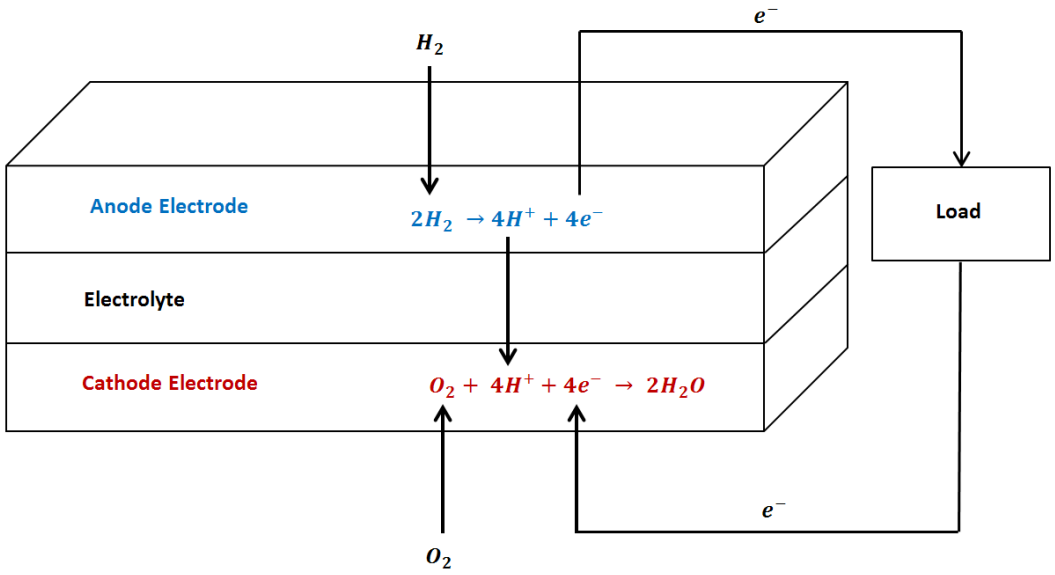

Figure 6 The oxidation and reduction half reactions that occur at the anode and cathode electrodes respectively in order to generate an external load.

The reactions are catalyzed by platinum particles that make up the microstructure of an electrode which is supported by carbon powder. The platinum particles typically have a diameter of 2-4 nm and are dispersed in a layer about 5-50 µm thick on the carbon powder. The carbon particles are typically 30 nm in diameter and overall the electrode is 10-40 weight percent platinum. Most often the anode and

cathode are very similar or identical; however, it is possible for the cathode to have a thicker layer of catalyst particles to promote the slower oxygen reduction reaction. Often an electrode is made with PTFE and the platinum particles are coated in a solution of the Nafion electrolyte as shown in Figure 4. The PTFE repels water from the catalyst and the electrolyte coating increases the three phase contact.

2.4.2.3 Gas Diffusion Layer (GDL)

The gas diffusion layer (GDL) joins the electrode with the current collecting plate and therefore serves to conduct electrical charge as well as diffuse reactant gases for uniform contact with the inner MEA. The GDL is a cloth or paper made of compressed carbon-based fibers and also provides protection for the catalyst electrode. It is usually about 200-500 µm thick with a pores about 10-50 µm in diameter. This is known as the mesoporous fibrous layer and in recent GDL manufacturing is combined with a microporous layer (MPL) as a transitioning layer between the GDL and catalyst electrode. The MPL is made of finer carbon black particles and enhances the uniform distribution of gases to the electrode.

The GDL absorbs water from the electrode and often swells separating the cell layers. Therefore, the particular GDL used is determined by the allowable separation based on application and the type of plates utilized. However, to avoid flooding PTFE can be added to the GDL and MPL to increase hydrophobicity and repel water from the cell.

2.4.3 Application of Faraday's Law

Through the application of Faraday's Law of Electrolysis a correlation between the reactant and product quantities of the electrochemical reactions in a fuel cell and the electrical output can be established. Faraday's Law states that the amount of substance reacted or produced is proportional to the current produced. Current is the flow of electrons in a circuit and can vary with time as in Equation 1.

$$\int_0^{\Delta t} I dt \tag{1}$$

If a constant current is generated Equation 1 simplifies and is equivalent to the product of Faraday's constant F, the number of moles of electrons in the reaction Δn_e, and the moles of reactant consumed n_{cons} as shown in Equation 2.

$$I\Delta t = n_{cons} * F * \Delta n_e \quad (2)$$

Equation 2 is applied to the half reactions shown in Figure 6 and rearranged as shown in Equations 3 and 4.

$$n_{H_2 cons} = \frac{I\Delta t}{2F} \quad (3a) \qquad \dot{n}_{H_2 cons} = \frac{I}{2F} \quad (3b)$$

$$n_{O_2 cons} = \frac{I\Delta t}{4F} \quad (4a) \qquad \dot{n}_{O_2 cons} = \frac{I}{4F} \quad (4b)$$

However the reactants flow rates entering the cell are in excess and dependent on anode and cathode stoichiometric coefficients, λ_A and λ_C. The inlet molar flow rates are expressed in Equations 5 and 6.

$$\dot{n}_{H_2 in} = \lambda_A * \dot{n}_{H_2 cons} \quad (5)$$

$$\dot{n}_{O_2 in} = \lambda_C * \dot{n}_{O_2 cons} \quad (6)$$

When air instead of pure oxygen is used as a reactant Equation 7 is used to calculate the molar flow rate of air into the cell, based on air composition of 21% oxygen and 79% nitrogen.

$$\dot{n}_{O_2 in} = .21 * \dot{n}_{Air\ in} \quad (7)$$

The oxidation and reduction reactions when combined yield the overall reaction of the fuel cell below.

$$H_2 + \frac{1}{2}O_2 \rightarrow H_2O$$

For every mole of hydrogen consumed one mole of water will be produced. Faradays' Law establishes the basic relationship between the reactants and products of reverse electrolysis and the electrical output of a fuel cell.

2.4.4 Water Management

It was necessary during operation to monitor the cell's relative humidity RH for water management. Relative humidity is the ratio of the water vapor partial pressure $P_{w\,T_{hum}}$ to the saturated water vapor pressure $P_{sat\,T_{cell}}$ in Equation 8.

$$RH = \frac{P_{w\,T_{hum}}}{P_{sat\,T_{cell}}} \tag{8}$$

Since only dry hydrogen was fed to the anode of the cell, the RH of the cell was determined by the partial pressure of the water vapor in the cathode. The partial pressure was calculated using the temperature of the air humidifier. The saturated water vapor pressure was calculated using the temperature of the cell which was fixed at 55C. Experiments were conducted at approximately 22% and 55% RH.

The saturated pressures were calculated using Antoine's equation, Equation 9.

$$P_{sat\,T} = \exp(a - \frac{b}{(T+273.15)+c}) \tag{9}$$

The variables a, b, and c are in units of atmosphere and Kelvin and are 11.6703, 3816.44, and -46.13, respectively.

The water transport coefficient of the experiments was calculated by analyzing the water management and gas flow of hydrogen in the anode. The initial fraction of water vapor in the anode $y^A_{H_2O}$ was found in Equation 10 in which the total pressure on the anode is assumed to be standard atmospheric

pressure, 1atm and the partial pressure of the saturated water $P_{H_2O\ sat}$ was found at the cell temperature.

$$y_{H_2O} = \frac{P_{H_2O\ sat}}{P_{Total}} \tag{10}$$

The molar flow of hydrogen exiting the anode $\dot{n}_{H_2out}$ was found as the difference between the molar flows of hydrogen in and the molar flow of hydrogen consumed, as in Equation 11.

$$\dot{n}_{H_2out} = \dot{n}_{H_2in} - \dot{n}_{H_2cons} \tag{11}$$

Equation 12 below is derived from Equations 5 and 11.

$$\dot{n}_{H_2out} = \dot{n}_{H_2in} * (1 - \frac{1}{\lambda_A}) \tag{12}$$

The molar flow of the water vapor coming out of the anode was determined in Equation 13.

$$\dot{n}^A_{H_2O\ vapor\ out} = \frac{y^A_{H_2O} * \dot{n}_{H_2out}}{(1 - y^A_{H_2O})} \tag{13}$$

Equation 13 is derived from Equation 14 and 15. Equation 14 relates water vapor and hydrogen leaving the cell and Equation 15 shows that the sum of the water vapor and hydrogen fractions is equal to one.

$$\frac{\dot{n}^A_{H_2O\ vapor\ out}}{\dot{n}_{H_2out}} = \frac{y^A_{H_2O}}{y_{H_2out}} \tag{14}$$

$$1 = y^A_{H_2O} + y_{H_2out} \tag{15}$$

The moles of water vapor leaving the anode was found for the specific time of the experiment and added to the moles of liquid water collected from the anode to find the total moles of water leaving the anode as shown in Equation 16.

$$n^A_{H_2O\ Total\ out} = n^A_{H_2O\ vapor\ out} + n^A_{H_2O\ liquid\ out} \tag{16}$$

Ultimately the water transport coefficient was calculated via Equation 17, assuming that hydrogen fed to the anode was completely dry and therefore that the amount of water in to the anode was equivalent to zero.

$$\alpha = \frac{n^{A}_{H_2O\ Total\ out} - n^{A}_{H_2O\ in}}{n_{H_2O\ prod}} \tag{17}$$

The moles of water produced by the cell $n_{H_2O\ prod}$ are equivalent to the moles of hydrogen consumed because for every mole of hydrogen used in the anode, one mole of water is produced in the cathode.

Analysis of the water transport coefficient indicates the net flow of water. Positive values of the coefficient show that water is moving from the cathode to the anode while negative values signify water flow from the anode to the cathode.

As previously explained no water enters the anode, however, water vapor enters the cathode through the humidified air supply. The molar flow of water vapor entering the cathode $\dot{n}^{C}_{H_2O\ \ vapor\ in}$ was calculated by Equation 18, similar to the calculation for the flow of water vapor leaving the anode in Equation 13.

$$\dot{n}^{C}_{H_2O\ vapor\ in} = \frac{y^{C}_{H_2O} * \dot{n}_{Air\ in}}{(1 - y^{C}_{H_2O})} \tag{18}$$

The fraction of water vapor in the cathode $y^{C}_{H_2O}$ was found in Equation 10. The total pressure on the cathode is assumed to be standard atmospheric pressure, 1atm and the partial pressure of the saturated water $P_{sat\ T_{hum}}$ was determined using Equation 9 at the temperature of the humidified air.

An overall water balance was completed with the amount of water vapor entering the cathode and the amount of water produced by the cell as shown in Equation 19.

$$n^{C}_{H_2O\ \ vapor\ in} + n_{H_2O\ prod} = n_{H_2O\ Total\ out} \tag{19}$$

The total moles of water out $n_{H_2O\ Total\ out}$ can be compared with the moles of liquid water collected from both the anode and cathode $n_{H_2O\ collected}$. This comparison assumes that all water vapor exiting the anode and cathode is completely condensed.

If this assumption is not followed then the total moles of water out of the cell can be compared with the actual total moles of water exiting the cell $n_{H_2O\ Actual\ Total\ out}$. The actual total represented in Equation 20 is the sum of the water moles collected and the amount of water vapor exiting the cathode.

$$n^C_{H_2O\ \ vapor\ out} + \ n_{H_2O\ collected} = \ n_{H_2O\ Actual\ Total\ out} \tag{20}$$

The amount of water vapor exiting the cathode was based on the measured temperature of the cathode outlet and the assumption that the vapor out was completely saturated and did not condense. The molar rate of water vapor exiting the cathode was calculated in Equation 21.

$$\dot{n}^C_{H_2O\ vapor\ out} = \frac{y^C_{H_2O\ out} * \dot{n}_{Air\ out}}{(1 - y^C_{H_2O\ out})} \tag{21}$$

Following Equation 10 the fraction of water vapor in the cathode outlet $y^C_{H_2O\ out}$ was found as the ratio of the partial pressure of the saturated water vapor to total pressure assumed to be standard atmospheric pressure, 1atm. Using Equation 9 the partial pressure of the saturated water vapor was determined at the temperature of the cathode outlet line. The molar flow rate of air leaving the cathode was calculated via Equation 22 which was derived from the difference of the molar flow of air into the cathode and the molar flow of oxygen consumed by cell and is similar to Equation 12.

$$\dot{n}_{Air\ out} = \ \dot{n}_{O_2 in} * (\frac{1}{0.21} - \frac{1}{\lambda_C}) \tag{22}$$

Further analysis was completed to determine if liquid water was present in the anode and cathode for each experiment. Liquid water was present if the amount of water collected from one side of the cell

was greater than the capacity or maximum amount of water possible for that side of the cell and its specific temperature.

The maximum molar flow rate of water in the anode $\dot{n}^{A}_{H_2O\ max}$ was calculated by Equation 23 and the maximum amount of water was determined based on the length of the experiment.

$$\dot{n}^{A}_{H_2O\ max} = \frac{y^{cell}_{H_2O} * \dot{n}_{H_2\ cell}}{(1 - y^{cell}_{H_2O})} \tag{23}$$

The vapor fraction of water in the cell $y^{cell}_{H_2O}$ is equivalent to the initial fraction of water vapor in the anode found in Equation 10 based on the temperature of the cell. The molar flow rate of hydrogen in the anode $\dot{n}_{H_2\ cell}$ is equivalent to the molar flow rate of hydrogen out of cell found in Equation 11.

2.5 Fuel Cell Testing Techniques

A variety of techniques used to analyze and characterize fuel cells are explained in the following sections.

2.5.1 Chronoamperometry

Chronoamperometry (CA) is a technique in which the potential of a working electrode is changed stepwise from a value with no faradaic reaction to one in which the concentration of the electroactive species at the surface is zero (Wang, 2001). The technique is often used to understand how current decays over time using the Cottrell equation, seen below.

$$i(t) = \frac{nFACD^{0.5}}{\pi^{0.5} t^{0.5}}$$

In the Cottrell equation, C is the reactant concentration, A is the electrode area, n is the electron number, and D is the diffusion coefficient of the reactant species. Often chronoamperometry is used to calculate the diffusion coefficient, measure fuel crossover, or calculate the surface are of the working

electrode (Yaun, Song, Wang, & Zhang, 2010). The Cottrell equation is derived from the fact that mass transport is only possible through diffusion during the test. The expansion of the diffusion layer over time can be seen through a concentration profile. As reactants are depleted there is a decrease slope, see Figure 7.

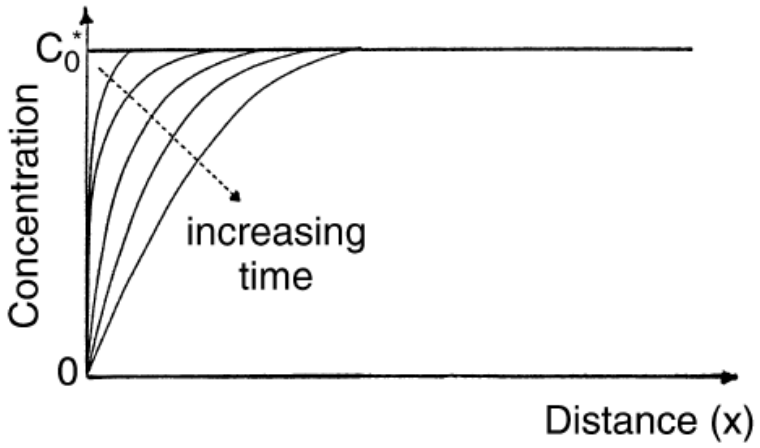

Figure 7 Change of concentration profiles with time (Wang, 2001).

2.5.2 Chronopotentiometry

In this test, current is input and voltage is the output. The technique applies a constant current between the working and the counter electrode. It is utilized to establish a steady state polarization curve. This curve is created based on the steady state voltages obtained from multiple testing at varying currents. An example curve is shown in Figure 8.

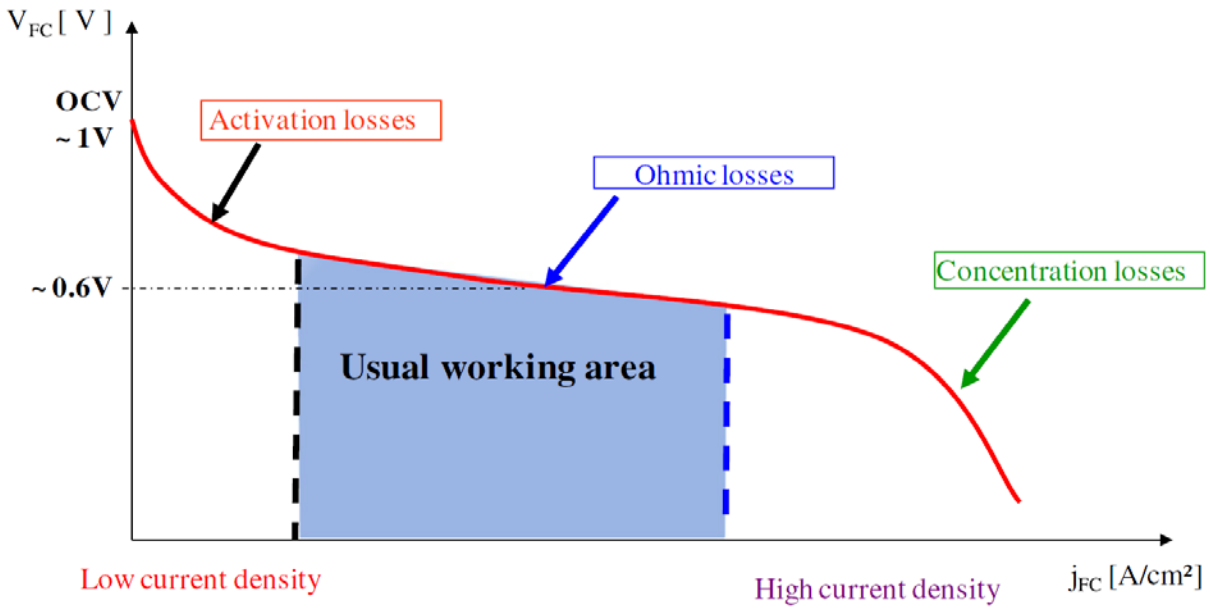

Figure 8: Polarization curve indicating the three distinct regions of PEMFC operation.

There are three easily identified regions of operation shown by the polarization curve. There is an initial sharp drop in voltage at low current densities, due to activation losses. The losses are caused by the FC kinetics, especially the slow reaction rate at the cathode. The second region is the typical working region in which potential decreases linearly with increased current density. This decline is primarily due to ohmic resistances or the resistance of the FC to the flow of electrons and protons. Finally the third region shows a significant decline in voltage at very high current densities. The final drop-off is represents concentration losses due to mass transport resistances , specifically “the mass transport resistance of oxygen in the GDL” (Vilekar, 2010). The initial point on the polarization curve is the open circuit voltage (OCV) at which no current is drawn from the cell. At about 0.6V and 0.4-0.8 A/cm2 a PEMFC typically operates at a median performance.

Polarization curves are useful tools for the characterization of a FC and its particular membrane. Establishing polarization curves for an FC at different operating conditions, such as varying RH levels,

shows the effects on the FC performance. Analysis of a polarization curve provides information on the appropriate operating conditions necessary for a particular FC application.

2.5.3 Cyclic Voltammetry

Cyclic voltammetry (CV) is one tool used for evaluation of the catalyst. This technique captures the process occurring at the surface of the electrode (Ramani, 2007). It is a linear potential scan of a stationary working electrode with respect to a non-polarizable electrode(*EC-Lab Software: Techniques and Applications*, 2011). From the initial potential (E_{int}), the scan goes forward to a first vertex potential, backwards to the second vertex potential and then returns to the first vertex potential to complete one cycle (Application Note 41). This can be seen in Figure 9a below.

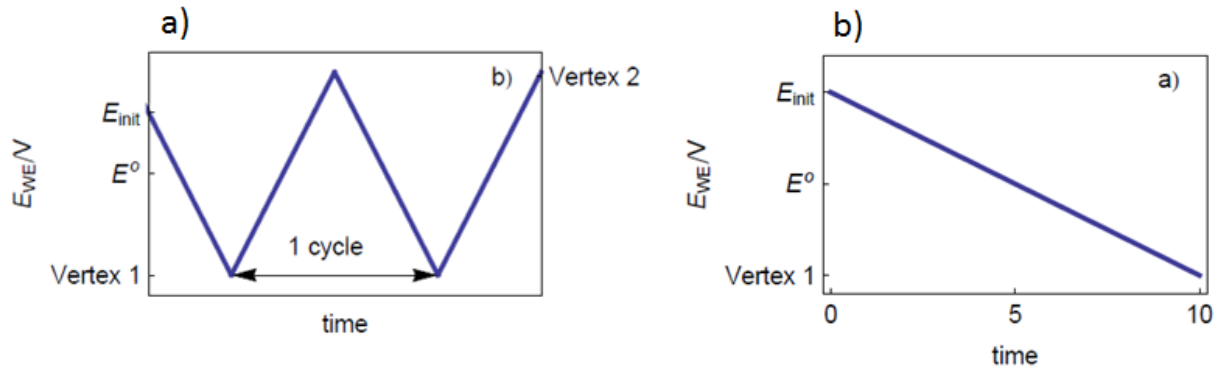

Figure 9: Potential voltage versus time for a) cyclic voltammetry and b) linear sweep voltammetry (Application Note 41).

In fuel cells, tests are done with hydrogen fed to the anode and nitrogen fed to the cathode. The resulting graph of the current versus the potential is known as a cyclic voltammogram, an example can be seen below. A lot of information can be gained from the voltammogram. The area under the first peak, in Section 1 in Figure 10, is the anode charge (Q_a) and signifies the desorption of hydrogen. Q_c, the cathode charge, represents the adsorption of hydrogen. In Section 2 of Figure 10 the double layer is

charged and discharged, information on" hydrogen crossover from the anode," and evaluation of the catalyst on the cathode side may be seen (Ramani, 2007).

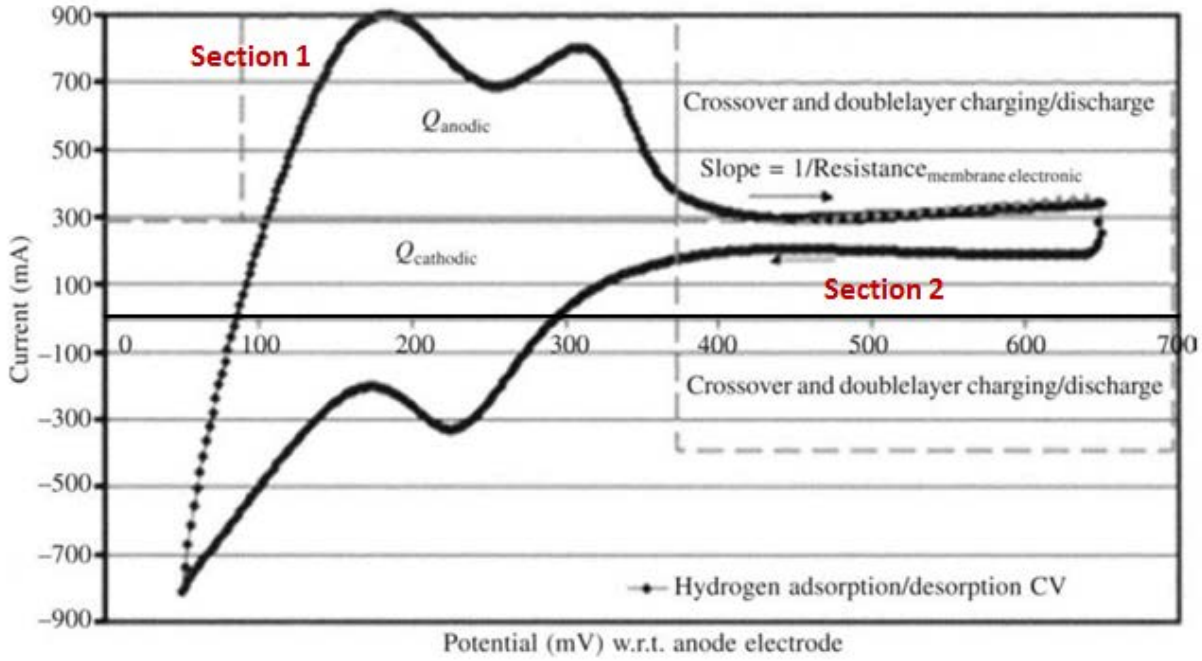

Figure 10: Cyclic voltammogram of fuel cell fed with H_2/N_2 (Ramani, 2007).

The MEA acts as a barrier between the anode and cathode electrodes however depending on how it is assembled and compacted, an electrical resistance results, this resistance can be seen in various techniques, including CV. In Section 2 of Figure 10, the membrane electronic resistance can be found by the inverse of the slope from 500 to 600 mV during the forward sweep.

If tests are done with both chambers fed with nitrogen, the double layer capacitance can be targeted. Double layer capacitance (C_{DL}) is calculated using the peak current (I_{peak}) from the CV and the scan rate (R).

$$C_{DL} = I_{peak} \times R$$

This capacitance is due to the Platinum-Carbon structure and allows for better understanding of the state of the components in an electrode. Reduced capacitance might signify organic contamination, a less wetted area, or carbon oxidation (Ramani, 2007).

2.5.4 Linear Sweep Voltammetry (LSV)

Similar to cyclic voltammetry, this test enables evaluation of the catalyst. However, in LSV a forward potential scan is conducted from the initial potential (E_{int}) to the first vertex, seen above in Figure 9b. LSV however is an irreversible scan. The scan will occur with a voltage range of 0 to 0.8. Like CV the cathode side contains nitrogen so any current that is generated "is attributed solely to the electrochemical oxidation of H_2 gas that crosses over from the anode side" (Yuan & Wang, 2008).

2.6 Prospective Applications

Fuel cells present a potential alternative energy source that is quiet, fairly simple, and completely clean. Many types of FCs are currently used as sources of distributed power, because they provide power on site and energy is not lost in transport. In particular PEMFCs have been used as power sources for back-up applications and vehicles and provide sustained power. However, one disadvantage of PEMFCs is that they do provide a fast voltage supply due to slow gas reactant flows. A potential application for PEMFCs is their conjunction with batteries or supercapacitors which could provide a potential during times of transient gas flows. In contrast batteries and supercapacitors are not sustained power supplies but can deliver a fast potential. Therefore, the combination of the two types of devices is an attractive possibility.

Very little work has explored this prospect. Experiments have been done that investigate the combination of FCs with a specific supercapacitor, superconducting coils. It was determined if FCs could produce a high current while operating at a very low voltage in order to sufficiently load the coils.

Operation at low voltages means that the FC working area was within the third region of Figure 8 in which mainly concentration losses exist. In this situation the current induced by the fuel cell is directly controlled by the inlet flow of hydrogen following Faraday's Law. It was found that the by short-circuiting the FC a desired current could be produced based on the inlet hydrogen and that the current was ideal for superconducting coils due to low oscillations. Operation at low voltages for combination with supercapacitors is an original application that has the potential for greater developments of FC technology.

This report intends to further explore the possibility of FC operation at low voltages. Unlike the previous experiments the FC is not short-circuited by a superconducting coil. Instead it is forced to operate at a low voltage via CA testing techniques to determine if an expected current is obtainable based on the inlet hydrogen flow. Figure 11 depicts a circuit in which a FC operates at low voltages in conjunction with a supercapacitor. This is a theoretical circuit representing how the FC/supercapacitor combination could be realistically applied. Ideally the additional wire shown would provide zero resistance and essentially reduce the FC voltage to zero. Simultaneously the FC would generate a high current for loading the supercapacitor. The potential for these applications is yet unknown, however, if proved viable could yield a clean and continuous power source unattached to the electrical grid.

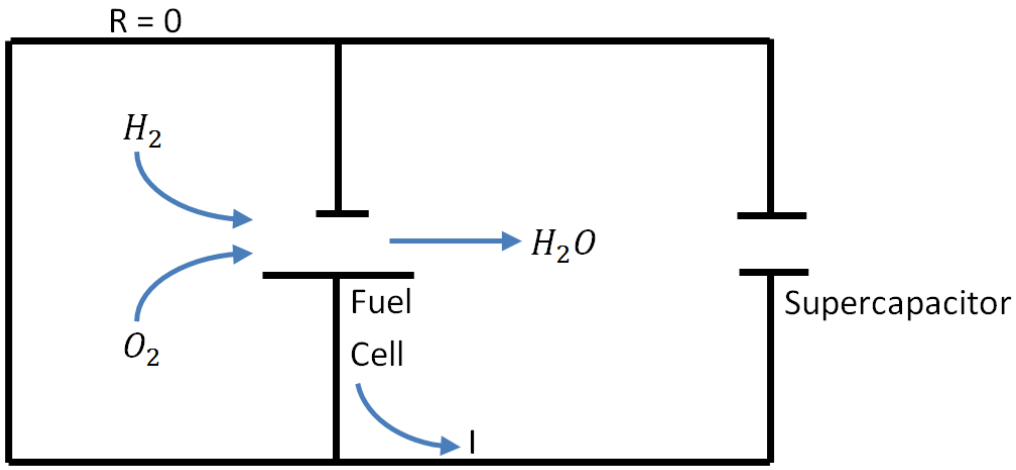

Figure 11 Theoretical circuit combining a FC and supercapacitor with a zero resistance wire minimizing the cell voltage.

As suggested by the previous work with superconducting coils it is necessary to analyze experimental results for the presence of flooding and degradation effects within the cell. Flooding is a prospective problem because of a fast decrease in anode pressure. As hydrogen is rapidly reacted anode pressure decreases and it may be possible that water vapor condenses. Also generation of a high current means that a lot of water is produced by the reaction increasing the risk of flooding. Therefore, these experiments target a low relative humidity in the cell to avoid flooding. Additionally these experiments analyze changes in resistance and the electrode electrochemical surface area to determine the degradation affects from low voltage operation.

3.0 Methodology

3.1 Equipment

The following sections details the equipment used in the experiments.

3.1.1 Fuel Cell

The fuel cell consisted of two end plates, two current collecting plates, bipolar flow plates, and a membrane-electrode assembly (MEA) shown in Figure 12. The MEA was a PIMEA Series 5760 MESGA.

The Perfluorosulfonic Acid (PFSA) membrane was reinforced with expanded polytetrafluoroethylene (ePTFE). On the anode side there was 0.45 milligrams of a 50% Platinum-50% Ruthenium mixture per square centimeter. The cathode side had 0.4 milligrams of Platinum per square centimeter. The gas diffusion layer (GDL) was a Sigracet® 30BC. The GDL had micro-porous layers (MPL) and was made with carbon felt.

Figure 12: Parts of the fuel cell; A. Membrane-electrode assembly (MEA) used; B. Red end plate, current collecting plate and a channel plate; C. Bipolar plates in which fuel (H_2 or Air) flows on the side with a serpentine path (left plate) and water flows on the plate with a rectangular path (right).

Air and Hydrogen enter the fuel cell through connectors at the end plate. Preheated water is used to maintain the temperature of the fuel cell around 55 °C. Water that has been produced and that has

entered the fuel cell in the humidified gases leaves through water outlet tubes from the anode and cathode side. Figure 13 shows all inlets and outlets of the fuel cell used.

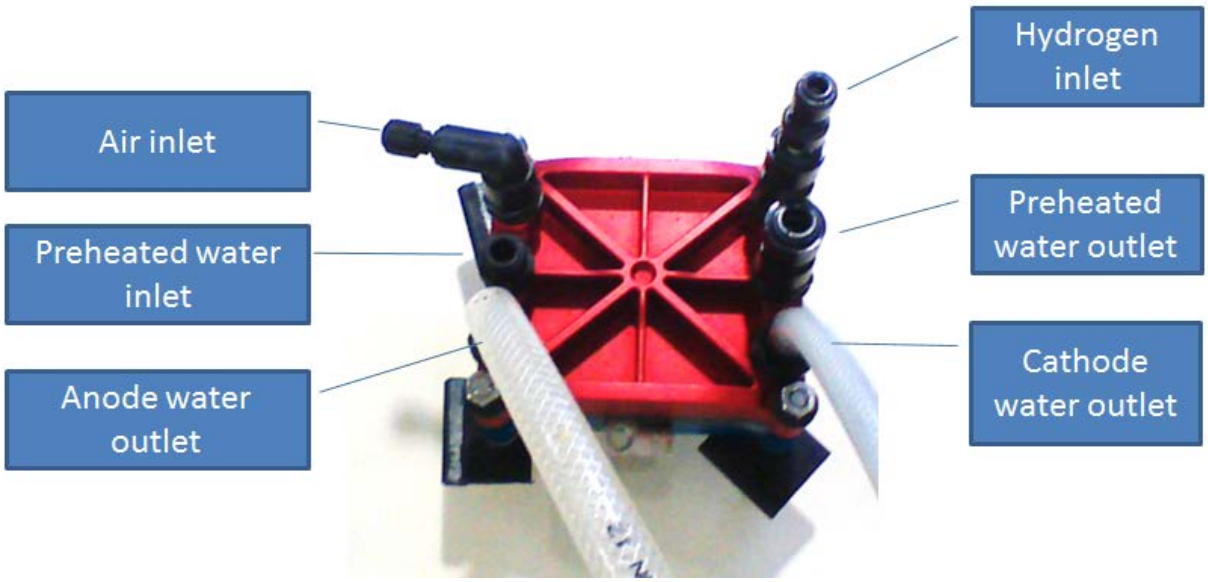

Figure 13: View of fuel cell inlets and outlets.

3.1.2 Fuel Cell Bench

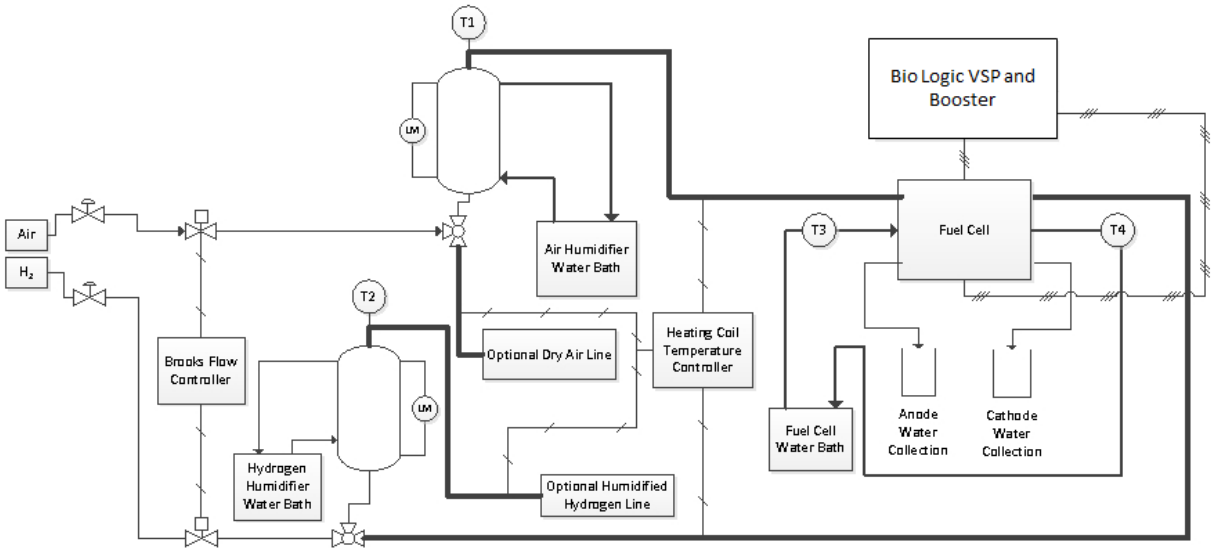

Figure 14: Schematic of fuel cell bench.

Figure 14 details the bench setup that was used to run experiments on the fuel cell. Air and hydrogen entered from a house feed. Regulators and valves were on each line to allow the gases to flow to the bench. Brooks® mass flow controllers were located down line and connected to a display where flows were set. Beyond the flow controllers were three way valves. The gas was able to flow either into a humidifier or directly to the fuel cell. For most operations hydrogen was kept dry and air was humidified. Each house-made humidifier had a water bath that supplied heated water to the humidifier. The air humidifier had insulated hoses to carry the water to and from the water bath. Air flowed from the humidifier through tubes that were wrapped in heating coils and insulation. Air entered the fuel cell on the cathode side. Hydrogen also flowed through tubes that were wrapped in heating coils and insulation to the humidifier as well. The heating coils were controlled by temperature probes that were connected to a temperature controller. All heating coils were set at 60 °C. The hydrogen entered the fuel cell at the anode side. As mentioned in the previous section, the fuel cell temperature was maintained at 55 °C with a water bath. Water was collected from the anode and cathode in beakers. The fuel cell was connected to an 80 amp BioLogic external current booster. The booster was connected to a potentiostat (VSP model). The VSP was connected to a computer with EC-Lab® software. A photo of the bench can be seen below in Figure 15.

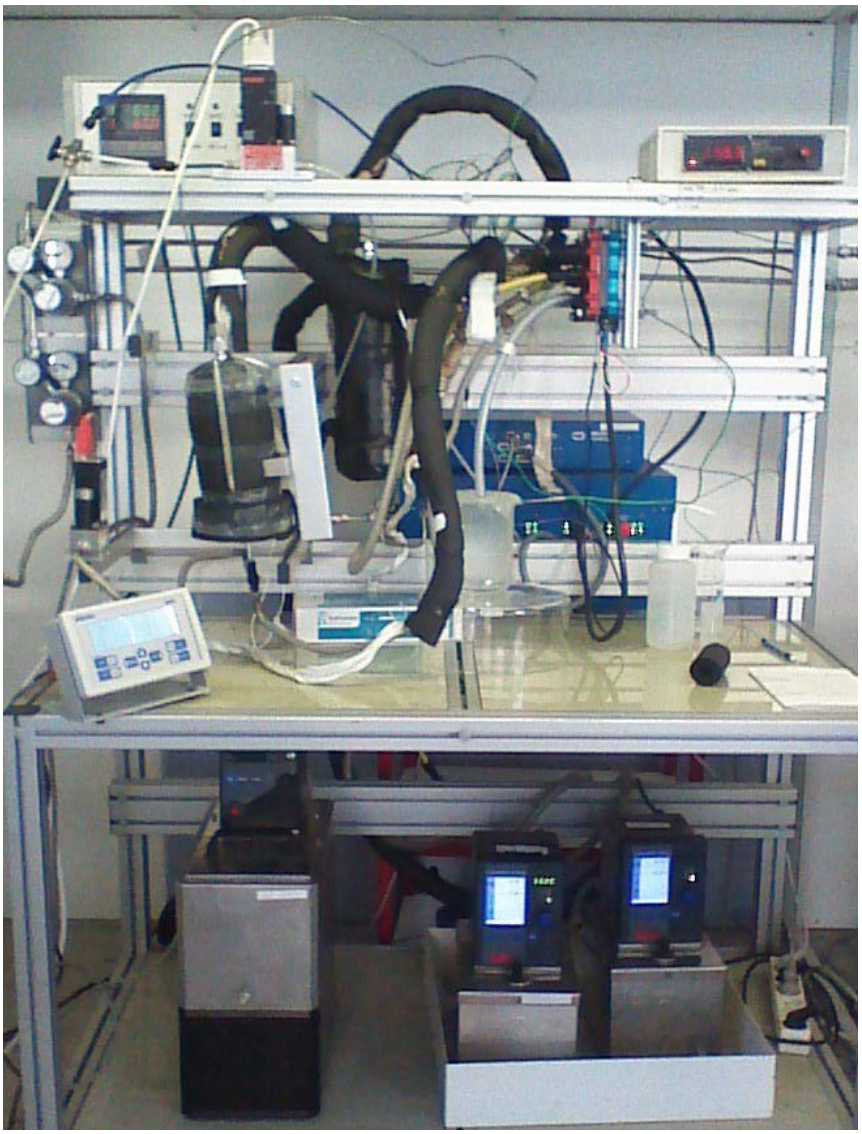

Figure 15: Photo of the fuel cell test bench.

3.2 Procedures

Tests were done to characterize the fuel cell, to understand the cathode, anode and ohmic resistances, to determine the active surface area of the fuel cell, and to learn how hydrogen flowrates affect the current when the cell was run at low voltages.

3.2.1 Characterization of the Fuel Cell

A current was first selected and then the required flow rates of hydrogen and air were calculated using Faraday's Law. The experimental flow rates are shown in Table 2

Table 2: Calculated flowrates for currents maintaining a $\lambda_{hydrogen}$=1.44 and λ_{Air}=2.40

Current (Amps)	Hydrogen Flow Rate (L/min)	Air Flow Rate (L/min)
10	0.1	0.4
20	0.2	0.8
30	0.3	1.2
40	0.4	1.6
50	0.5	2.0
60	0.6	2.4
70	0.7	2.8
80	0.8	3.2

The Brooks Flow controller was set to the desired flow rates (Air set on Channel 1 and Hydrogen on Channel 3). The EC-Lab software was next opened and a chronopotentiometry (CP) test was selected. The current and time of the experiment were specified using the software, see Figure 16, and the CP was started.

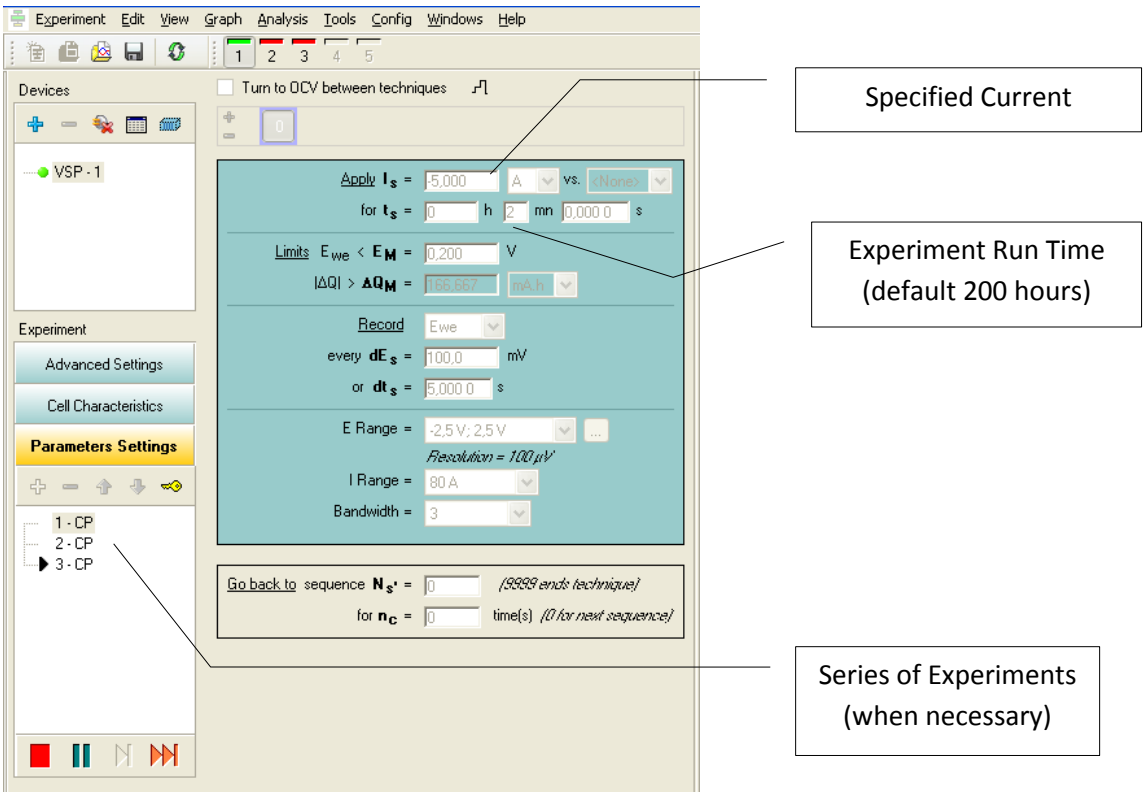

Figure 16: Snapshot of EC-Lab® display for Chronopotentiometry experiments

The time was noted and collection beakers were placed under the anode and cathode water tubes. Upon reaching a transient state, the experiment was stopped and the time was recorded. From the graph of voltage versus time a median voltage of the transient state was obtained as well as the fluctuation of the voltage. Temperatures of the humidifier, the cell, the atmosphere and exiting water vapor were also recorded. The water collected was weighed. Next a galvanostatic electrochemical impedance spectroscopy (GEIS) was setup. The current, amplitude and often the number of runs was specified.

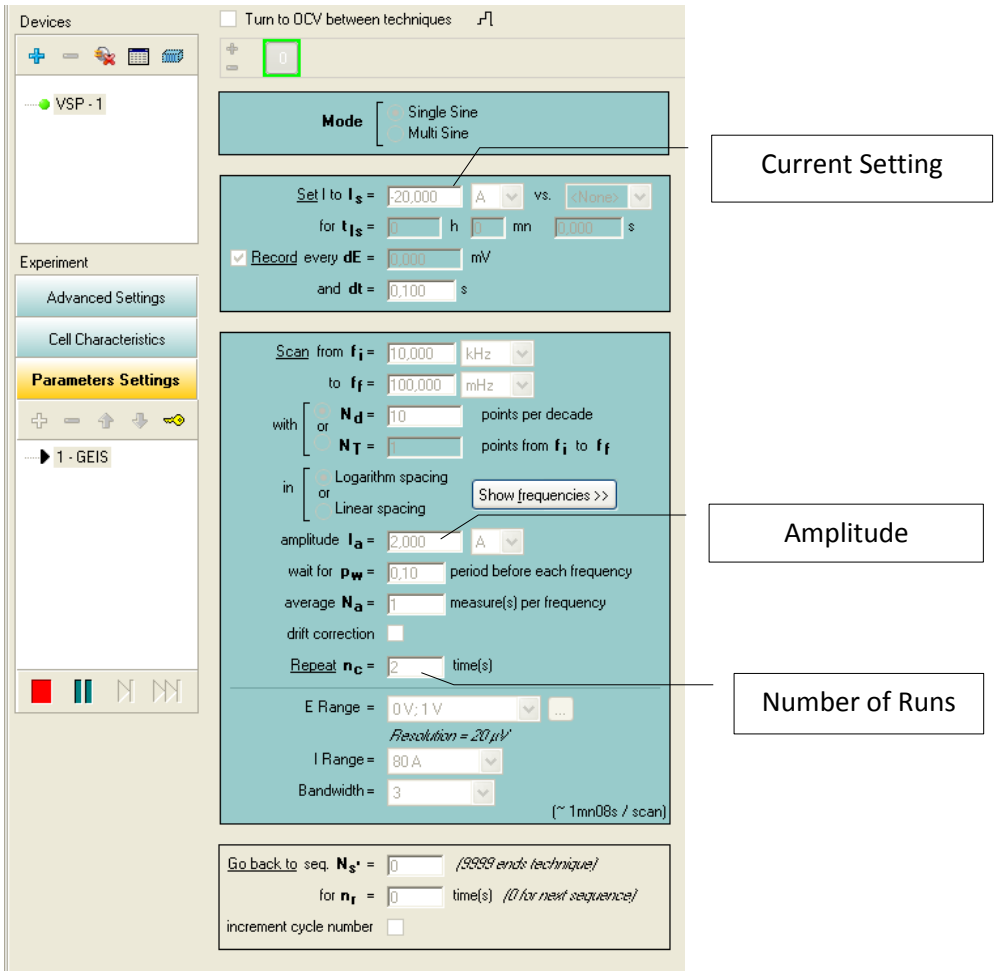

Figure 17: Snapshot of galvanostatic electrochemical impedance spectroscopy display in EC-Lab ®

Upon completion of the GEIS, the procedure was repeated at other currents. Tests were completed at two relative humidities (22% and 55%). The relative humidity was controlled by the air humidifier water bath. The water bath was set to 28 °C for 22% RH.

3.2.2 Dry Air and Hydrogen Test Procedures

In order to allow dry air to go to the fuel cell, all gas flow to the fuel cell was first shut off. Then the humidified air stream was disconnected and the dry air line was connected to the cathode side of the cell. Next, the three-way valve below the air humidifier was turned to allow flow though the dry air line. A temperature probe was inserted between the heating coil and interior tube and the heating coil was turned on and set to 60°C. Gas was next set at the necessary ratio based on Table 2. Due to the use of

dry gases, it was found that there were large charge transfer and ohmic resistances; this made it impossible to set CP at the desired current immediately. Instead, a stepwise technique was used. A series of CP tests were setup to run for two minutes each. Starting at 5 amps and increasing by 10 amps each time until the desired current was reached, see Table 3. The experiment for the desired current was run until a transient state was reached. The beginning and final voltage for each step was recorded as well as the open circuit voltage.

Table 3: Dry gas CP series settings for 30A

Experiment #	Current Setting (Amp)	Time (min)
1	5	2
2	15	2
3	25	2
4	30	120

3.2.3 Cyclic Voltammetry and Linear Sweep Voltammetry

In order to complete cyclic voltammetry (CV) and linear sweep voltammetry (LSV) testing the FC needed to operate with only the hydrogen reduction reaction and therefore nitrogen an inert gas was fed to the cathode. The air inlet line prior to the humidifier was closed via a three way valve and a nitrogen inlet line was opened for flow. Additionally as close to complete saturation of the FC was desired for these experiments. All water baths for both gas humidifiers and the cell were set to 58 °C and allowed to reach a steady temperature. The three-way valve below the hydrogen humidifier was adjusted to direct hydrogen gas through the humidifier. A heating element and insulation were wrapped around the hydrogen humidifier outlet stream in order to prevent the condensation of water vapor prior to entering

the cell, see Figure 18. This line was connected to the fuel cell hydrogen inlet and testing was completed.

Figure 18: Interior line wrapped in a heating coil and insulation.

Linear sweep voltammetry is a test in which the FC voltage is varied to determine the hydrogen crossover within the PEM. LSV varies current at a very low rate (2 mV/s) in order to avoid any effects on the FC from capacitive current. At 0.4 V the current at which hydrogen leakage or crossover occurs was observed. This leakage current was applied via Faraday's Law in Equation 3b to determine the flow of hydrogen crossover within the membrane.

Cyclic voltammetry is a test in which the FC voltage is varied to determine the electrochemical surface area (ECSA) of the electrodes. CV varies voltage at a very high rate (30 mV/s) and the resulting adsorption-desorption curves for hydrogen, as shown in Figure 9, reflect several reactions within the FC. From 50-450 mV these reactions include hydrogen oxidation at the anode and loading of the capacitance double layer shown by regions A and B, respectively.

Hydrogen oxidation occurs on the platinum catalyst at the anode electrochemical area. The ECSA was calculated using the area of region A. This was determined by subtracting the area under the curve in region B from the total area under the curve from 50-450 mV. The area of region A was divided by the rate of change in the voltage, 30 mV/s to obtain the desorption charge. The desorption charge was

divided by the standard value that 210 µC/cm^2 of charge is consumed in hydrogen oxidation for polycrystalline platinum to calculate the final ECSA.

3.2.4 Chronoamperometry

To run chronoamperometry (CA) tests dry hydrogen and humidified air were used. The flow of hydrogen and air were set using the calculated flows in Table 2. In EC-Lab a series of CA tests were setup, each applying a different potential step (E_i). The initial tests were run for 2 minutes each while the final test at 20 millivolts was run until steady state was reached (2-4 hours).

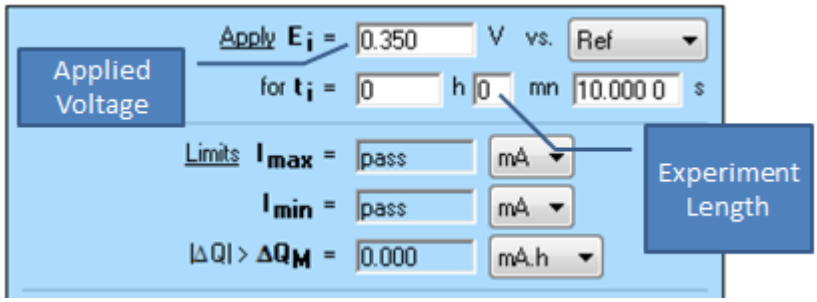

Figure 19: EC-Lab display for CA tests.

Tests were done at varying flow rates. GEIS was run after each series of CA tests. The current for the GEIS test was based on the flow rate of reactants and corresponded to the current in Table 2.

4.0 Results

4.1 Polarization

Characterization of all three membranes was established at approximately 22% relative humidity and for the first membrane also at 55% RH. Current density was varied and the resulting voltages are shown in Figure 20. For all tests it was found that as the current density increases the cell voltage decreases in a nearly linear relationship. The results are as expected and correspond to the second region of the polarization curve as shown in Figure 8. The decrease in voltage observed is attributed to greater resistances and potential loss as the demanded current increases. The membranes exhibited very

similar characterization at 22% RH as shown by the large overlap in measured potentials, visible in Figure 20. This indicates that all the membranes were activated and at a similar state prior to experimental testing. For M1 the potential of the FC at different RH conditions was minimal; at 22% RH the cell voltage measured was about 27mV lower than the voltage recorded at 55% RH.

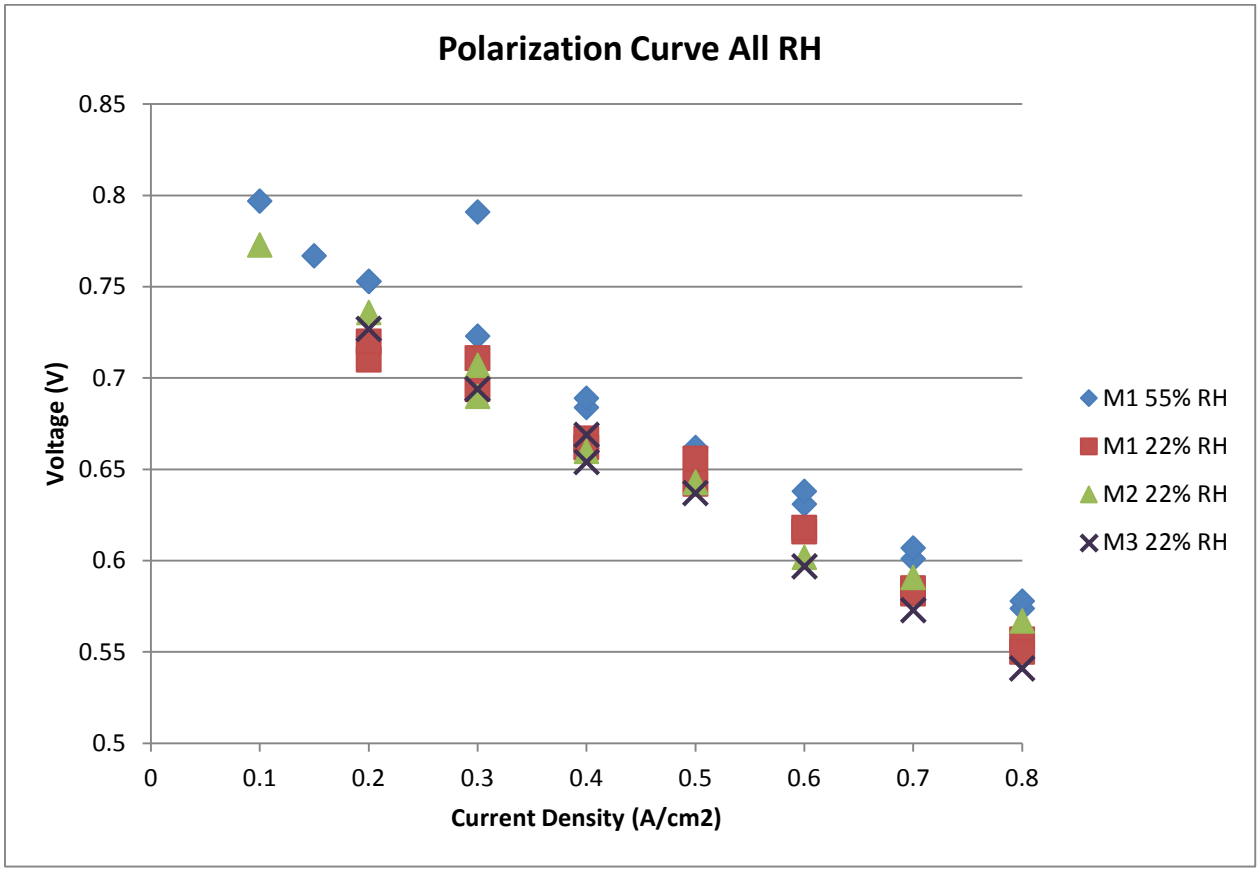

Figure 20 Polarization curves for all three membranes, primarily at 22% RH.

The voltages were approximate averages recorded after a transient period in which the cell reached steady state. The transient period for most experiments was about 1-3 hours. At 22% RH the transient periods were longer, especially at lower current densities, ranging from 4-12 hours. The fluctuation in the steady state voltage was recorded as shown in Table 4. At 22% RH the fluctuation was relatively constant for all experiments 1.0-3.0 mV except for some tests at lower current densities. In particular at

20A M1 showed a fluctuation of about 10.0mV and M2 showed a fluctuation of about 6.0mV. At 55% RH the fluctuation did not vary as much at lower current densities and on average the fluctuation observed for all experiments was about 1.6mV. Therefore, the voltages supplied for all membranes have the same evenness and testing at 22% RH has the same repeatability as testing at 55% RH, except at low current densities.

Table 4 Fluctuation of steady states voltages obtained in the characterization of all three membranes.

	M1 55% RH		M1 22% RH		M2 22% RH		M3 22% RH	
Current Density (A/cm2)	Voltage (V)	Fluctuation ± V	Voltage (V)	Fluctuation ± V	Voltage (V)	Fluctuation ± V	Voltage (V)	Fluctuation ± V
10	0.797	0.0035			0.773	0.0060		
15	0.767	0.0015						
20	0.753	0.0005	0.710	0.0100	0.736	0.0030	0.727	0.0030
	0.753	0.0020	0.720	0.0110				
30	0.791	0.0015	0.711	0.0025	0.707	0.0020	0.694	0.0020
	0.723	0.0015	0.694	0.0035	0.690	0.0020		
40	0.684	0.0015	0.667	0.0015	0.660	0.0020	0.669	0.0010
	0.689	0.0010	0.662	0.0025			0.654	0.0020
50	0.661	0.0010	0.656	0.0015	0.643	0.0030	0.637	0.0020
	0.662	0.0005	0.642	0.0020	0.643	0.0020		
60	0.631	0.0010	0.616	0.0015	0.602	0.0020	0.597	0.0010
	0.638	0.0025	0.618	0.0020				
70	0.601	0.0010	0.585	0.0020	0.591	0.0010	0.573	0.0010
	0.607	0.0015	0.582	0.0020				
80	0.574	0.0035	0.557	0.0015	0.567	0.0030	0.541	0.0030
	0.578	0.0020	0.550	0.0020				

Additionally performance curves for all membranes were obtained in which the specific electrical power of the cell is the product of the cell voltage and current. Independent of the humidity conditions the cell power for all membranes increased with current density as shown in Figure 21. This is logical for the testing at lower current densities because as the load of the cell is increased the cell must supply more power. At both humidity conditions and between all membranes the cell achieved similar performance levels. Only slight variations among the membranes were found as shown in Figure 21.

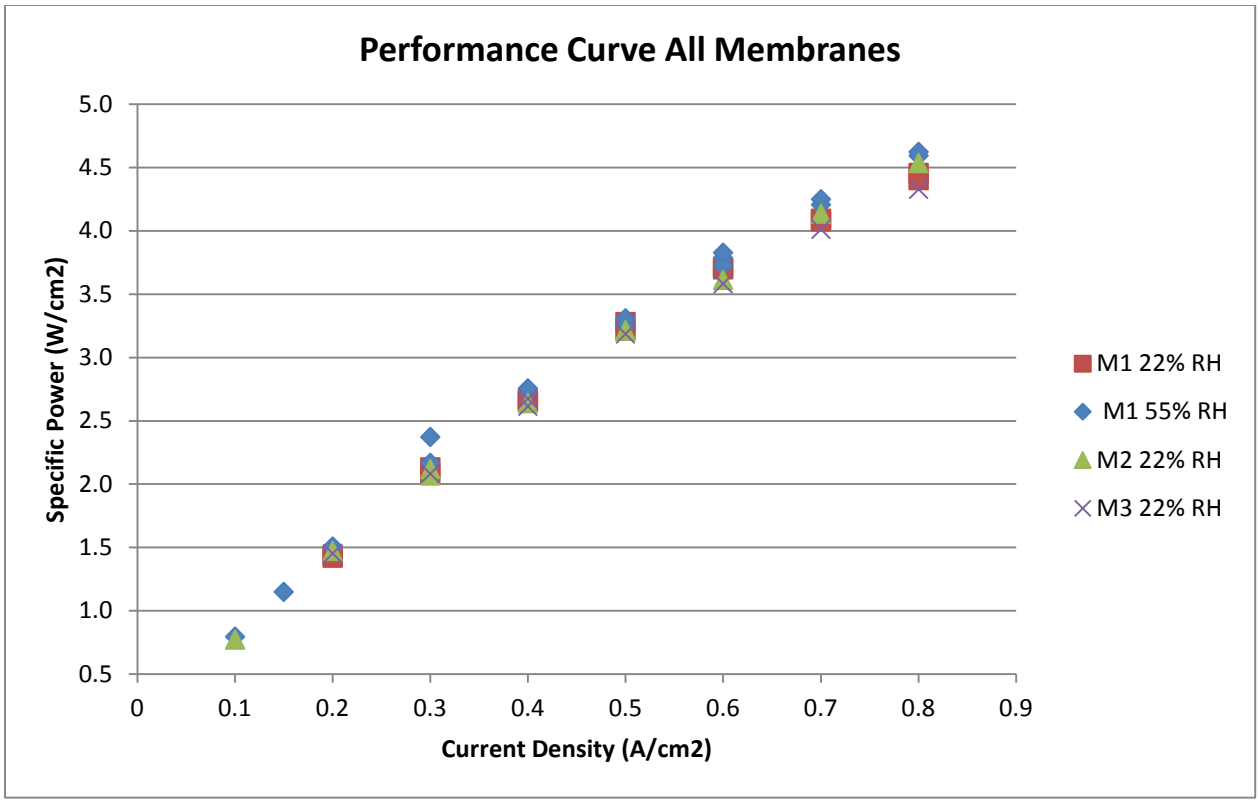

Figure 21 Performance curves for all three membranes, primarily at 22% RH.

4.2 GEIS

Our experimental GEIS data was fit to an impedance model in Excel in order to analyze the different resistance parameters. For each experiment a value for the ohmic resistance parameter of the cell was determined as shown in Figure 22. As the current density increases the resistance decreases because at higher currents more water is produced which increases the conductivity of the membrane. For 22% RH the ohmic resistance was greater than at 55% RH for most of the current densities which can be attributed to less water in the cell and therefore less membrane conductivity.

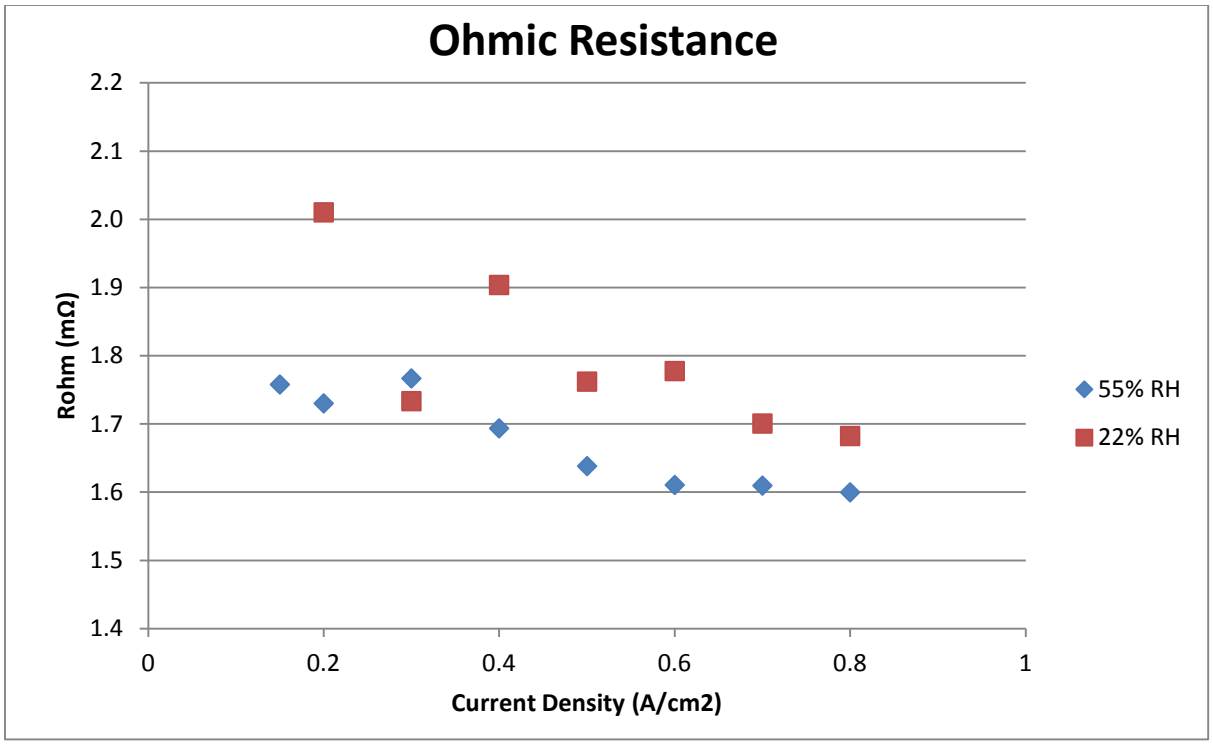

Figure 22 Values of the cell ohmic resistance parameter as determined from fitting data to the GEIS model for both 22% and 55% RH.

Additionally, the impedance spectra were fit to the model in order to analyze the charge transfer resistance and the capacitance resistance in both the anode and cathode and the diffusion resistance in the cathode.

In fitting the data to the model it was established that the anode charge transfer resistance for both RH conditions was about 10% of the charge transfer resistance parameter for the cathode, therefore only the charge transfer resistance parameter values for the cathode are shown in Figure 23. For both humidity conditions the charge transfer resistance parameter decreases significantly as current density increases from 0.10-0.30 A/cm2. At 80 A/cm2 the charge transfer resistance is about half of its original value at low current density. This is as expected because at high current densities the cell voltage is lower and there is less resistance to electron flow.

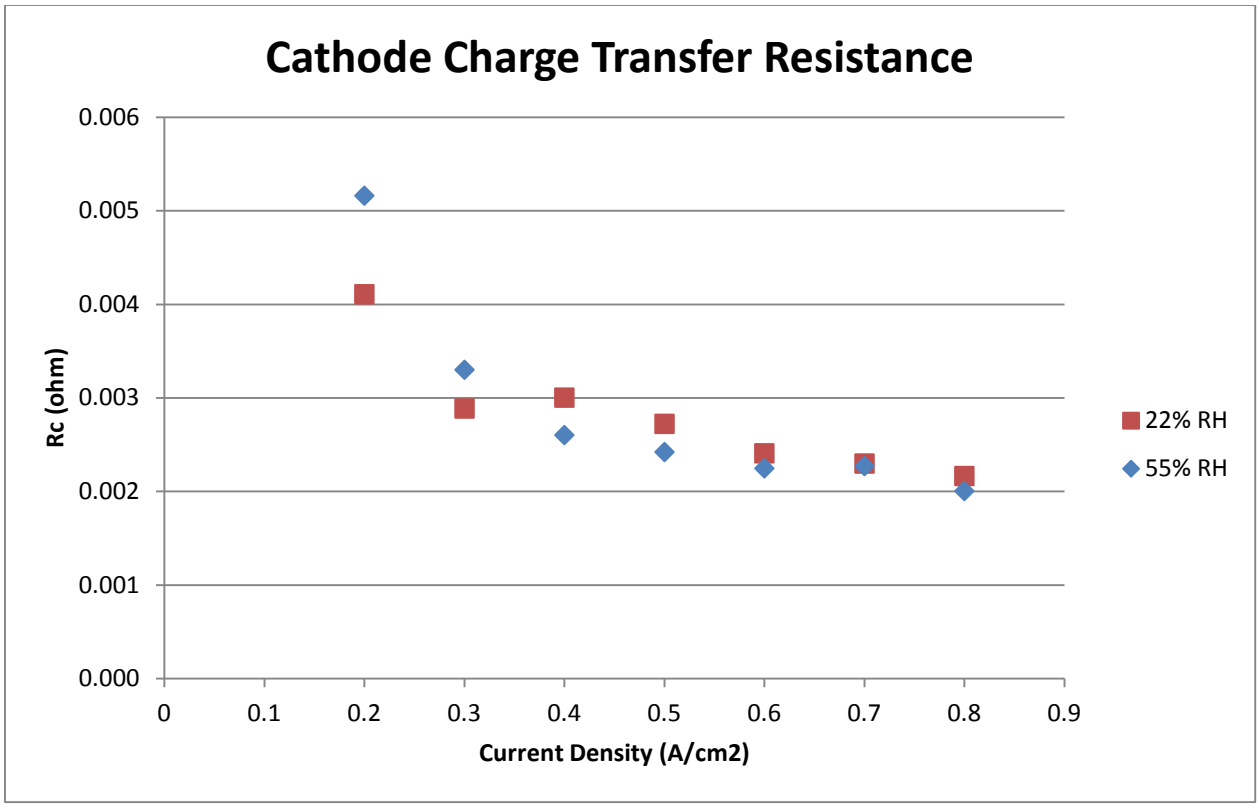

Figure 23 Charge transfer resistance parameter of the cathode at 22% and 55% RH.

A pseudo capacitance parameter was used to model the double layer capacitance at the surface of the anode and cathode electrodes. A pseudo capacitance is necessary because the electrode surfaces are not completely flat but rather three dimensional due to the contours of the catalyst layer. Therefore instead of considering a pure capacitor a constant phase element (CPE) is considered for each electrode and the CPE is dependent on the fractional constant parameter. If this parameter is equal to one then there is pure capacitance. As shown in Figure 24 the pseudo capacitance parameter of the cathode is about 2.5 $F*rad^{(1-n)}*s^{(n-1)}$ for both humidity conditions. This is logical since the electrodes do not change with differences in humidity. It was also found that the anode pseudo capacitance parameter at 22% RH and 55% RH was about 2.4 $F*rad^{(1-n)}*s^{(n-1)}$ for most of the experiments. This is because in order to fit the data to the model the parameter was initially optimized for the anode and then left constant for

additional fittings. The similarity in the anode and cathode pseudo capacitance parameters is as expected since the electrodes have similar carbon and platinum catalyst content and structure.

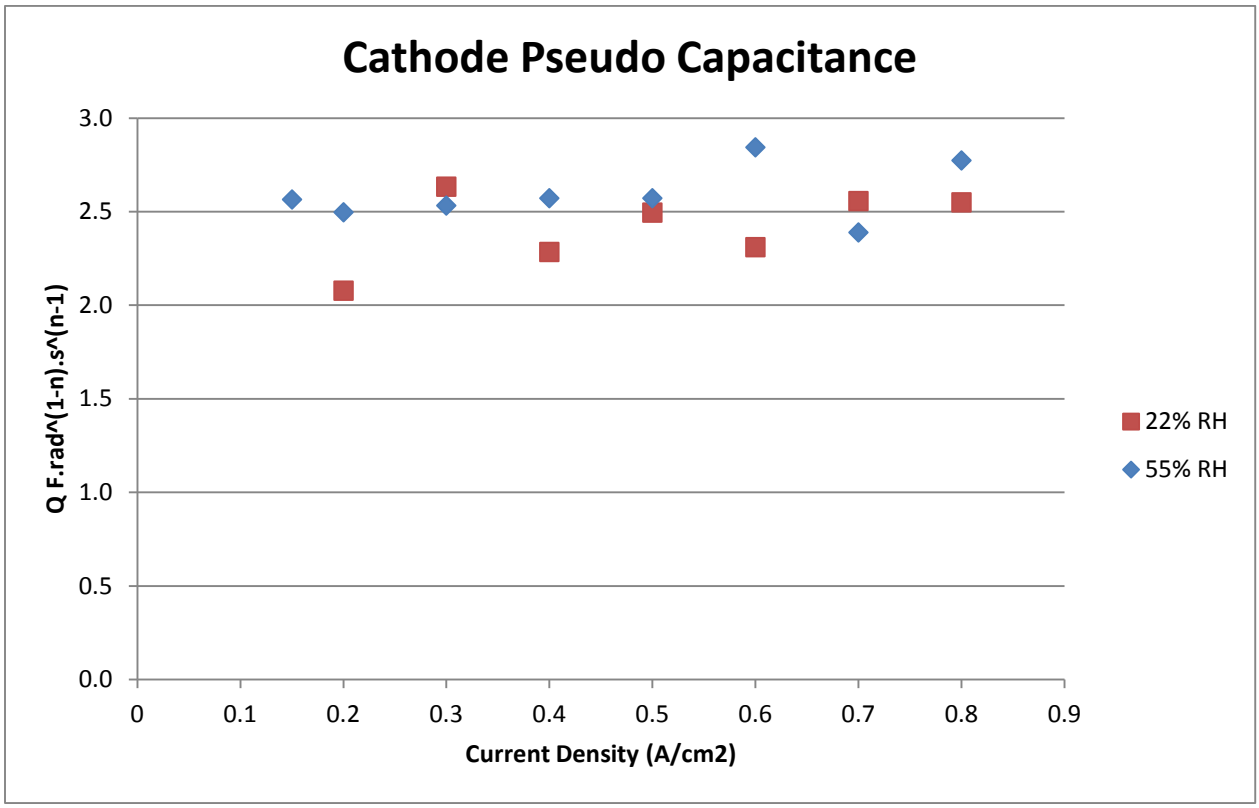

Figure 24 Pseudo capacitance parameter for the cathode at 22% and 55% RH.

Also of importance is the value for the CPE constant used in the model to signify the degree of variation the element has from a pure capacitor. Figure 25 shows the cathode CPE constant values obtained from the fitting for both humidity conditions. It is apparent that for all current densities the CPE has a lower constant at 22% RH and therefore behaves less like a pure capacitor. It is possible that less water in the cathode reduces the polarization and therefore the capacitance of the CPE.

At 55% RH at 0.15 and 0.20 A/cm2 the CPE constant parameter for the anode was included in the modeling and was about 0.986. However, the anode parameter was not varied at 0.30 A/cm2 and

above. At 22% RH the anode parameter similar to the pseudo capacitance was initially optimized to be 0.938 and then left constant for additional fittings.

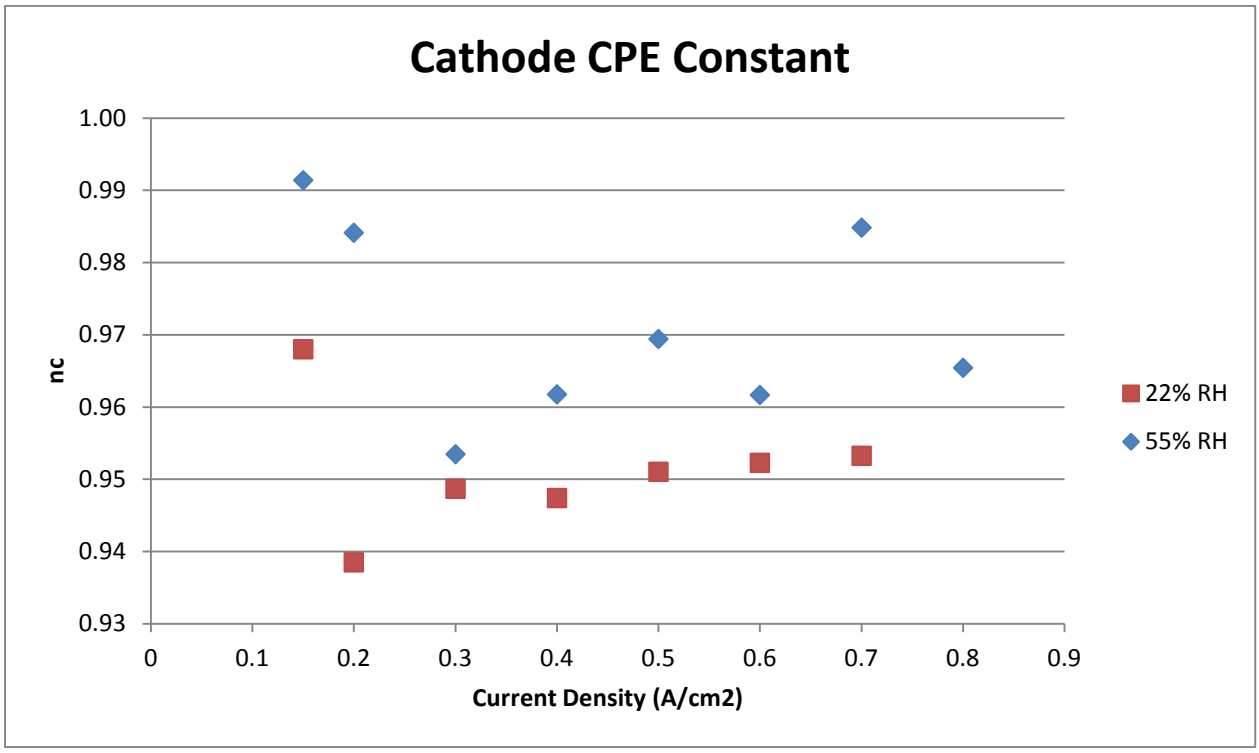

Figure 25 Constant phase element constant for the cathode 22% and 55% RH.

Fitting impedance data to the model also allowed for an estimation of a diffusion resistance parameter for the cathode. The model was developed to assume that the Warburg diffusion resistance on the anode is negligible. This assumption is based on the dominant resistance in the cathode due to the rate of the slow oxygen reduction reaction in comparison to the fast hydrogen oxidation reaction in the anode. The diffusion resistance in the cathode is greater at 22% RH than 55% RH for all experiments, as shown in Figure 26. It is possible that less water limits the medium and mobility of the gases to flow to the electrodes, causing a greater diffusion resistance. Also, the diffusion resistance reaches a minimum value for both humidity conditions at median current densities.

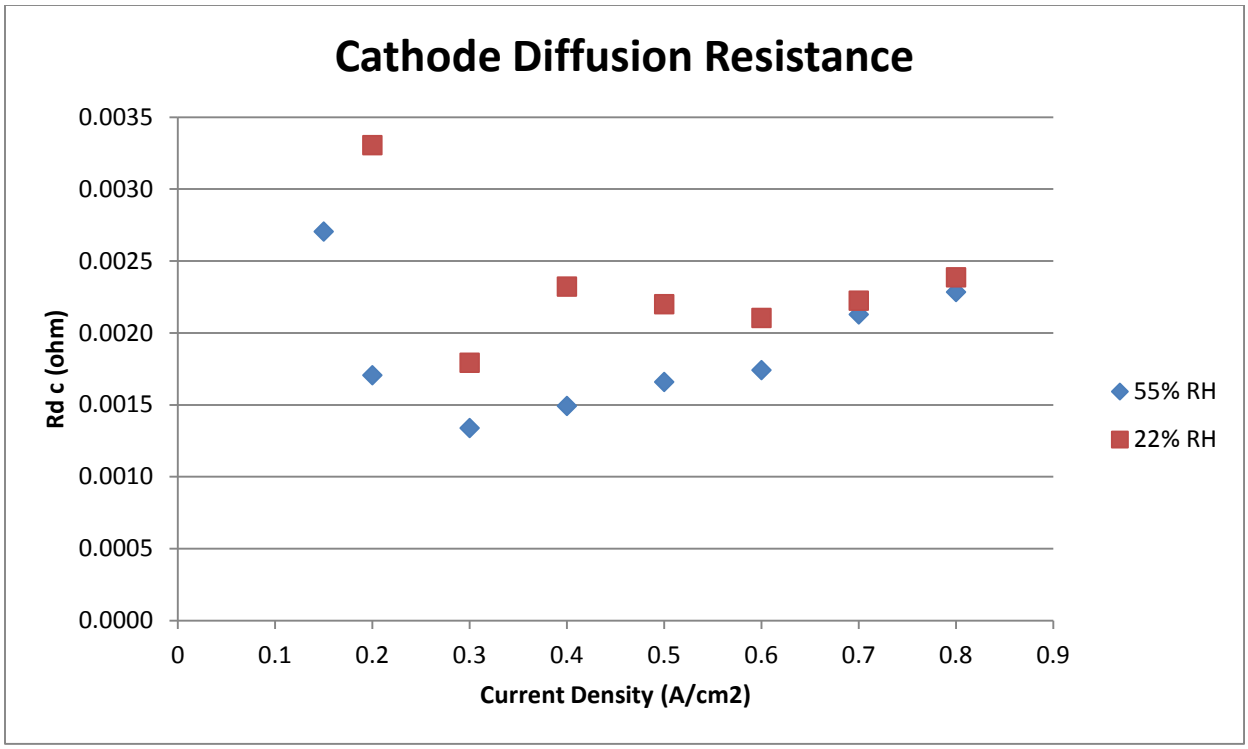

Figure 26 Warburg diffusion resistance parameter for the cathode at 22% and 55% RH.

4.3 Water Management

For experiments operated with humidified conditions it is necessary to analyze the water management of the cell. As explained in Sections 2.4.4 water balance calculations were completed for testing with M1. The water balance was based on, theoretical gas flows calculated from Faraday's law and Antoine's equation together with the collected quantities of water from the cell anode and cathode. Two different methods were used to calculate the water balance.

The first method followed the assumption that all water vapor exiting the anode and cathode of the cell was completely condensed as a part of the collected liquid water quantity. It was assumed that any vapor exiting the cathode outlet was condensed at ambient temperature. The second water balance calculations were based on a measured temperature at the cathode outlet and included any water vapor that may have evaporated into the environment upon exiting. The measured temperature at the

outlet is not completely accurate because it was an independent temperature probe placed within the water collection container and it was not directly at the cathode outlet.

For either method the percent difference shown in Figure 27 and Figure 28, is the difference between the theoretical production of water (based on the humidified air in and the air produced) and the collected water (calculated via either of the two methods) divided by the theoretical water. The figures show that for both humidity conditions the calculations via the total condensation assumption yielded greater percent differences in the water balance overall than calculations including water vapor leaving the cathode. Therefore, it can be determined that the most accurate analysis of the cell water management includes calculations of water vapor entering the environment at the cathode outlet.

It is important to note that the water balance calculations were completed using the actual temperatures of the cell, humidified air and cathode outlet. However, there is a limited amount of data at 55% RH because some temperature values were not recorded.

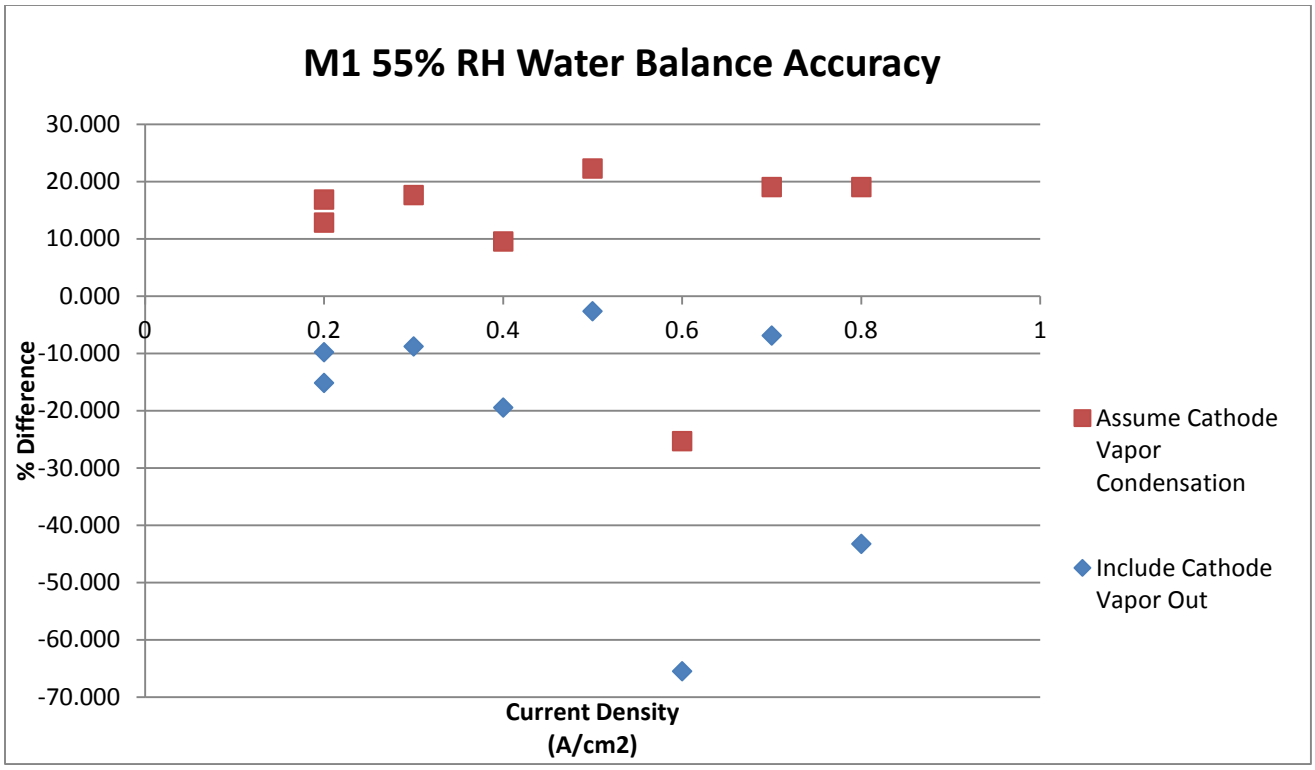

Figure 27 Water balance of the cell shown as the percent difference of the amount of water in and out of the cell. Limited data calculated at actual experimental temperatures. Experimental conditions at 55% RH.

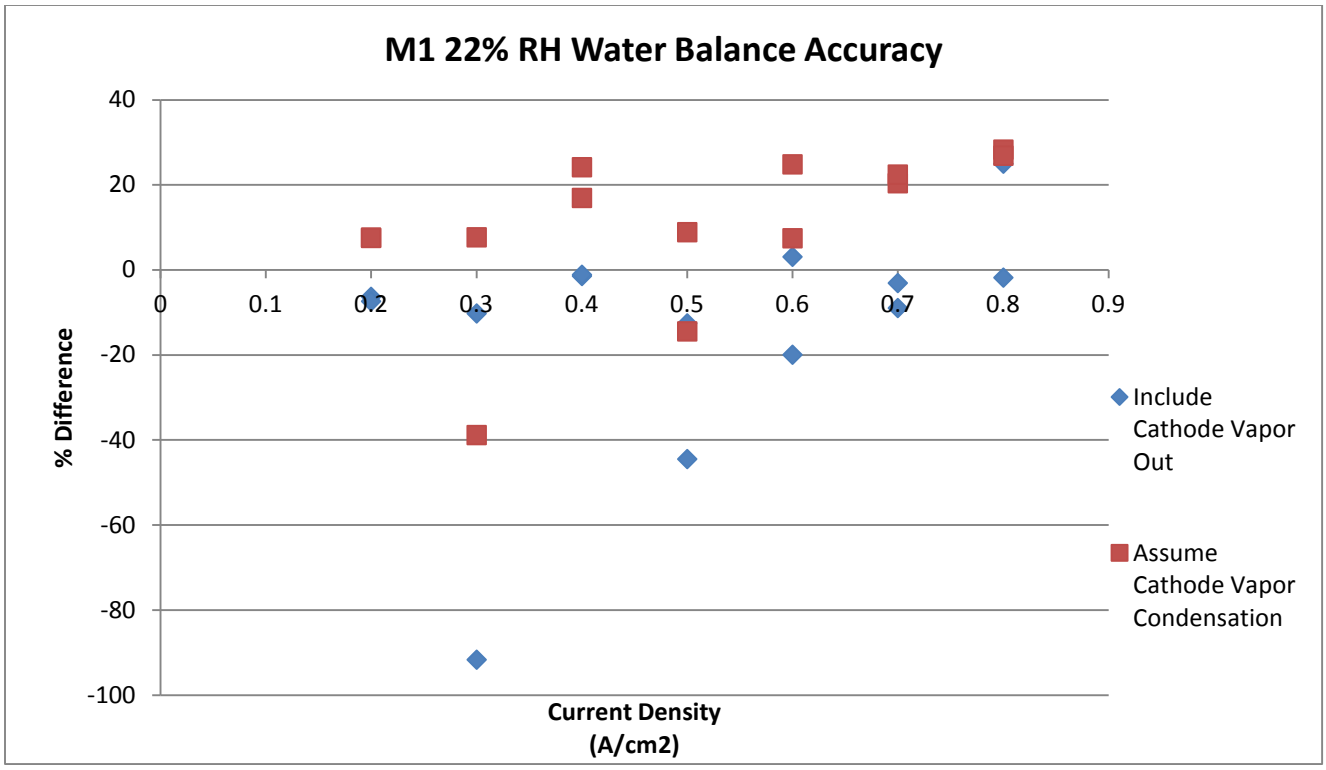

Figure 28 Water balance of the cell shown as the percent difference of the amount of water in and out of the cell. Data calculated at actual experimental temperatures. Experimental conditions at 22% RH.

Positive values of the percent difference signify that the water out of the cell is less than the water predicted or theoretical amount of water in the cell. The inclusion of water vapor exiting the cathode attempts to account for this difference. However, negative values of the percent difference signify that the water out of the cell is greater than the predicted or theoretical amount of water in the cell. Therefore not all water vapor exiting the cathode is lost to the environment but rather some condenses to liquid water in the collection beaker.

Analysis of the cell water management, including water vapor exiting the cathode, was completed for comparison at the different RH conditions as shown in Figure 29. The average percent difference for the experiments at 22% RH was about 17% while the average percent difference at 55% RH was about 23%. Consequently at lower RH a slightly more accurate water management within the cell was found.

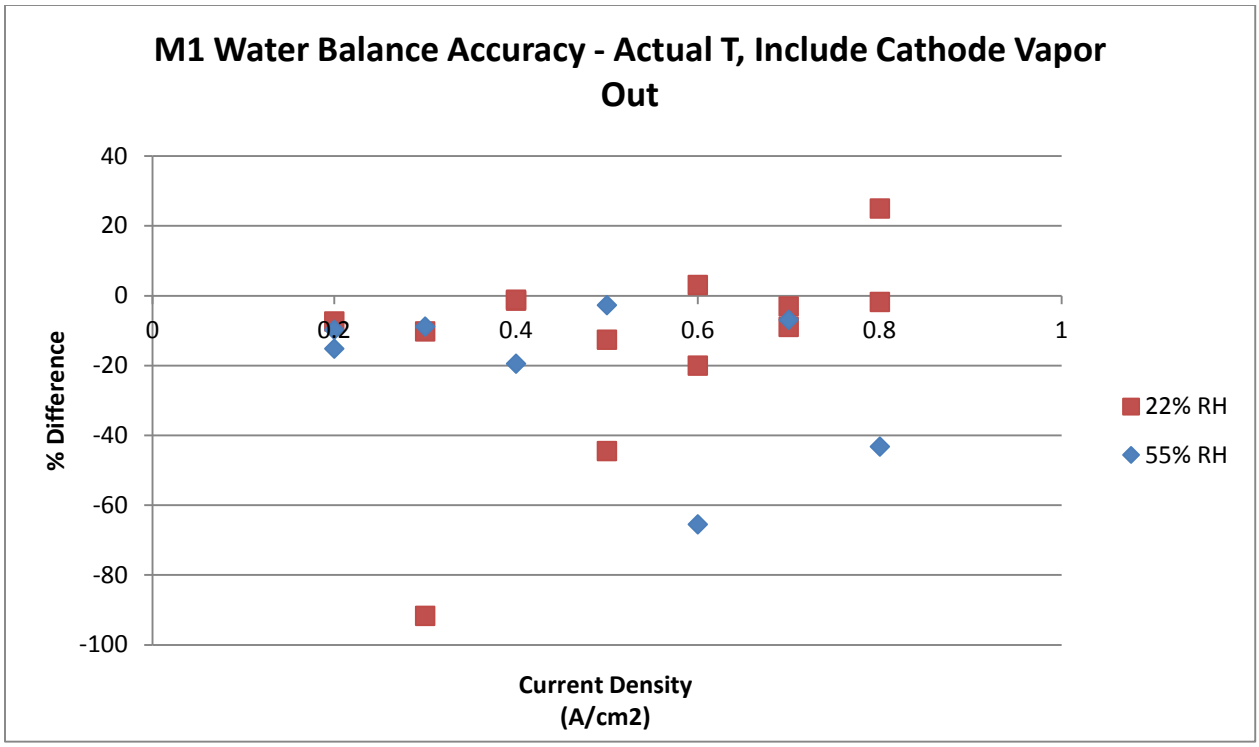

Figure 29 Water balance of the cell indicated by the percent difference of the amount of water in and out of the cell. Data calculated at actual experimental temperatures and including water vapor exiting the cathode.

The water transport coefficient was calculated for each experiment, see Section 2.4.4 and the values are shown in Figure 30. For all experiments at both humidity conditions the coefficient was a positive value indicating that the net flow of water in the cell was from the cathode to the anode. As the current density increases the coefficient increases indicating that more water back diffused to the anode. The back diffusion is contrary to the flow of water in electro-osmotic drag and at higher values of the coefficient less water drags protons across the membrane and the cell voltage declines. Therefore the increase in the coefficient is consistent with the decrease in voltage shown in Figure 20. Also, the coefficient is lower at 22% RH for all experiments. At lower humidity there is less water present on the cathode creating a smaller diffusion gradient from the cathode to the anode. A smaller diffusion gradient results in less back diffusion.

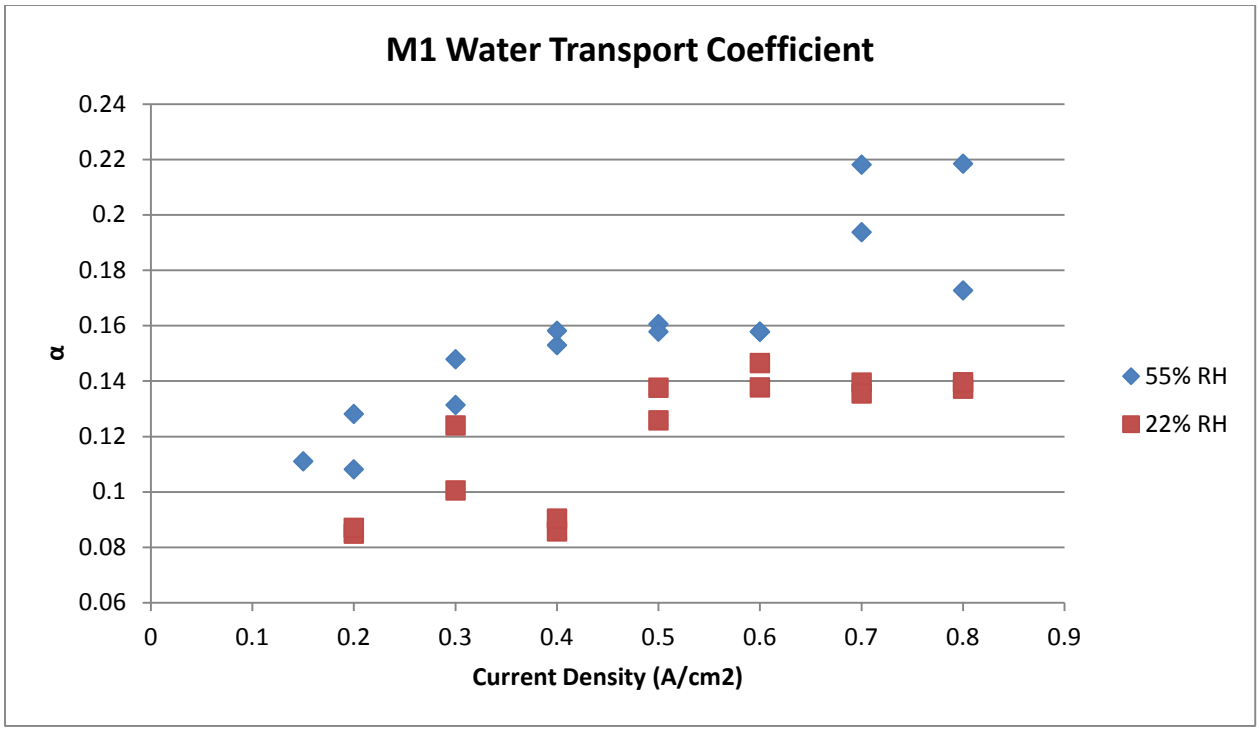

Figure 30 Water transport coefficient for 22% and 55% RH.

To investigate the potential of flooding in the membrane it was determined if liquid water was present in the anode and cathode at both RH conditions following the calculations outlined in Section 2.4.4. The maximum amount of water was calculated for the length of time in which water was collected during the experiment. The difference between the maximum amount of water vapor that could be present at the cell temperature and the amount of water collected indicates whether only vapor or both vapor and liquid water were present in the cell. If the difference divided by the maximum amount of water vapor was a positive percent difference then only water vapor was present. If the percent difference was negative this indicates that both water vapor and liquid were present. For the anode liquid water was not present during any experiments at 22% RH as shown in Figure 30. At 55% RH liquid water was only present for current densities at 0.60 A/cm2 and higher.

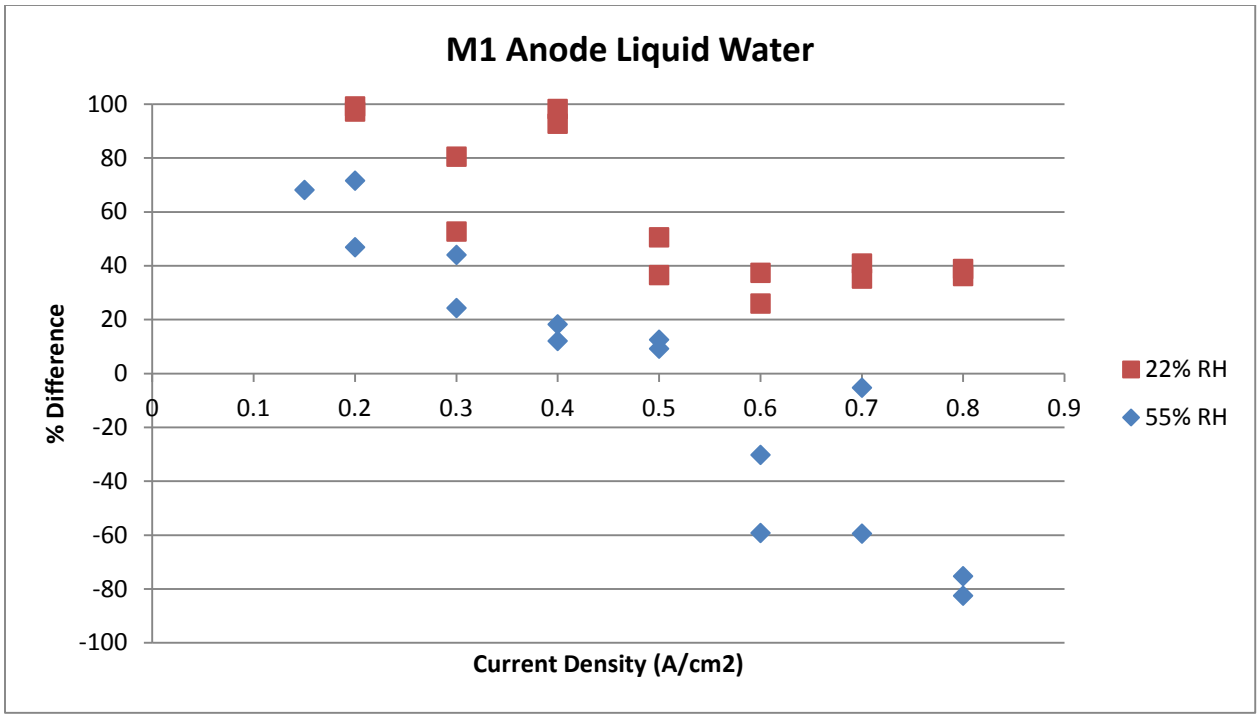

Figure 31 Presence of liquid water in the anode for both RH conditions indicated by the percent difference between the maximum and collected amounts of water.

As shown in Figure 32 liquid water was present in the cathode at 20, 30, 50, and 60 A/cm2 at 22% RH and at 55% RH liquid water was present for all current densities.

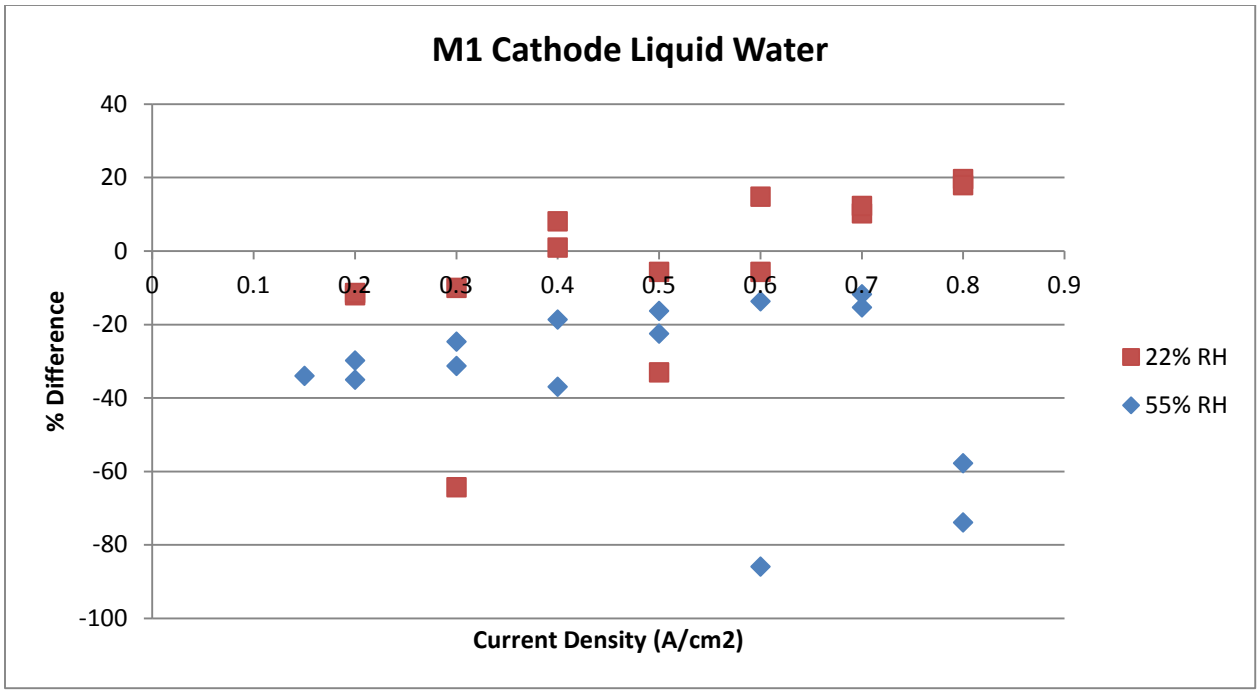

Figure 32 Presence of liquid water in the cathode for both RH conditions indicated by the percent difference between the maximum and collected amounts of water.

At 22% and 55% RH it was found that the cell achieved very similar performance and that the variation in the voltages achieved at both conditions were reliable within about 1.6-2.0mV. The water management at both RH conditions was also comparable and the experiments at 22% RH even had a slightly more accurate water balance when actual temperatures and water vapor exiting the cathode were considered. The main differences between the RH conditions were found in the presence of liquid water in the anode and cathode at varying current densities. At 55% RH liquid water was found more often in both the anode and cathode at 55% RH. However, it can be assumed that flooding did not occur during any experiments due to the cell voltages achieved. Operation of the cell at 22% RH is comparable alternative to operation at 55% RH. Operation at 22% RH would serve as an adequate option for experiments at low voltage in order to minimize the amount of liquid water present in the cell.

4.4 Dry Air Experiments

It was expected that operating the cell at high currents would produce large quantities of water. Therefore in order to avoid flooding it was desired to investigate testing with both dry hydrogen and dry air flows. CP testing at various currents was attempted with λ_A for hydrogen equal to 1.44 and λ_C for air equal to 2.4. It was found that in order to run the fuel cell at the desired current an incremental technique had to be applied. For example gas flows following the stoichiometric coefficients for 40A would be fed to the cell and a series of CP tests would run consecutively in which the current drawn from the cell was increased in steps from 5A, 15A, 25A, 35A and finally 40A. Each current would be tested for about 1-2 minutes in order to produce water and gradually hydrate the membrane.

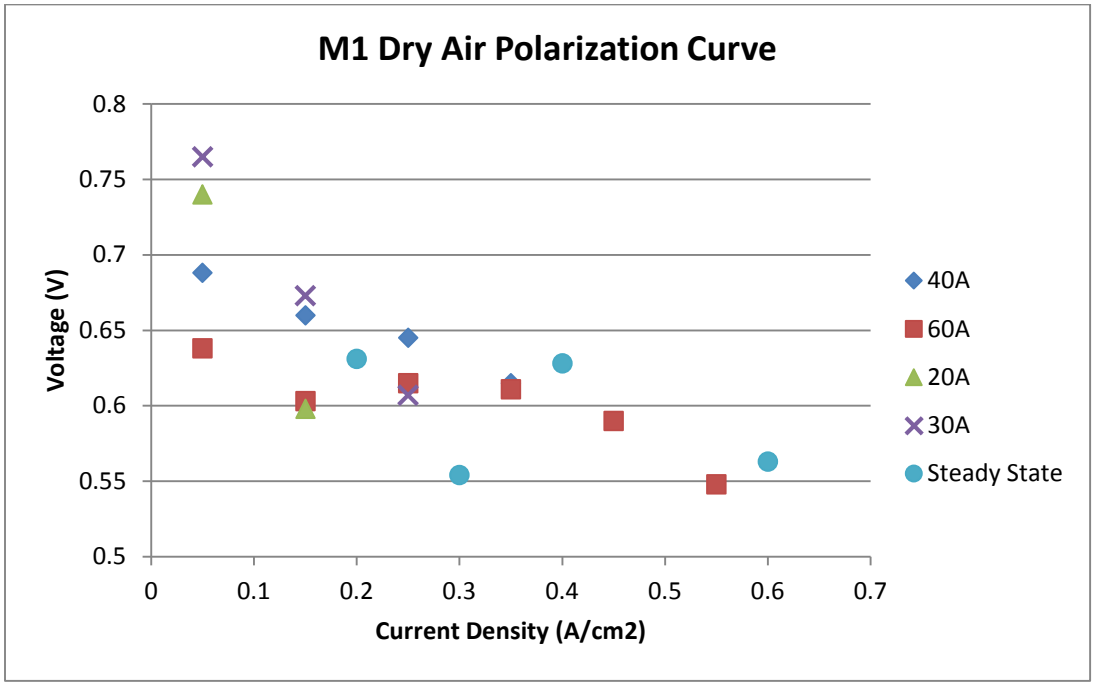

Figure 33 Voltages obtained with M1 operating at dry conditions for both inlet hydrogen and air. Steady state values as a part of a partial polarization curve are designated by the circular data points.

Figure 33 shows the intermediate voltages that were obtained at each current as a part of the applied techniques. The tests were completed in chronological order as listed in the legend beginning with 40A. The data set is very limited because even with the incremental technique it was difficult to reach the desired current densities. The cell voltage would often drop below 0.2 V and the test would

automatically stop. It was not possible to optimize the technique for all current densities in order to obtain a complete set of data.

The series of circular points is the steady voltage obtained at the final current corresponding to the gas flows. These would be the typical points plotted on a polarization curve. It is evident that there was a lot of variation among the voltages reached at each current density. The circular points do not resemble a linear voltage decline due to ohmic losses which is typical for FCs. The tests at 40A and 60A were run on the same day and it is possible they represent a portion of the linear polarization region. In contrast the tests at 20A and 30A were run the following day and it is possible that they represent a portion of the linear polarization region but at a lower performance. The difficulty running experiments with dry air and the inconsistency within the data obtained resulted in further experimental testing at 22% RH.

4.5 Short CA Experiments

Short CA tests were completed at 22% RH with M1 and M2 to investigate if at low voltages the FC operated in accordance with the third region of a typical polarization curve. For testing with M1 the applied potential was incrementally decreased from 0.6V to 0.02 V. Several tests were run targeting a specific current by controlling the hydrogen flow rate following an anode stoichiometric coefficient of 1.0. The cathode stoichiometric coefficient was changed by experimental error to 1.68; however, air was still fed in excess.

The “polarization curves” for each of the tests completed with M1 are shown in Figure 34. The legend designates the targeted currents for each test based on the set hydrogen flow rate. It is shown that regardless of voltage the current obtained is fairly constant around the targeted value.

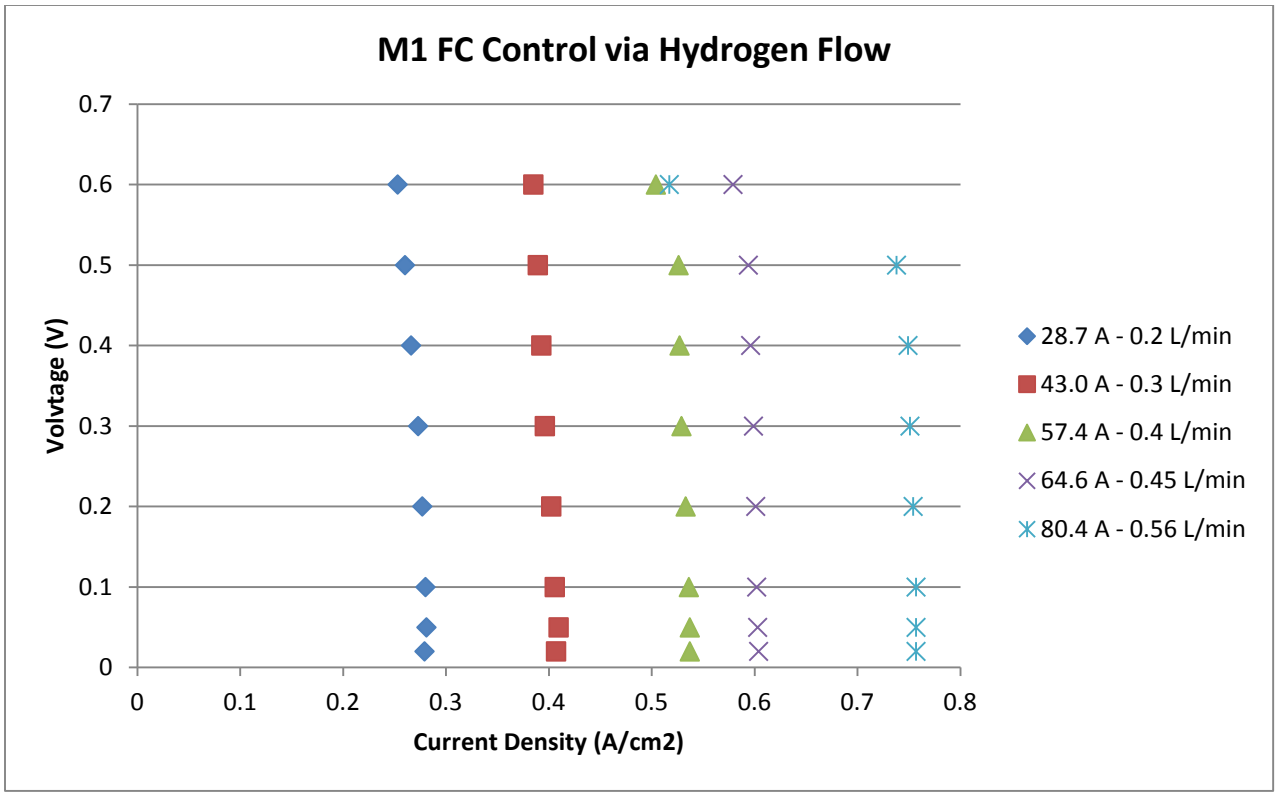

Figure 34 Low voltage CA testing at targeted currents controlled by hydrogen flow rate.

As the voltage decreases the current produced by the FC is closer to the target value. This is most likely due to less resistance present at low voltages and consequently less limitation on the current achievable. The percent difference between the final current obtained at 0.02V and the targeted current for all tests was on average 6%. The actual stoichiometric coefficient at each voltage increment was calculated for all tests of varying hydrogen flows and is shown in Figure 35. One outlier data point for experiments with 0.56 L/min at 0.6 V has been removed from the graph to allow for data analysis on a smaller scale. It was found that the actual stoichiometric coefficient was the closest to 1.0 for all hydrogen flow rates at the lowest voltages. Also, at a hydrogen flow rate of 0.20 L/min and a target current of about 30 A the lowest actual values of the coefficient were found.

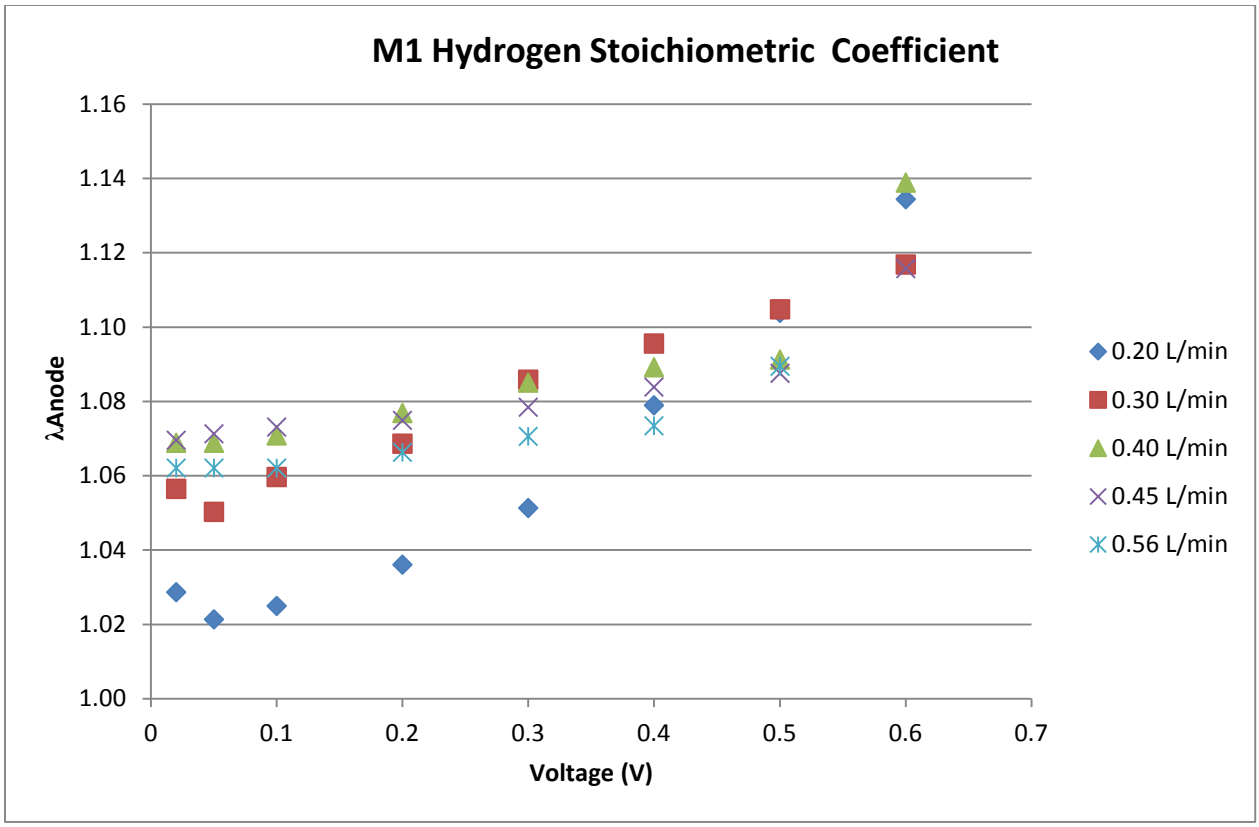

Figure 35 Actual hydrogen stoichiometric coefficient calculated based on performance of M1.

Consequently, short CA tests show that FC operation at low voltages is successful and that it is possible to control the current produced via the hydrogen flow rate. In particular, at only 0.2 V it is estimated that for the majority of hydrogen flows an anode stoichiometric coefficient of about 1.07 is obtained.

During short CA testing with M2 the voltage was maintained at 20 mV and the hydrogen flow rates were changed throughout the test corresponding to a series of target currents. The flow rates were changed once it was observed that the voltage reached a steady state value (about 2 minutes) and the flows tested followed an anode stoichiometric coefficient of 1.0 and a cathode stoichiometric coefficient of 1.68 as well as 2.4.

It was found that for both coefficients the currents obtained were very similar and differed by ± 0.1 A. Table 5 shows the actual currents obtained at the different hydrogen flow rates with a cathode stoichiometric coefficient equal to 2.4. At the lowest hydrogen flow rate the difference between the

target current and the achieved value was smallest and the anode stoichiometric coefficient most closely reached the theoretical value of 1.0. Additionally, for all hydrogen flows at 20 mV the difference between the target and achieved currents was minimal; therefore, indicating that with M2 it was possible to very closely control the current directly through the hydrogen flow rate. However, there is a degree of uncertainty in the values obtained based on the unknown accuracy of the actual gas flows compared to the set flow values.

Table 5 Current controlled by H2 flow rate in short CA testing on M2 with λ Cathode equal to 2.4.

H2 (L/min)	Target I (A)	Actual I (A)	% Difference	Actual λ Anode
0.14	20	19.8	1.2	1.01
0.21	30	29.4	2.2	1.02
0.28	40	39.1	2.5	1.02
0.35	50	48.7	2.6	1.03
0.42	60	58.5	2.6	1.03
0.49	70	68.2	2.6	1.03
0.56	80	78.1	2.5	1.02

4.6 CV and LSV Experiments

The flow rate of hydrogen crossover through M2 and M3 was determined via LSV testing following membrane characterization. The leak currents were observed at 0.4 V as discussed in Section 2.5.4. It was found that the leak currents for M2 and M3 were about 93 mA and 96 mA, respectively. These values correspond to hydrogen crossover rates of approximately 6.5E-4 and 6.7E-4 L/min of hydrogen. Given that a flow of 0.3 L/min of hydrogen is used in LSV testing, less that 0.25% of the inlet hydrogen crossed through the membranes un-oxidized.

4.7 Dead Membrane Analysis

Throughout experimentation M1 and M2 performance declined and via different testing and analysis it was observed that both membranes "died." This means that the membranes were significantly degraded and no longer operated as expected. The performance of the "dead" membranes was not adequate for further testing and subsequently the membranes were replaced. LSV and CV experimental results were the dominant indicators of a "dead" membrane. Figure 36 shows the LSV results for M1 and

M2 after undergoing various testing. Contrary to the expected curve as shown by M2 initial in Figure 36 the data does not plateau and instead continues to increase. Therefore, it was not possible to determine a rate of hydrogen crossover and it is expected that there may have been holes in the membrane allowing un-oxidized hydrogen to cross the membrane.

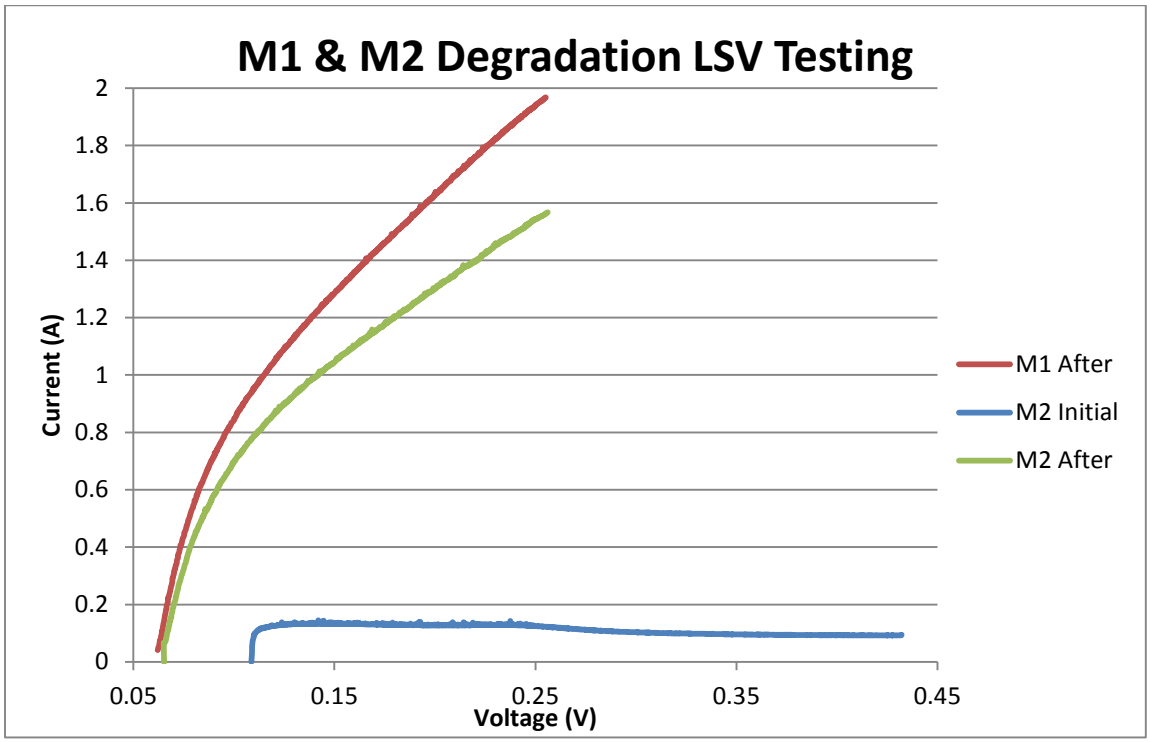

Figure 36 LSV testing of M1 and M2 to determine degradation.

Additionally the data obtained from CV testing on M1 and M2 is shown in Figure 37. It is obvious that after undergoing various tests M1 and M2 were not in the same initial state. Degradation is obvious by the angled curves that were obtained. It was not possible to calculate a value for the ECSA of the membranes, showing the anode electrode experienced serious degradation in both membranes.

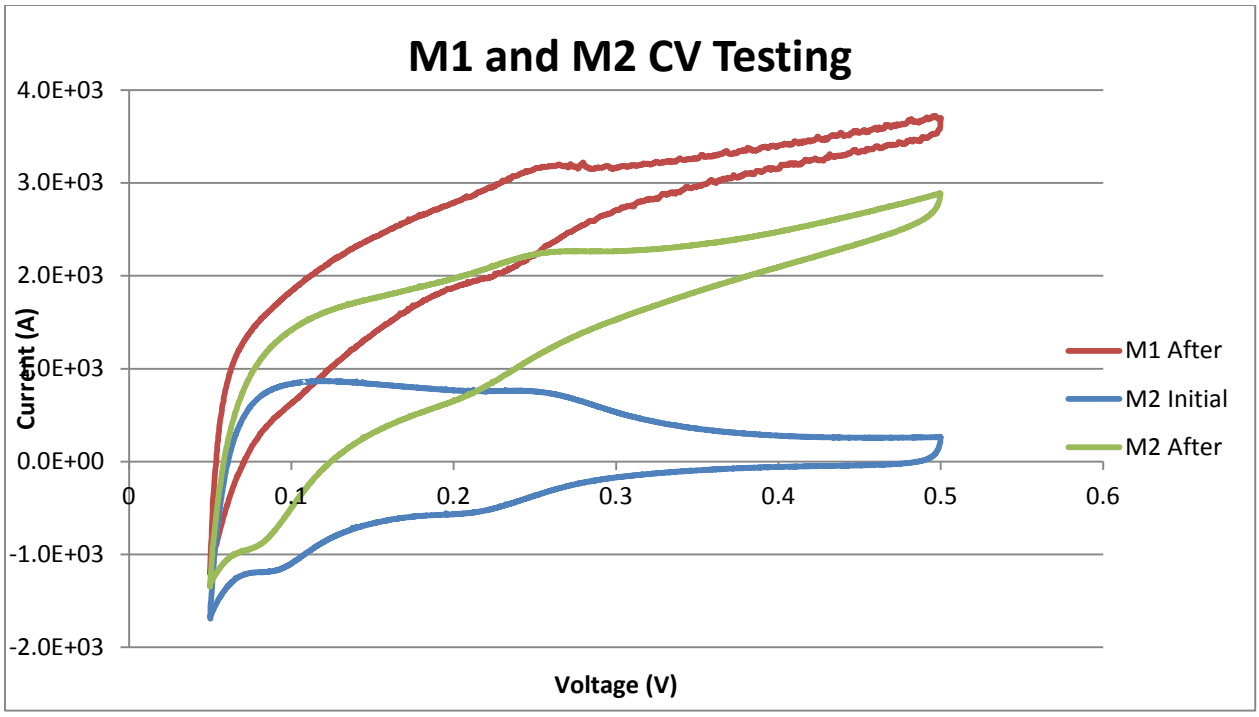

Figure 37 CV test data for M1 after dry air testing, and CV test data for M2 before and after various testing.

Also other observations about the membranes' operation were made that confirmed their failure. For M1 it was observed that following dry air and short CA experiments routine experiments that the FC were expected to be able to run failed. For example, it was not possible to complete a CP experiment at 40 A with stoichiometric coefficients of 2.4 and 1.4 for air and hydrogen respectively. Following the short and long CA testing with M2 it was observed that the FC had a very low OCV.

The membrane "deaths" of M1 and M2 are attributed to different stresses that they underwent during testing, however, these stressors cannot be the definite causes of the membrane degradation and failures without additional testing. For M1 it is theorized that the membrane was severely degraded during the dry air experiments. This was a harsh operating condition in which it is possible the dry air and hydrogen were too abrasive on the fragile membrane. For M2 the membrane failure is attributed to extended operation at OCV of about 1.0 V when a long CA experiment ended prematurely. Running at

OCV is very demanding on a membrane and it is estimated the FC was at OCV for about 14 hours thus leading to significant degradation.

4.8 Long CA Experiments

Following characterization M3 was tested several times with an extended CA test at 22% RH and 0.2 V. The target current for all tests was 60 A and the air stoichiometric coefficient was 2.4 and the hydrogen coefficient was 1.0. Consequently this corresponded to flow rates of 2.4 L/min and 0.42 L/min for air and hydrogen, respectively. Each long CA test ran continuously for about two days. CV and LSV tests were completed initially and following each long CA test. Table 6 shows the results of the long CA tests. It is apparent that initially M3 experienced significant degradation because the rate of hydrogen crossover is about twice as much as the initial leakage. However, in subsequent testing the rate of hydrogen crossover continued to increase but only slightly following each test. Additionally the ECSA of the electrodes decreased throughout testing but in minimal amounts. The results of long CA experiments and the consequent degradation of the MEA indicate that testing under these conditions does exhaust the FC, especially initially. However, the slight degradation during repeated testing shows that it has a minimal long-term impact.

Table 6 Degradation data for M3 after each long CA test. Rate of hydrogen crossover obtained from CV testing and ECSA data obtained from LSV data.

Long CA Test	Approx. Experimental Time (hr)	Leak Current (A)	Rate of H2 Crossover (L/min)	% Difference from Initial	ECSA (cm2 Pt/cm2 electrode)	% Change
Initial		0.096	6.7E-04		201.9	
Test 1	64	0.182	1.3E-03	89.6	192.8	4.5
Test 2	43	0.195	1.4E-03	103.1	194.2	-0.7
Test 3	42	0.211	1.4E-03	119.8	164.2	15.4

5.0 Conclusions and Future Experimentation

Characterization of a FC membrane yielded very comparable performance independent of the RH maintained in the anode. For both 55% and 22% RH the FC obtained similar voltages. This proved the effectiveness of operation at lower humidity levels, presenting the opportunity to minimize flooding. Also, the water balance at both humidity conditions was maintained. The balance was most accurate under the assumption that water vapor exiting the cathode did not completely condense but instead evaporated into the laboratory environment.

Experimentation proved the validity of Faraday's law by controlling the FC current directly through the hydrogen feed. At a given hydrogen flow the current produced was found to be very similar to the expected or target value, differing by only a few percentage. This was demonstrated via short and long duration CA testing. Additionally these experiments were carried out at very low voltage corresponding to an extreme operating condition and region of a FC polarization curve. Through extended duration testing the degradation of the membrane and electrodes was monitored. It was found that the cell experienced an initial degree of degradation during the primary CA testing but after it continued to operate at a constant level. This was supported by the rate of hydrogen crossover, the quantity of electrochemical active surface area, and the impedance parameters which were maintained fairly consistently throughout repeated CA tests.

The impact of these results is very promising for potential applications with supercapacitors. The success of current control via hydrogen allows for a simple and efficient process that can be easily controlled. Also, the opportunity for operation at low voltages is ideal for conjunction with supercapacitors. Low-voltage allows for the loading of supercapacitors at a steady current. Additional experimentation is recommended to further explore this original application. It is necessary to investigate other conditions such as the effect of different humidity levels or the effect of environment temperature on the FC performance. Testing at lower voltages or targeting other current values is recommended to determine

the extents of this process. Finally at the minimum it is necessary to complete preliminary research in which a FC is put in circuit with a supercapacitor to determine if its performance is as efficient and beneficial as theorized.

Other conclusions that can be made from this research are important to the general study of FC technology. It is important to analyze the various ways in which the experimental membranes failed. Of significance is the degradation and ultimate failure of the membrane after being subjected to testing with dry inlet gases. This is an important result that can be validated in repeated experiments. This enables scientists to better understand the limits and extremes at which a FC can successfully run. In the same respect, the membrane failure attributed to OCV shows that a FC membrane can quickly deteriorate when place under high electrical stress. These results provide information to scientists indicating the fragility of a FC MEA.

References

Asghari, Saeed, Ali Mokmeli, and Mahrokh Samavati. "Study of Pem Fuel Cell Performance by Electrochemical Impedance Spectroscopy." *International Journal of Hydrogen Energy* 35.17 (2010). Print.

Boillot, M., et al. "Effect of Gas Dilution on Pem Fuel Cell Performance and Impedance Response." *Fuel cells* 6.1 (2005). Print.

Boillot, Mathieu, et al. "Investigation of the Anode Response of a Polymer Electrolyte Membrane Fuel Cell without Reference Electrode." Print.

Brunetto, Carmelo, Antonino Moschetto, and Giuseppe Tina. "Pem Fuel Cell Testing by Electrochemical Impedance Spectroscopy." *Electric Power Systems Research* 79.1 (2009). Print.

Dandekar, N., and A. Mendonca. "*Electrochemical Characterization and Aging in Pem Fuel Cells*." Worcester Polytechnic Institute, 2012. Print.

Ec-Lab Software: Techniques and Applications: Bio-Logic Science Instruments, 2011. Print.

Fuel Cell Testing. Part Ii: Eis Characterization: Bio-Logic Science Instruments. Print.

Hinaje, M., et al. "Superconducting Coil Fed by Pem Fuel Cell." *International Journal of Hydrogen Energy* 38.16 (2013). Print.

Hinaje, M., et al. "An Innovating Application of Pem Fuel Cell: Current Source Controlled by Hydrogen Supply." *International Journal of Hydrogen Energy* 37.17 (2012). Print.

Lapicque, François, et al. "Analysis and Evaluation of Aging Phenomena in Pemfcs." *Advances in Chemical Engineering*. Vol. 41: Elsevier, 2012. Print.

Larminie, James, and Andrew. Dicks. *Fuel Cell Systems Explained*. 2nd ed. ed. Chichester, West Sussex: J. Wiley, 2003. Print.

Madhusudana Rao, R., and R. Rengaswamy. "A Distributed Dynamic Model for Chronoamperometry, Chronopotentiometry and Gas Starvation Studies in Pem Fuel Cell Cathode." *Chemical Engineering Science* 61.22 (2006). Print.

Montville, Laura, and Andrew Emerson. "*Electrochemcial Characterization and Water Balance of Pem Fuel Cell*." Worcester Polytechnic Institute, 2010. Print.

Qi, Zhigang. "Electrochemical Methods for Catalyst Activity Evaluation." *Pem Fuel Cell Electrocatalysts and Catalyst Layers*. Ed. Zhang, Jiujun: Springer London, 2008. 547-607. Print.

Ramani, Manikandan. "Electro-Analytical Techniques in Fuel Cell Research and Development." *Recent Trends in Fuel Cell Science and Technology*. Ed. Basu, S. New Delhi, India: Anamaya Publishers, 2007. Print.

Thampan, Tony, et al. "Pem Fuel Cell as a Membrane Reactor." *Catalysis Today* 67.1 (2001). Print.

Vilekar, Saurabh. "Catalytic and Electrocatalytic Pathways in Fuel Cells." Worcester Polytechnic Institute, 2010. Print.

Wadsö, Lars, and Patric Jannasch. "Water Vapor Sorption Thermodynamics of the Nafion Ionomer Membrane." *The Journal of Physical Chemistry B* 117.28 (2013). Print.

Wang, Joseph. *Analytical Electrochemistry*. Second Edition ed: Wiley-VCH, 2001. Print.

Wu, Jinfeng, et al. "Diagnostic Tools in Pem Fuel Cell Research: Part I Electrochemical Techniques." *International Journal of Hydrogen Energy* 33.6 (2008). Print.

Yaun, Xiao-Zi, et al. *Electrochemical Impedance Spectroscopy in Pem Fuel Cells*. Springer London, 2010. Print.

Yuan, Xiao-Zi, et al. "Pem Fuel Cells and Their Related Electrochemical Fundamentals." *Electrochemical Impedance Spectroscopy in Pem Fuel Cells*. Springer London, 2010. 1-37. Print.

Yuan, Xiao-Zi, and Haijiang Wang. "Pem Fuel Cell Fundamentals." *Pem Fuel Cell Electrocatalysts and Catalyst Layers*. Ed. Zhang, Jiujun: Springer London, 2008. Print.

Yuan, Xiaozi, et al. "Ac Impedance Technique in Pem Fuel Cell Diagnosis - a Review." *International Journal of Hydrogen Energy* 32.17 (2007). Print.

Zhao, Nana, et al. "The Importance of Water Transport on Short-Side Chain Perfluorosulfonic Acid Membrane Fuel Cells Operating under Low Relative Humidity." *Journal of Power Sources* 242 (2013). Print.

Appendix I: Membrane One Data Sheets

Linear Sweep Voltammetry

Potential (V)	Current (A)	Elapsed Time (s)
0.06210032	0.04158153	5.0072
0.06226959	0.043365	5.0622
0.06242871	0.05019634	5.1523
0.06263934	0.05318283	5.2424
0.06282599	0.05879287	5.3425
0.06296454	0.06644769	5.4426
0.06321322	0.07463921	5.5327
0.06344122	0.0756044	5.6228
0.06364244	0.08324718	5.7229
0.06379762	0.09151728	5.823
0.06407806	0.09770787	5.9231
0.06418298	0.10793545	6.0119
0.06451883	0.11147575	6.1033
0.06454821	0.12056247	6.1934
0.06472873	0.12514486	6.2835
0.06485789	0.13311255	6.3836
0.06523635	0.14042615	6.4837
0.06531083	0.1493086	6.5727
0.06551728	0.15523856	6.6639
0.06574441	0.1633509	6.764
0.06597982	0.17321944	6.8641
0.06614292	0.1819344	6.9542
0.06645159	0.18537292	7.0343
0.06643654	0.1892617	7.1144
0.06658221	0.19476823	7.2045
0.06674676	0.2017384	7.3046
0.06707649	0.20838977	7.4047
0.06721006	0.21627718	7.5048
0.06717215	0.22308523	7.5949
0.06762884	0.22685276	7.685
0.06784256	0.23261682	7.7851
0.06795404	0.23802821	7.8852
0.06821265	0.24501484	7.9853

0.06835943	0.25255638	8.0854
0.06858239	0.25700851	8.1855
0.06875146	0.26367758	8.2856
0.06897315	0.26903863	8.3789
0.06922369	0.27508203	8.4658
0.06932612	0.28204069	8.5659
0.06944339	0.29106935	8.6514
0.06962412	0.29361091	8.7461
0.06978946	0.30130967	8.8462
0.07009736	0.30665365	8.9397
0.07021268	0.3118888	9.0264
0.07043315	0.32095573	9.1064
0.07043988	0.32002259	9.1865
0.07076063	0.32693195	9.2866
0.07097737	0.33431315	9.3768
0.07126135	0.3375357	9.4568
0.07123502	0.34002961	9.5446
0.07155605	0.34627323	9.6298
0.07165088	0.3518934	9.7271
0.07181644	0.35640666	9.8272
0.07217334	0.36320436	9.9273
0.07213274	0.36788614	10.0274
0.07225259	0.3749388	10.1148
0.07263169	0.37848413	10.2076
0.07280054	0.38444667	10.3077
0.07287186	0.38838582	10.403
0.07316656	0.39611037	10.4882
0.07329993	0.39911205	10.588
0.07342112	0.40559479	10.6781
0.07367413	0.40761236	10.7682
0.07399038	0.41290155	10.8683
0.0742221	0.41808659	10.9684
0.0743452	0.4246966	11.0635
0.07442702	0.42784316	11.1586
0.07464976	0.43202779	11.2587
0.07492596	0.43631992	11.3588
0.07526141	0.44224977	11.4451
0.07519861	0.44841682	11.5091
0.07546434	0.44974561	11.5756
0.07539368	0.45140493	11.6591
0.07574122	0.4558719	11.7592
0.0760887	0.4611054	11.8593
0.07626689	0.4672913	11.9594

0.07634678	0.47155485	12.0595
0.07664111	0.47554998	12.1596
0.07673501	0.47902561	12.2597
0.07694404	0.48434138	12.3598
0.07714005	0.4891513	12.46
0.07722965	0.49300902	12.5601
0.07746081	0.49666228	12.6602
0.07764385	0.5000312	12.7603
0.07795086	0.50499644	12.8604
0.07806675	0.50922598	12.9605
0.07832952	0.51375951	13.0606
0.07849366	0.51838615	13.1507
0.07859236	0.52048741	13.2408
0.07883441	0.52551996	13.339
0.07915028	0.53082714	13.4242
0.079326	0.53579192	13.511
0.07948799	0.53678856	13.6011
0.07969271	0.54032574	13.7012
0.07978181	0.5449674	13.8014
0.08000486	0.54850224	13.9015
0.08030533	0.55439879	13.9916

Cyclic Voltammetry

Ewe/V vs. SCE	<I>/mA	Potential (V)	Current (A)	Elapsed Time (s)
0.0572088	84.5808	0.05720883	0.08458082	0
0.0570244	37.2049	0.05702438	0.0372049	0.0036
0.0566502	-21.6173	0.05665017	-0.02161725	0.0104
0.0563468	-73.3926	0.05634679	-0.07339263	0.017
0.0561503	-123.776	0.05615033	-0.12377648	0.0238
0.05599	-170.189	0.05598995	-0.17018935	0.0304
0.0558536	-217.934	0.05585363	-0.21793438	0.037
0.0557227	-263.393	0.05572265	-0.2633927	0.0438
0.0553939	-302.725	0.05539389	-0.30272485	0.0504
0.0550758	-346.787	0.0550758	-0.34678737	0.057
0.0549047	-385.653	0.05490474	-0.38565286	0.0638
0.0549555	-421.642	0.05495553	-0.42164192	0.0704
0.0545706	-457.69	0.05457062	-0.4576904	0.077
0.054469	-491.626	0.05446905	-0.49162608	0.0838
0.0542178	-526.156	0.05421779	-0.52615571	0.0904
0.0539746	-560.363	0.05397455	-0.56036292	0.0972
0.0538021	-590.93	0.05380215	-0.59093011	0.1038

0.0535896	-619.011	0.05358965	-0.61901119	0.1104
0.0533718	-649.697	0.0533718	-0.64969715	0.1172
0.0532074	-674.766	0.05320741	-0.67476605	0.1238
0.0530444	-702.219	0.05304436	-0.70221922	0.1304
0.0529669	-729.384	0.05296686	-0.72938389	0.1372
0.0526087	-755.938	0.05260868	-0.75593762	0.1438
0.0524483	-781.189	0.0524483	-0.78118899	0.1506
0.0522559	-808.044	0.05225585	-0.80804395	0.1572
0.0519632	-832.46	0.05196316	-0.8324595	0.1638
0.0517239	-858.767	0.05172393	-0.85876716	0.1706
0.0515489	-880.964	0.05154886	-0.88096392	0.1772
0.0514125	-904.497	0.05141253	-0.90449707	0.1838
0.051053	-926.482	0.05105303	-0.92648166	0.1906
0.0509902	-950.265	0.05099022	-0.95026506	0.1972
0.0507897	-972.178	0.05078974	-0.97217752	0.2038
0.0507042	-991.723	0.0507042	-0.99172269	0.2106
0.0503982	-1014.41	0.05039815	-1.01440726	0.2172
0.0501242	-1037.49	0.05012418	-1.03748647	0.224
0.0500533	-1056.76	0.05005334	-1.05676014	0.2306
0.0500721	-1068.02	0.05007207	-1.06801953	0.2342
0.0500721	-1077.69	0.05007207	-1.07769244	0.235
0.0495909	-1069.04	0.04959094	-1.06903772	0.2352
0.0502324	-1082.53	0.05023245	-1.08252893	0.236
0.0499411	-1030.08	0.04994108	-1.03007908	0.2396
0.0502418	-942.192	0.05024179	-0.94219156	0.2462
0.050338	-857.108	0.05033801	-0.85710838	0.253
0.0505786	-780.858	0.05057858	-0.78085806	0.2596
0.0506227	-702.987	0.05062268	-0.70298708	0.2664
0.0508258	-632.188	0.05082583	-0.63218835	0.273
0.0510517	-566.778	0.05105168	-0.56677758	0.2796
0.0513497	-496.7	0.05134972	-0.49670009	0.2864
0.051601	-435.888	0.05160098	-0.43588823	0.293
0.051609	-378.827	0.051609	-0.37882669	0.2996
0.0518001	-318.893	0.05180011	-0.31889297	0.3064
0.052058	-268.938	0.05205805	-0.26893763	0.313
0.0523654	-219.555	0.05236544	-0.219555	0.3196
0.0525151	-166.337	0.05251513	-0.16633716	0.3264
0.052725	-120.896	0.05272495	-0.12089583	0.333
0.0529294	-73.7787	0.05292943	-0.0737787	0.3398
0.0529655	-29.3386	0.05296552	-0.02933859	0.3464
0.0533985	11.4827	0.05339853	0.01148267	0.353
0.0535121	51.4766	0.05351213	0.05147665	0.3598
0.0537514	90.5797	0.05375136	0.0905797	0.3664

0.0539305	130.37	0.05393045	0.13037001	0.373
0.0542298	166.771	0.05422982	0.16677061	0.3798
0.0542646	203.863	0.05426457	0.20386273	0.3864
0.0546227	238.265	0.05462274	0.23826508	0.3932
0.054572	272.315	0.05457196	0.27231534	0.3998
0.0549542	299.896	0.05495419	0.29989576	0.4064
0.0552255	327.442	0.05522549	0.32744225	0.4132
0.0552763	353.36	0.05527628	0.35335964	0.4198
0.0555569	382.603	0.05555694	0.38260313	0.4264
0.0557534	412.012	0.0557534	0.41201209	0.4332
0.0560447	441.646	0.05604475	0.44164592	0.4398
0.0560153	468.887	0.05601535	0.46888695	0.4464
0.0562359	496.658	0.05623586	0.49665831	0.4532
0.056701	521.833	0.05670096	0.52183327	0.4598
0.0566863	543.207	0.05668625	0.54320692	0.4666
0.0570805	563.062	0.05708051	0.56306182	0.4732
0.0572168	582.62	0.05721683	0.5826197	0.4798
0.0572756	604.999	0.05727564	0.60499883	0.4866
0.0573932	626.831	0.05739325	0.62683071	0.4932
0.0577594	647.725	0.05775944	0.64772496	0.4998
0.0580414	666.057	0.05804143	0.66605678	0.5066
0.0583061	685.649	0.05830606	0.68564861	0.5132
0.0584414	705.296	0.05844139	0.70529564	0.5199
0.0585279	721.311	0.05852791	0.72131094	0.5266
0.0586161	740.835	0.05861612	0.74083487	0.5332
0.0589195	753.571	0.0589195	0.75357085	0.54
0.059148	770.515	0.05914804	0.77051542	0.5466
0.059271	787.256	0.05927099	0.78725625	0.5532
0.0594528	804.523	0.05945275	0.80452316	0.56
0.0597802	820.441	0.05978019	0.820441	0.5666
0.0600368	836.164	0.06003679	0.8361637	0.5732
0.0601838	851.008	0.0601838	0.85100822	0.58
0.0602814	865.31	0.06028136	0.86530962	0.5866
0.0605968	876.522	0.06059678	0.87652249	0.5934
0.0607104	889.386	0.06071037	0.8893858	0.6
0.0610939	901.354	0.06109393	0.90135384	0.6066
0.0611086	914.344	0.06110865	0.91434433	0.6134

Water Collection

Liquid Water Out/Collected

	Anode				Cathode					
Time	Measured	Actual	nH20 liq out		Measured	Actual	nH20 liq out		Total	
sec	g	g	mole	L	g	g	mole	L	mole	L
70080	36.945	0.0939	0.005211	9.41E-05	409.67	146.34	8.120977	1.47E-01	8.13E+00	1.47E-01
49740	37.0664	0.2153	0.011948	2.16E-04	367.16	103.83	5.761931	1.04E-01	5.77E+00	1.04E-01
14220	38.4355	1.5844	0.087925	1.59E-03	328.65	65.32	3.624861	6.55E-02	3.71E+00	6.70E-02
62940	39.7413	2.8902	0.160388	2.90E-03	456.91	193.58	10.74251	1.94E-01	1.09E+01	1.97E-01
70620	244.13	0.4	0.022198	4.01E-04	505.18	241.85	13.4212	2.42E-01	1.34E+01	2.43E-01
233220	42.1791	5.328	0.295671	5.34E-03	1124.3	860.97	47.77858	8.63E-01	4.81E+01	8.68E-01
12960	40.0811	3.23	0.179245	3.24E-03	343.67	80.34	4.45838	8.05E-02	4.64E+00	8.37E-02
38700	44.3742	7.5231	0.417486	7.54E-03	453.85	190.52	10.5727	1.91E-01	1.10E+01	1.98E-01
9480	39.6693	2.8182	0.156393	2.82E-03	308.75	45.42	2.520533	4.55E-02	2.68E+00	4.83E-02
25860	45.878	9.0269	0.500938	9.05E-03	416.13	152.8	8.479467	1.53E-01	8.98E+00	1.62E-01
26220	46.2474	9.3963	0.521437	9.42E-03	417.68	154.35	8.565483	1.55E-01	9.09E+00	1.64E-01
19440	43.2501	6.399	0.355105	6.41E-03	375.79	112.46	6.240844	1.13E-01	6.60E+00	1.19E-01
53940	57.8636	21.0125	1.166065	2.11E-02	590.1	326.77	18.13374	3.27E-01	1.93E+01	3.49E-01
68520	64.6835	27.8324	1.544528	2.79E-02	687.1	423.77	23.51665	4.25E-01	2.51E+01	4.53E-01

Appendix II: Membrane Two Data Sheets

Linear Sweep Voltammetry – 2/19/2014

Potential (V)	Current (A)	Elapsed Time (s)
0.11938535	0	0
0.10876572	0	4.9998
0.10900629	0.03504548	5.0018
0.10894783	0.05383179	5.0468
0.1091797	0.06330955	5.1369
0.10926019	0.07371531	5.237
0.10957203	0.08113412	5.3371
0.10981259	0.08709802	5.4372
0.10991868	0.09318994	5.5272
0.11023135	0.09406575	5.6174
0.11008488	0.09765142	5.7175
0.11051646	0.09929635	5.8176
0.11063278	0.10180718	5.9177
0.11097531	0.10369559	6.0178
0.11107771	0.10521881	6.1179
0.11130052	0.10637425	6.218
0.11151116	0.10856683	6.3081
0.11165693	0.10810895	6.3982
0.11190211	0.10968993	6.4983
0.11194226	0.1099736	6.5946
0.11218551	0.11286874	6.6798
0.11261918	0.11137449	6.7786
0.11265082	0.11229157	6.8787
0.11290429	0.11343681	6.9788
0.1129624	0.11348184	7.0789
0.11320116	0.11740604	7.1641
0.11323401	0.11483778	7.2591
0.11367498	0.1157148	7.3592
0.11393338	0.11601865	7.4593
0.11393782	0.11666346	7.5594
0.11416435	0.11788196	7.6495
0.11437441	0.11739176	7.7396
0.11449925	0.11794484	7.8397
0.11460681	0.11803369	7.9319
0.1149226	0.11830677	8.0099
0.11513126	0.12023402	8.09

0.11517151	0.11854548	8.1801
0.11541241	0.11912411	8.2802
0.1156489	0.11933464	8.3803
0.11582226	0.11960846	8.4804
0.11595569	0.12005722	8.5805
0.11619648	0.12128189	8.6806
0.11646375	0.12097513	8.7807
0.11664195	0.12107094	8.8808
0.1168958	0.12209069	8.9809
0.1169939	0.12265717	9.081
0.11710039	0.12253595	9.1811
0.11731466	0.12265717	9.2812
0.11755077	0.12283592	9.3814
0.11776535	0.12341248	9.4815
0.11801853	0.12362233	9.5816
0.11836161	0.12350597	9.6817
0.11868796	0.12692565	9.7718
0.11850465	0.12424265	9.8619
0.1189585	0.12442133	9.962
0.11910217	0.12740184	10.052
0.11916789	0.12472411	10.1422
0.11941738	0.12473798	10.2423
0.11953767	0.12559745	10.3424
0.11981852	0.12543391	10.4425
0.11987177	0.12582843	10.5426
0.12017954	0.1257007	10.6427
0.12047319	0.12600167	10.7428
0.12045539	0.12620969	10.8429
0.1208073	0.12652726	10.943
0.12091404	0.12651705	11.0431
0.12115479	0.12644359	11.1432
0.12130146	0.12721012	11.2433
0.12140425	0.12740404	11.3434
0.12169404	0.12729703	11.4435
0.1218681	0.12996426	11.5336
0.12219688	0.12730397	11.6237
0.1222596	0.12785658	11.7238
0.12261594	0.12813443	11.8239
0.122665	0.12862494	11.924
0.12280335	0.12801831	12.0241
0.12306631	0.12799695	12.1243
0.12333865	0.13031162	12.2144
0.1234847	0.12815237	12.3044

0.12371635	0.12873802	12.4046
0.12388483	0.13829873	12.4946
0.12405898	0.12860998	12.5847
0.12422421	0.1293544	12.6848
0.12436231	0.12862262	12.785
0.12443814	0.12957496	12.8851
0.12474709	0.13150837	12.9752
0.12484771	0.12913295	13.0653
0.12491129	0.13077885	13.1474
0.12536997	0.13221104	13.2204
0.12548539	0.12933557	13.3155
0.12560523	0.12945812	13.4156
0.12597468	0.12990808	13.5157
0.12615828	0.13289063	13.6058
0.12617525	0.13002572	13.6959
0.12637591	0.13009094	13.796
0.12656382	0.13264954	13.8861
0.12691051	0.1307721	13.9762

Linear Sweep Voltammetry – 2/12/14

Potential (V)	Current (A)	Elapsed Time (s)
0.06543801	0	0
0.0652288	0	4.9998
0.06506843	0.06648466	5.002
0.06535351	0.06624264	5.057
0.06544884	0.06670903	5.1505
0.06569654	0.06899319	5.2372
0.06602143	0.07245063	5.3373
0.06624006	0.07744988	5.4374
0.06633417	0.08206004	5.5375
0.0665608	0.08780156	5.6376
0.06672116	0.09484566	5.7377
0.06676127	0.10144588	5.8378
0.06713552	0.10812179	5.9379
0.06743841	0.11525638	6.038
0.06752495	0.12076755	6.1294
0.06779481	0.12619996	6.2182
0.06800757	0.13241933	6.3159
0.06798282	0.14073874	6.3855
0.06821356	0.14196875	6.4584
0.0684162	0.14706771	6.5485

0.06844399	0.15339318	6.6286
0.06883691	0.15624964	6.7187
0.06895309	0.16387886	6.8188
0.06924859	0.17183127	6.9089
0.06931394	0.17487636	6.999
0.0693614	0.18152056	7.0979
0.06966732	0.1873253	7.1831
0.06984407	0.1909554	7.2792
0.07000857	0.19845614	7.3694
0.07022096	0.20145436	7.4494
0.07017761	0.20278896	7.5395
0.07053334	0.20967093	7.6296
0.07085557	0.21270079	7.7197
0.07098898	0.21886745	7.8198
0.07089659	0.22601584	7.9058
0.07134983	0.22878899	8
0.07147067	0.2346792	8.1001
0.07162157	0.24009051	8.2002
0.07179569	0.2452309	8.3003
0.07203142	0.25109272	8.4004
0.07218275	0.25743957	8.5005
0.07245444	0.26569252	8.5906
0.07259268	0.26756489	8.6807
0.07277094	0.27239237	8.7808
0.07290629	0.27737831	8.8709
0.07317632	0.28025042	8.961
0.07332952	0.285929	9.0511
0.07358619	0.29026388	9.1412
0.07371978	0.29359545	9.2413
0.07386553	0.29951242	9.3314
0.07400087	0.30224168	9.4215
0.07435688	0.30695688	9.5216
0.07441487	0.31294815	9.6217
0.07472219	0.31762204	9.7218
0.07502397	0.3245015	9.8119
0.07509194	0.32560144	9.902
0.07523973	0.32998932	10.0003
0.07545932	0.33522348	10.0855
0.07557307	0.33887928	10.1822
0.07588466	0.3435564	10.2823
0.07600966	0.34700011	10.3824
0.07623687	0.35220065	10.4826
0.0764956	0.35854082	10.5827

0.07658435	0.36405258	10.6828
0.07678088	0.36835063	10.7829
0.07695855	0.37321285	10.883
0.07722155	0.37735004	10.9831
0.07741121	0.38313184	11.0732
0.07756427	0.38511939	11.1633
0.07776488	0.38912219	11.2634
0.07795672	0.39568426	11.3534
0.0780688	0.39932524	11.4313
0.07829947	0.40068532	11.5236
0.07849976	0.40542485	11.6237
0.07880734	0.40952385	11.7238
0.07901395	0.41414419	11.8037
0.07910699	0.41461941	11.876
0.07919515	0.41931623	11.9541
0.07922611	0.42127437	12.0442
0.07960626	0.42467305	12.1358
0.07972505	0.42698091	12.2244
0.07992106	0.43124541	12.3244
0.08012157	0.43693509	12.4146
0.08028636	0.43715309	12.5046
0.08046855	0.4398124	12.6047
0.08066057	0.44363585	12.7048
0.08069722	0.44607199	12.7857
0.08089668	0.44740872	12.865
0.08105763	0.45458008	12.9551
0.08127981	0.45376363	13.0452
0.0815383	0.45670883	13.1453
0.08182332	0.460026	13.2454
0.08182297	0.46350016	13.3455
0.08215318	0.46757053	13.4436
0.08228656	0.4715338	13.5288
0.08253609	0.47334626	13.6258
0.08263435	0.47629764	13.7259

Cyclic Voltammetry- 2/19/14

		Potential (V)	Current (A)	Elapsed Time (s)
Ewe/V vs. SCE	<I>/mA	0.08671393	0.04028919	0
0.0867139	40.2892	0.08641053	0.02263618	0.0036
0.0864105	22.6362	0.08623546	-0.00723944	0.0102
0.0862355	-7.23944	0.08609111	-0.03566839	0.017

0.0860911	-35.6684	0.08574764	-0.05907846	0.0236
0.0857476	-59.0785	0.08542421	-0.08498736	0.0304
0.0854242	-84.9874	0.08544827	-0.10974231	0.037
0.0854483	-109.742	0.08519033	-0.13244389	0.0436
0.0851903	-132.444	0.08507407	-0.15548487	0.0504
0.0850741	-155.485	0.08486958	-0.17481367	0.057
0.0848696	-174.814	0.08457556	-0.19671766	0.0636
0.0845756	-196.718	0.08440048	-0.21766284	0.0704
0.0844005	-217.663	0.08426816	-0.23728015	0.077
0.0842682	-237.28	0.08400488	-0.25609559	0.0836
0.0840049	-256.096	0.08369616	-0.27475832	0.0904
0.0836962	-274.758	0.08370284	-0.29188103	0.097
0.0837028	-291.881	0.08358923	-0.31117586	0.1038
0.0835892	-311.176	0.0830199	-0.32737372	0.1104
0.0830199	-327.374	0.08306668	-0.34276548	0.117
0.0830667	-342.765	0.08279702	-0.35556966	0.1234
0.082797	-355.57	0.08264034	-0.37280658	0.1298
0.0826403	-372.807	0.08241181	-0.39100688	0.1364
0.0824118	-391.007	0.08215653	-0.40147735	0.143
0.0821565	-401.477	0.08194403	-0.41804429	0.1498
0.081944	-418.044	0.08182508	-0.43045782	0.1564
0.0818251	-430.458	0.08159655	-0.44488651	0.1632
0.0815966	-444.887	0.08143619	-0.45733403	0.1698
0.0814362	-457.334	0.08116087	-0.46945905	0.1764
0.0811609	-469.459	0.08104326	-0.48369261	0.1832
0.0810433	-483.693	0.08079201	-0.49175758	0.1898
0.080792	-491.758	0.08073989	-0.50608027	0.1964
0.0807399	-506.08	0.08043784	-0.51776409	0.2032
0.0804378	-517.764	0.08033893	-0.53027094	0.2098
0.0803389	-530.271	0.07983323	-0.53936536	0.2165
0.0798332	-539.365	0.07993533	-0.55180163	0.2232
0.0799353	-551.802	0.07961992	-0.56142358	0.2298
0.0796199	-561.424	0.07937267	-0.57245826	0.2366
0.0793727	-572.458	0.0792751	-0.58092633	0.2432
0.0792751	-580.926	0.07894366	-0.59124407	0.2498
0.0789437	-591.244	0.07886347	-0.60109935	0.2566
0.0788635	-601.099	0.07873918	-0.60942314	0.2632
0.0787392	-609.423	0.07850397	-0.61841724	0.2698
0.078504	-618.417	0.07824469	-0.62966835	0.2766
0.0782447	-629.668	0.07802685	-0.63769941	0.2832
0.0780268	-637.699	0.07791859	-0.6463753	0.29
0.0779186	-646.375	0.07765664	-0.65625603	0.2966
0.0776566	-656.256	0.07754304	-0.6651865	0.3032

0.077543	-665.187	0.0771675	-0.67131266	0.31
0.0771675	-671.313	0.07711002	-0.68017942	0.3166
0.07711	-680.179	0.07686011	-0.68897836	0.3232
0.0768601	-688.978	0.07659815	-0.69494333	0.33
0.0765982	-694.943	0.07634021	-0.70386957	0.3366
0.0763402	-703.87	0.07622795	-0.71134059	0.3434
0.0762279	-711.341	0.0760943	-0.71790795	0.35
0.0760943	-717.908	0.07586043	-0.72594746	0.3566
0.0758604	-725.947	0.07562789	-0.73071604	0.3634
0.0756279	-730.716	0.07544611	-0.74116105	0.37
0.0754461	-741.161	0.07539266	-0.74607386	0.3766
0.0753927	-746.074	0.07506923	-0.75399455	0.3834
0.0750692	-753.995	0.07478991	-0.76244988	0.39
0.0747899	-762.45	0.07459612	-0.77050212	0.3966
0.0745961	-770.502	0.07446247	-0.77475735	0.4034
0.0744625	-774.757	0.07422859	-0.7825381	0.41
0.0742286	-782.538	0.07401209	-0.78921999	0.4168
0.0740121	-789.22	0.07375146	-0.79237217	0.4234
0.0737515	-792.372	0.0735109	-0.8005602	0.43
0.0735109	-800.56	0.07339863	-0.80648696	0.4368
0.0733986	-806.487	0.07327435	-0.81064456	0.4434
0.0732744	-810.645	0.07318748	-0.81844229	0.45
0.0731875	-818.442	0.07276515	-0.82533637	0.4568
0.0727651	-825.336	0.07257403	-0.8304061	0.4634
0.072574	-830.406	0.0721771	-0.83662138	0.4702
0.0721771	-836.621	0.07217845	-0.84403721	0.4768
0.0721784	-844.037	0.07200737	-0.8478979	0.4834
0.0720074	-847.898	0.07175879	-0.85380348	0.4902
0.0717588	-853.803	0.07153828	-0.86085024	0.4968
0.0715383	-860.85	0.07146877	-0.86581822	0.5034
0.0714688	-865.818	0.07128167	-0.87112559	0.5102
0.0712817	-871.126	0.07104377	-0.87767172	0.5168
0.0710438	-877.672	0.07074708	-0.88489671	0.5234
0.0707471	-884.897	0.0705867	-0.88932589	0.5302
0.0705867	-889.326	0.07043167	-0.89580414	0.5368
0.0704317	-895.804	0.07028199	-0.90057272	0.5436
0.070282	-900.573	0.06999197	-0.90667766	0.5502
0.069992	-906.678	0.06973404	-0.91212075	0.5568
0.069734	-912.121	0.06955227	-0.91669844	0.5636
0.0695523	-916.698	0.06945738	-0.92357554	0.5702
0.0694574	-923.576	0.06935581	-0.92880654	0.5768
0.0693558	-928.807	0.0690257	-0.93346904	0.5836
0.0690257	-933.469	0.0688092	-0.94005335	0.5902

0.0688092	-940.053	0.06857665	-0.94508072	0.597
0.0685766	-945.081	0.0684831	-0.95090992	0.6036
0.0684831	-950.91	0.06830668	-0.95753668	0.6102
0.0683067	-957.537	0.06809151	-0.96188946	0.617
0.0680915	-961.889	0.06762107	-0.96684473	0.6236
0.0676211	-966.845	0.06765849	-0.97441757	0.6302
0.0676585	-974.418	0.06736581	-0.97819762	0.637

Cyclic Voltammetry – 2/21/14

		Potential (V)	Current (A)	Elapsed Time (s)
Ewe/V vs. SCE	<I>/mA	0.06362504	0.06065316	0
0.063625	60.6532	0.06333367	0.03500305	0.0038
0.0633337	35.0031	0.06303162	0.00559409	0.0104
0.0630316	5.59409	0.06294475	-0.02059905	0.017
0.0629448	-20.5991	0.06263469	-0.04745828	0.0238
0.0626347	-47.4583	0.06243289	-0.07469932	0.0304
0.0624329	-74.6993	0.06214154	-0.09907244	0.037
0.0621415	-99.0724	0.06202259	-0.12184614	0.0438
0.0620226	-121.846	0.0617446	-0.14889204	0.0504
0.0617446	-148.892	0.06153237	-0.1720462	0.0571
0.0615324	-172.046	0.06129956	-0.19385822	0.0638
0.0612996	-193.858	0.06123675	-0.22053502	0.0704
0.0612368	-220.535	0.06108306	-0.2437669	0.0772
0.0610831	-243.767	0.06092134	-0.26503452	0.0838
0.0609213	-265.035	0.0608064	-0.28491062	0.0904
0.0608064	-284.911	0.06052709	-0.30690371	0.0972
0.0605271	-306.904	0.06028251	-0.32668218	0.1038
0.0602825	-326.682	0.06018435	-0.34525915	0.1101
0.0601844	-345.259	0.05989093	-0.36605252	0.1164
0.0598909	-366.053	0.0596116	-0.38444799	0.1232
0.0596116	-384.448	0.05945924	-0.40331861	0.1298
0.0594592	-403.319	0.05919729	-0.42353407	0.1366
0.0591973	-423.534	0.05894737	-0.43931614	0.1432
0.0589474	-439.316	0.05884981	-0.45846677	0.1498
0.0588498	-458.467	0.05875626	-0.47658645	0.1566
0.0587563	-476.586	0.05843818	-0.49398915	0.1632
0.0584382	-493.989	0.05825776	-0.51103547	0.1698
0.0582578	-511.035	0.05808535	-0.52856548	0.1766
0.0580853	-528.565	0.05775257	-0.54374933	0.1832
0.0577526	-543.749	0.05766035	-0.56012536	0.19
0.0576604	-560.125	0.05752804	-0.57683227	0.1966

0.057528	-576.832	0.05731554	-0.59146465	0.2032
0.0573155	-591.465	0.05722332	-0.60994068	0.21
0.0572233	-609.941	0.05687183	-0.62465369	0.2166
0.0568718	-624.654	0.05658583	-0.63895516	0.2232
0.0565858	-638.955	0.05640407	-0.65646815	0.23
0.0564041	-656.468	0.05636531	-0.66978536	0.2366
0.0563653	-669.785	0.05609936	-0.68453649	0.2432
0.0560994	-684.536	0.05586547	-0.70160409	0.25
0.0558655	-701.604	0.05565698	-0.71606247	0.2566
0.055657	-716.062	0.05536162	-0.72945177	0.2634
0.0553616	-729.452	0.05522396	-0.74598049	0.27
0.055224	-745.98	0.05508364	-0.75894129	0.2766
0.0550836	-758.941	0.05483371	-0.77246215	0.2834
0.0548337	-772.462	0.05487915	-0.78583875	0.29
0.0548791	-785.839	0.0544889	-0.80064503	0.2966
0.0544889	-800.645	0.05428977	-0.81338949	0.3034
0.0542898	-813.389	0.05418285	-0.82957462	0.31
0.0541829	-829.575	0.05388603	-0.84041129	0.3167
0.053886	-840.411	0.05368434	-0.85466466	0.3234
0.0536843	-854.665	0.05338364	-0.8673201	0.33
0.0533836	-867.32	0.05319921	-0.87970392	0.3368
0.0531992	-879.704	0.05305754	-0.8912053	0.3434
0.0530575	-891.205	0.0528143	-0.90558313	0.35
0.0528143	-905.583	0.05274348	-0.9201603	0.3568
0.0527435	-920.16	0.05238396	-0.93090652	0.3634
0.052384	-930.907	0.05240935	-0.94410073	0.37
0.0524094	-944.101	0.05212736	-0.95913187	0.3768
0.0521274	-959.132	0.05185071	-0.97042113	0.3834
0.0518507	-970.421	0.0516342	-0.98427713	0.3902
0.0516342	-984.277	0.05143506	-0.99530332	0.3968
0.0514351	-995.303	0.05125998	-1.00783991	0.4034
0.05126	-1007.84	0.05104882	-1.02262496	0.4102
0.0510488	-1022.62	0.05082162	-1.03554331	0.4168
0.0508216	-1035.54	0.05067729	-1.04723574	0.4234
0.0506773	-1047.24	0.05056975	-1.05267326	0.4298
0.0505698	-1052.67	0.05023491	-1.07297488	0.4362
0.0502349	-1072.97	0.05000504	-1.08182054	0.4428
0.050005	-1081.82	0.04979756	-1.09357802	0.4482
0.0497976	-1093.58	0.04983265	-1.09652905	0.4504
0.0498326	-1096.53	0.04959209	-1.10874744	0.451
0.0495921	-1108.75	0.04989678	-1.08040772	0.4546
0.0498968	-1080.41	0.05005315	-1.03429606	0.4614
0.0500531	-1034.3	0.05036722	-0.99115417	0.468

0.0503672	-991.154	0.05055581	-0.94755178	0.4743
0.0505558	-947.552	0.05072273	-0.91270629	0.4806
0.0507227	-912.706	0.0508096	-0.87213107	0.4874
0.0508096	-872.131	0.0510956	-0.83403768	0.494
0.0510956	-834.038	0.05121855	-0.79759042	0.5006
0.0512186	-797.59	0.05142704	-0.75933164	0.5074
0.051427	-759.332	0.05167964	-0.72341049	0.514
0.0516796	-723.41	0.05183864	-0.69030506	0.5207
0.0518386	-690.305	0.05202578	-0.6538039	0.5274
0.0520258	-653.804	0.05231045	-0.62103911	0.534
0.0523105	-621.039	0.05243341	-0.58722218	0.5408
0.0524334	-587.222	0.0525577	-0.55566228	0.5474
0.0525577	-555.662	0.05291187	-0.52709331	0.554
0.0529119	-527.093	0.05315644	-0.49401884	0.5608
0.0531564	-494.019	0.05310833	-0.46590808	0.5674
0.0531083	-465.908	0.05336226	-0.43769552	0.574
0.0533623	-437.696	0.05364425	-0.40816777	0.5808
0.0536443	-408.168	0.05387412	-0.38110066	0.5874
0.0538741	-381.101	0.05403049	-0.35423295	0.5942
0.0540305	-354.233	0.05430714	-0.32559612	0.6008
0.0543071	-325.596	0.0543459	-0.30261878	0.6074
0.0543459	-302.619	0.05467734	-0.277622	0.6142
0.0546773	-277.622	0.05499676	-0.25098763	0.6208

Appendix III: Membrane Three Data Sheets

Linear Sweep Voltammetry- 2/28/14

Potential (V)	Current (A)	Elapsed Time (s)
0.27268612	0	0
0.24363819	0	4.9998
0.24363819	0.01127055	5.0058
0.24396777	0.03265153	5.0608
0.24412394	0.04634501	5.1609
0.24421726	0.05572361	5.261
0.24444897	0.06306018	5.3611
0.24460039	0.06836742	5.4612
0.2448259	0.07538369	5.5563
0.24504873	0.07890995	5.6414
0.24514854	0.07812217	5.7243
0.24526498	0.08148459	5.7996
0.24552092	0.08462222	5.8816

0.24558491	0.08429604	5.9718
0.24570991	0.0868791	6.0719
0.24615067	0.08823053	6.172
0.24633287	0.08957103	6.2721
0.24644025	0.09147957	6.3722
0.24663843	0.0932276	6.4595
0.24682686	0.09466854	6.5347
0.2470372	0.09514225	6.6324
0.24726442	0.09569939	6.7326
0.24745709	0.09859702	6.8226
0.24762459	0.10047825	6.9027
0.24771969	0.10027526	6.9828
0.24798633	0.09908082	7.0729
0.2482356	0.09927868	7.173
0.24838273	0.10010767	7.2731
0.24849397	0.10141053	7.3732
0.24873932	0.10087477	7.4733
0.24895893	0.10495456	7.5634
0.24898848	0.10261663	7.6535
0.24919337	0.10330433	7.7536
0.24943396	0.10363061	7.8537
0.24962769	0.10544776	7.9438
0.24970651	0.10750882	8.0239
0.249973	0.1043072	8.114
0.25027177	0.10454385	8.2141
0.25042692	0.10592721	8.2944
0.25057966	0.10640686	8.3596
0.25060111	0.10477614	8.4544
0.25079712	0.10534544	8.5544
0.25102434	0.10579411	8.6546
0.25131837	0.10570463	8.7547
0.25142974	0.10636953	8.8548
0.25162154	0.1058181	8.9549
0.2517772	0.10638957	9.055
0.25214285	0.10648154	9.1551
0.25234744	0.10683385	9.2552
0.25240609	0.10679126	9.3553
0.25266817	0.10725103	9.4554
0.25280195	0.10737325	9.5555
0.25302014	0.10749615	9.6556
0.2532742	0.10791367	9.7557
0.25362155	0.1078709	9.8558
0.25356331	0.10830524	9.9559

0.25386211	0.10813134	10.056
0.25421822	0.10813939	10.1561
0.25429869	0.1081502	10.2562
0.25440058	0.10796813	10.3563
0.25460607	0.10827865	10.4564
0.25493076	0.10870062	10.5565
0.25507826	0.10843539	10.6566
0.25533643	0.10850263	10.7567
0.25543913	0.10881014	10.8568
0.25568864	0.10893336	10.957
0.25592902	0.1087708	11.0571
0.25599155	0.10888792	11.1572
0.25617388	0.10876346	11.2573
0.25632566	0.10968339	11.3574
0.25670442	0.10871836	11.4575
0.2568959	0.10881368	11.5576
0.25717667	0.10929089	11.6577
0.25708747	0.10914954	11.7578
0.25750136	0.10977707	11.8579
0.25764433	0.10958557	11.958
0.25796959	0.1096709	12.0581
0.25791606	0.1092886	12.1582
0.25816104	0.10948072	12.2583
0.25836602	0.10954315	12.3584
0.25861979	0.10958967	12.4585
0.25882933	0.10932042	12.5586
0.25918981	0.10904504	12.6587
0.25919908	0.10933692	12.7588
0.2594125	0.1095996	12.8589
0.25970694	0.10934635	12.959
0.25978267	0.10979388	13.0592
0.26003623	0.10975091	13.1593
0.26034844	0.10942412	13.2594
0.26037076	0.10927083	13.3595
0.26066029	0.10930156	13.4596
0.26078442	0.10960371	13.5597
0.26112804	0.10922732	13.6598
0.26125321	0.1093544	13.7599
0.26157355	0.10926032	13.86

Ewe/V vs. SCE	<I>/mA	Potential (V)	Current (A)	Elapsed Time (s)
0.0873511	35.1982	0.08735114	0.03519822	0
0.0872482	12.2124	0.08724821	0.01221238	0.0036
0.0869475	-16.399	0.08694751	-0.01639899	0.0102
0.0866281	-42.0746	0.08662809	-0.04207455	0.017
0.086584	-66.6259	0.08658398	-0.06662586	0.0236
0.0863929	-91.7329	0.08639288	-0.09173293	0.0304
0.0862859	-111.388	0.08628595	-0.1113884	0.037
0.0858235	-133.118	0.08582353	-0.13311845	0.0436
0.0858615	-155.738	0.08586147	-0.15573843	0.05
0.0855643	-173.329	0.08556426	-0.17332881	0.0564
0.0853384	-194.69	0.0853384	-0.19468975	0.063
0.0852007	-215.495	0.08520073	-0.21549494	0.0696
0.0848452	-233.733	0.08484524	-0.23373342	0.0764
0.0847838	-254.28	0.08478376	-0.25427979	0.083
0.0845124	-271.759	0.08451245	-0.27175888	0.0898
0.0843026	-287.1	0.08430263	-0.28709974	0.0964
0.0841449	-305.092	0.08414493	-0.30509214	0.103
0.0840019	-320.84	0.08400192	-0.32084027	0.1098
0.0836852	-335.727	0.08368517	-0.3357272	0.1164
0.0835435	-353.147	0.08354352	-0.35314686	0.123
0.0833043	-367.766	0.08330428	-0.3677665	0.1298
0.0832441	-383.205	0.08324414	-0.38320494	0.1364
0.0829261	-393.68	0.08292606	-0.39367966	0.143
0.0826908	-410.751	0.08269085	-0.41075146	0.1498
0.0825933	-423.865	0.08259328	-0.42386499	0.1564
0.0822939	-435.383	0.08229391	-0.43538337	0.1632
0.0822819	-450.045	0.08228187	-0.45004541	0.1698
0.0817834	-462.62	0.08178338	-0.46262017	0.1764
0.0818288	-469.264	0.08182881	-0.46926392	0.1832
0.0814533	-484.261	0.08145328	-0.48426111	0.1898
0.0813624	-497.158	0.0813624	-0.4971583	0.1964
0.0810256	-507.446	0.08102559	-0.50744633	0.2032
0.0809855	-519.894	0.0809855	-0.51989382	0.2098
0.0806929	-528.35	0.0806929	-0.52834991	0.2165
0.0805739	-538.298	0.08057387	-0.53829773	0.2232
0.0804068	-551.874	0.08040681	-0.55187372	0.2298
0.080193	-560.316	0.08019298	-0.56031628	0.2366
0.0799431	-567.507	0.07994307	-0.56750732	0.2432
0.0797733	-578.831	0.07977333	-0.57883052	0.2498
0.0796049	-589.662	0.07960494	-0.58966162	0.2566
0.0794967	-594.68	0.07949668	-0.59468048	0.2632

0.0792735	-608.715	0.07927348	-0.6087146	0.2698
0.0790708	-600.18	0.07907079	-0.60017961	0.2759
0.0787402	-623.135	0.07874023	-0.62313488	0.282
0.0785571	-633.355	0.07855713	-0.63335504	0.2886
0.0783968	-640.096	0.07839676	-0.64009636	0.2952
0.0782431	-649.018	0.07824307	-0.64901832	0.302
0.0778394	-660.957	0.07783945	-0.66095671	0.3086
0.0777459	-666.052	0.07774591	-0.66605196	0.3152
0.0776537	-671.796	0.07765368	-0.67179627	0.322
0.0773503	-682.322	0.0773503	-0.68232189	0.3286
0.0771231	-689.763	0.07712311	-0.68976327	0.3352
0.0770429	-693.433	0.07704291	-0.69343304	0.342
0.0767315	-703.581	0.07673151	-0.70358105	0.3486
0.0766179	-710.322	0.07661791	-0.71032236	0.3554
0.0763159	-719.567	0.07631587	-0.71956675	0.362
0.0762624	-726.911	0.07626241	-0.72691055	0.3686
0.0761034	-732.506	0.07610337	-0.73250638	0.3754
0.0758895	-740.274	0.07588954	-0.74027439	0.382
0.0757211	-748.051	0.07572114	-0.74805088	0.3886
0.0752266	-751.848	0.07522665	-0.7518479	0.3954
0.0752387	-758.627	0.07523867	-0.75862738	0.402
0.0749804	-754.749	0.07498041	-0.75474872	0.408
0.074823	-774.851	0.07482303	-0.77485067	0.414
0.0746233	-778.241	0.0746233	-0.77824129	0.4207
0.0744395	-785.762	0.07443947	-0.78576239	0.4268
0.074223	-792.3	0.07422296	-0.79230008	0.4334
0.0741067	-785.698	0.07410669	-0.78569771	0.4394
0.0737258	-803.793	0.07372579	-0.80379293	0.4454
0.0738006	-809.686	0.07380063	-0.8096858	0.452
0.0733422	-814.23	0.07334223	-0.81422953	0.4588
0.0732714	-821.73	0.07327139	-0.82173018	0.4654
0.0730737	-827.479	0.07307371	-0.82747855	0.4721
0.0729987	-832.846	0.07299875	-0.83284557	0.4788
0.0728156	-839.231	0.07281565	-0.83923054	0.4854
0.0725564	-844.937	0.07255638	-0.84493665	0.4922
0.0723559	-849.459	0.0723559	-0.84945916	0.4988
0.0720859	-856.302	0.07208594	-0.85630231	0.5054
0.0719977	-862.03	0.07199774	-0.86202966	0.5122
0.0716957	-866.807	0.07169569	-0.8668067	0.5188
0.0713736	-874.872	0.0713736	-0.87487168	0.5254
0.0712226	-878.817	0.07122257	-0.87881722	0.5322
0.0711103	-885.317	0.07111032	-0.88531674	0.5388
0.0709366	-890.84	0.07093657	-0.89084048	0.5456

0.0707415	-896.033	0.07074145	-0.89603328	0.5522
0.0705036	-901.175	0.07050356	-0.90117515	0.5588
0.0703018	-907.904	0.07030176	-0.90790376	0.5656
0.070128	-914.234	0.07012801	-0.91423355	0.5722
0.06985	-916.944	0.06985002	-0.9169445	0.5788
0.0696415	-921.879	0.06964152	-0.92187855	0.5856
0.0694117	-929.464	0.06941166	-0.92946414	0.5922
0.0693501	-934.615	0.06935014	-0.93461515	0.5989
0.0690962	-941.352	0.06909624	-0.94135157	0.6056
0.0689626	-946.443	0.0689626	-0.94644254	0.6122
0.0687234	-951.334	0.06872338	-0.95133418	0.619

Linear Sweep Voltammetry – 3/3/2014

Potential (V)	Current (A)	Elapsed Time (s)
0.11776966	0.20971149	23.8937
0.11787584	0.2092641	23.9938
0.11819692	0.20967806	24.0939
0.11830799	0.21022219	24.194
0.11874864	0.21022738	24.2941
0.11872172	0.21062798	24.3903
0.11896667	0.21267429	24.4679
0.11913212	0.21054157	24.5544
0.11921209	0.21210056	24.6445
0.11940832	0.21111194	24.7346
0.11961007	0.21137853	24.8347
0.11992063	0.21124393	24.9348
0.12003944	0.2156677	25.0148
0.12025006	0.21146458	25.0949
0.1202503	0.21112726	25.195
0.12058282	0.2138172	25.2851
0.120825	0.21159275	25.3752
0.12090941	0.21564784	25.4653
0.12118585	0.21191919	25.5554
0.12127911	0.21212777	25.6555
0.12153333	0.21227745	25.7556
0.12164947	0.21279623	25.8557
0.12190308	0.21293622	25.9558
0.12207505	0.21258236	26.0466
0.1222951	0.213122	26.136
0.12218545	0.21373398	26.2273
0.1225713	0.21255793	26.3162

0.12274273	0.21317497	26.4141
0.12300083	0.21514648	26.4993
0.12311516	0.21360081	26.5965
0.12325738	0.21365981	26.6966
0.1234092	0.21684283	26.7867
0.12366456	0.2170572	26.8668
0.12399267	0.21594225	26.9469
0.12386324	0.21423371	27.037
0.12411761	0.21454069	27.1371
0.12432209	0.21425139	27.2372
0.12451801	0.2147191	27.3373
0.12474531	0.21477345	27.4374
0.12502597	0.21445669	27.5375
0.12526934	0.2178057	27.6276
0.12526192	0.21503462	27.7177
0.12557429	0.22614444	27.8078
0.12571637	0.21488952	27.8979
0.12588575	0.21538271	27.998
0.12607598	0.21632823	28.0786
0.1261792	0.21493488	28.1581
0.1264476	0.21571467	28.2583
0.12662531	0.21577268	28.3583
0.12680267	0.21877756	28.4436
0.12695363	0.21550544	28.537
0.12722357	0.21680067	28.6222
0.12751643	0.21570905	28.7187
0.12762763	0.21560428	28.8188
0.1278019	0.21562836	28.9189
0.12800182	0.21571976	29.019
0.12804422	0.21783553	29.1091
0.12830032	0.21542396	29.1992
0.12859899	0.21605332	29.2993
0.12884827	0.21573745	29.3994
0.12891065	0.21665575	29.4996
0.12918998	0.21868369	29.5896
0.12919508	0.21656156	29.6797
0.12938732	0.21678981	29.7798
0.12957887	0.21669822	29.88
0.12990859	0.2188314	29.968
0.13020203	0.21727579	30.0601
0.13019809	0.21669083	30.1602
0.13025591	0.21692043	30.2603
0.13065249	0.2164457	30.3604

0.13075517	0.21666431	30.4605
0.13112819	0.22005744	30.5556
0.1312851	0.21677279	30.6508
0.13141038	0.21732701	30.7509
0.13173062	0.21752872	30.851
0.13192199	0.2169334	30.9511
0.13209541	0.22492136	31.0312
0.13213153	0.21696776	31.1112
0.1323321	0.21734977	31.2113
0.13258046	0.2195385	31.3014
0.13279143	0.21726324	31.3915
0.13287105	0.21765246	31.4916
0.13319656	0.21753358	31.5917
0.13343681	0.21757822	31.6918
0.13356629	0.21718773	31.7919
0.13375758	0.21760059	31.892
0.1339654	0.22054841	31.9822
0.13414517	0.21779505	32.0722
0.13433263	0.21810752	32.1723
0.134555	0.21775616	32.2724
0.13471985	0.21752036	32.3726
0.13497886	0.21837093	32.4727
0.13494256	0.21782923	32.5728
0.13520944	0.21829876	32.6729
0.13559744	0.21797064	32.773

Cyclic Voltammetry – 3/3/2014

Ewe/V vs. SCE	<I>/mA	Potential (V)	Current (A)	Elapsed Time (s)
0.0777283	72.3624	0.07772826	0.07236244	0
0.0778605	40.0983	0.07786054	0.04009828	0.0036
0.0776948	5.86561	0.07769483	0.00586561	0.0102
0.077477	-27.6798	0.07747698	-0.02767977	0.017
0.0773367	-57.8227	0.07733665	-0.05782268	0.0236
0.0770653	-86.4425	0.07706534	-0.08644254	0.0302
0.0769183	-118.482	0.07691834	-0.11848185	0.037
0.0766096	-144.28	0.07660961	-0.14428044	0.0436
0.0765455	-170.206	0.07654546	-0.17020632	0.0502
0.0761793	-196.773	0.07617927	-0.19677282	0.057
0.0761084	-218.762	0.07610843	-0.21876166	0.0636
0.0757997	-244.03	0.07579971	-0.24402995	0.0704
0.0757008	-266.354	0.0757008	-0.26635394	0.077

0.0756179	-287.562	0.07561795	-0.28756217	0.0836
0.0752143	-309.661	0.07521433	-0.30966129	0.0904
0.074919	-330.814	0.07491898	-0.33081439	0.097
0.0747933	-349.337	0.07479334	-0.34933711	0.1036
0.0746717	-368.73	0.07467172	-0.36872956	0.1104
0.0743323	-387.587	0.07433226	-0.38758742	0.117
0.0743267	-404.142	0.0743267	-0.40414205	0.1237
0.0739794	-423.394	0.07397943	-0.42339408	0.1304
0.0738003	-439.189	0.07380035	-0.43918888	0.137
0.0737402	-454.127	0.0737402	-0.45412669	0.1438
0.073362	-471.368	0.07336199	-0.4713682	0.1504
0.0732136	-484.528	0.07321364	-0.48452839	0.157
0.0730345	-497.79	0.07303455	-0.49779042	0.1638
0.0729624	-514.51	0.07296238	-0.51451008	0.1704
0.072536	-527.895	0.07253604	-0.52789515	0.177
0.0724826	-541.106	0.07248259	-0.54110626	0.1838
0.0723276	-557.635	0.07232755	-0.55763501	0.1904
0.0720362	-567.677	0.07203621	-0.567677	0.1972
0.0716633	-579.501	0.07166333	-0.57950085	0.2038
0.0715724	-592.135	0.07157245	-0.59213499	0.2104
0.0715885	-604.417	0.07158849	-0.604417	0.2172
0.0711461	-614.709	0.07114611	-0.61470931	0.2238
0.0709403	-627.64	0.07094029	-0.62764046	0.2304
0.0706489	-639.418	0.07064894	-0.63941761	0.2372
0.0705367	-649.964	0.07053668	-0.6499644	0.2438
0.07036	-661.159	0.07035997	-0.66115917	0.2505
0.0702066	-670.922	0.07020658	-0.67092233	0.2572
0.0700061	-679.276	0.0700061	-0.67927582	0.2638
0.0697869	-691.719	0.06978692	-0.69171907	0.2706
0.0697041	-701.154	0.06970406	-0.70115433	0.2772
0.0694408	-709.521	0.06944077	-0.70952057	0.2838
0.0692924	-718.689	0.06929243	-0.71868856	0.2906
0.0690545	-728.866	0.06905454	-0.72886634	0.2972
0.0688033	-740.181	0.06880328	-0.74018103	0.3038
0.068675	-749.273	0.06867497	-0.7492727	0.3106
0.0684732	-755.87	0.06847317	-0.75586976	0.3172
0.0682099	-765.657	0.06820989	-0.76565721	0.324
0.067956	-776.255	0.06795596	-0.77625496	0.3306
0.0677354	-783.272	0.06773543	-0.783272	0.3372
0.0677635	-791.235	0.06776351	-0.79123517	0.344
0.0676192	-800.013	0.06761917	-0.80001289	0.3506
0.0672102	-809.075	0.0672102	-0.80907485	0.3572
0.0671661	-817.305	0.0671661	-0.81730528	0.364

0.0667023	-825.459	0.06670234	-0.82545937	0.3706
0.0667217	-832.077	0.06672174	-0.83207687	0.3773
0.0664698	-841.78	0.0664698	-0.84178023	0.384
0.0662359	-849.056	0.06623591	-0.84905613	0.3906
0.0658898	-855.59	0.06588977	-0.85558956	0.3974
0.0658791	-865.173	0.06587908	-0.86517338	0.404
0.0656024	-873.544	0.06560243	-0.87354383	0.4106
0.0654648	-881.863	0.06546477	-0.88186332	0.4174
0.0652946	-879.007	0.06529459	-0.87900724	0.4237
0.0648166	-896.466	0.06481658	-0.896466	0.43
0.0647284	-903.415	0.06472837	-0.90341514	0.4366
0.0647444	-909.55	0.06474442	-0.90954985	0.4434
0.0643769	-923.639	0.06437688	-0.92363918	0.45
0.0642031	-925.082	0.06420314	-0.92508158	0.4568
0.0640829	-933.83	0.06408286	-0.9338296	0.4634
0.0638984	-942.018	0.06389842	-0.94201764	0.47
0.0635095	-951.321	0.06350952	-0.9513214	0.4768
0.0634855	-958.067	0.06348545	-0.95806702	0.4834
0.0631954	-966.832	0.06319544	-0.96683195	0.49
0.063003	-973.548	0.06300299	-0.97354785	0.4968
0.0628974	-980.052	0.0628974	-0.98005158	0.5034
0.0625005	-989.194	0.06250048	-0.98919416	0.5102
0.0623628	-997.632	0.06236282	-0.99763249	0.5168
0.0621289	-1006.12	0.06212894	-1.00612173	0.5234
0.0618536	-1013.08	0.06185363	-1.0130751	0.5302
0.0618095	-1020.12	0.06180952	-1.02012192	0.5368
0.0617253	-1027.8	0.06172533	-1.02780082	0.5434
0.0613925	-1036.3	0.06139254	-1.03630277	0.5502
0.0612696	-1043.01	0.06126959	-1.04301012	0.5568
0.0610945	-1049.95	0.0610945	-1.04995083	0.5634
0.0608553	-1058.49	0.06085528	-1.05848673	0.5702
0.0606174	-1066.1	0.06061739	-1.06609781	0.5768
0.0603795	-1074.12	0.0603795	-1.07412466	0.5836
0.0603621	-1082.57	0.06036213	-1.08256723	0.5902
0.0600868	-1090.43	0.06008681	-1.09042845	0.5968
0.0598543	-1100.66	0.05985427	-1.10065712	0.6036
0.0598075	-1108.13	0.05980749	-1.10813243	0.6102
0.0594239	-1116.02	0.05942392	-1.116015	0.6168
0.0592007	-1123.7	0.05920073	-1.1236981	0.6236

Appendix IV: Calibration of Flow Meters

SV- set value

PV- present value (actual)

Brooks Flow Controller for Air on the very top of the unit (NW of cell) it leads to the Air humidifier. There is a thermometer probe into the humidifier (Channel 1 on Temp reader).

Calibration of Brooks flowmeters

1. Stop the experiment. (Pause)
2. Hydrogen comes from bottles and Air comes from compressor.
3. On Brooks 0254 Channel 3 -> Set Point -> set as 0.
4. Get DryCal ML500 (electronic bubble flow test)
5. Attach a tube from the flow meter to the DryCal
6. Set the flow on the machine to minimum (.020 L/min).
7. Push Auto on the DryCAL to get the value (25 sccm in comparison to the set point of 20). Must then adjust the set point when setting those values (create a calibration curve).

Set Point	DryCal reading
.05	.025
.1	.101
.2	.197
.3	.293
.4	.390
.5	.487
.6	.582
.7	.681
.8	.778
.9	.874
1.0	.970

Appendix V: Additional Photos

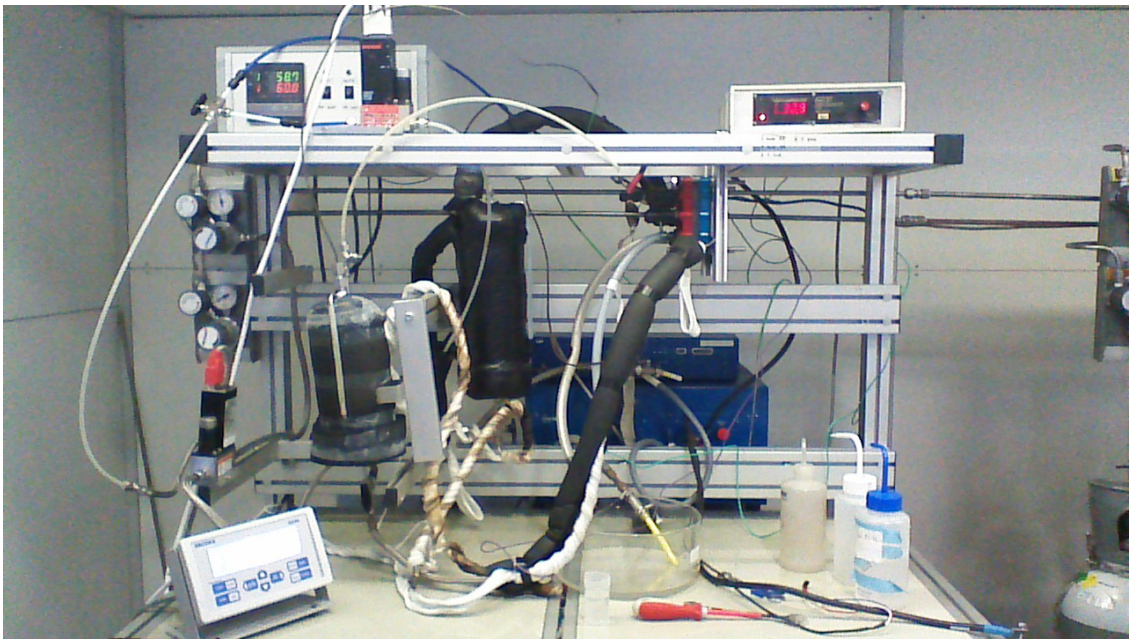

Figure 38: Additional photo of fuel cell bench

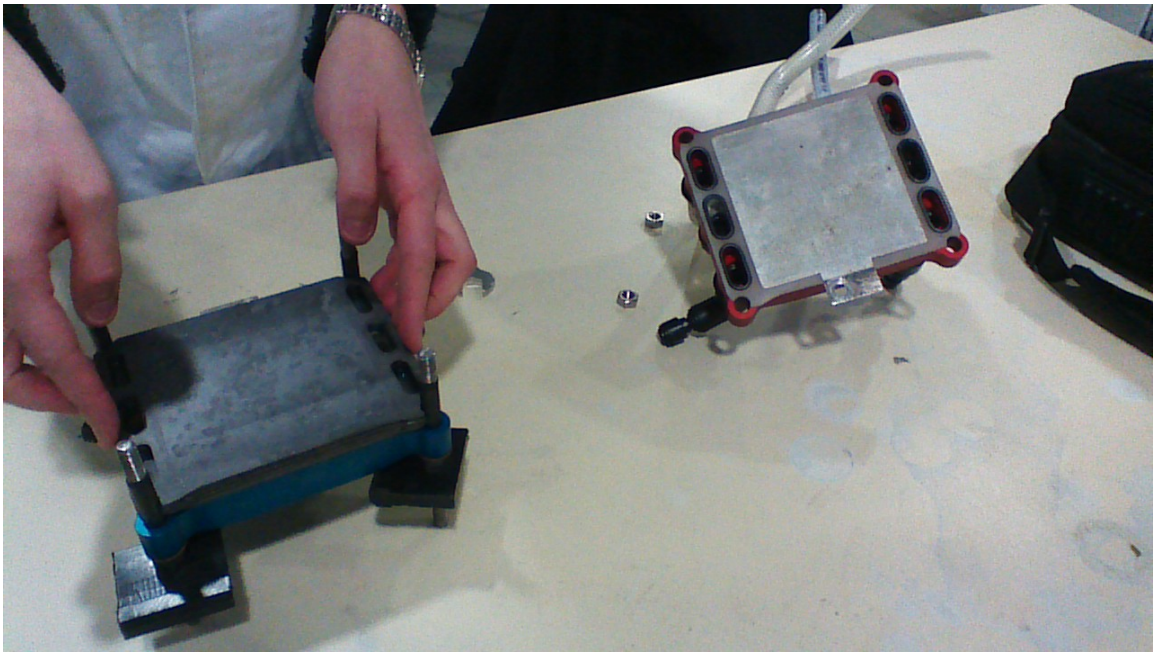

Figure 39: Disassembling the cell.

Figure 40: A bipolar plate (on left) and additional plate to protect the current collector plate.

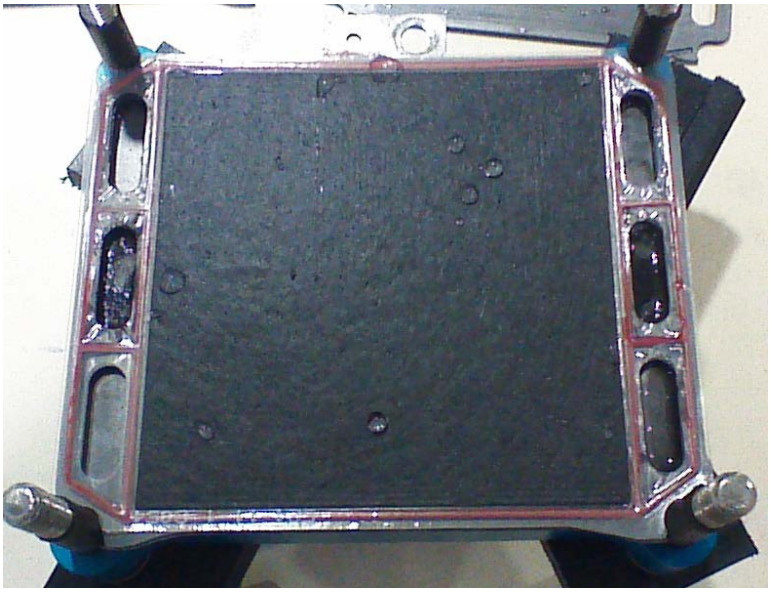

Figure 41: View of the Cathode side of the membrane.

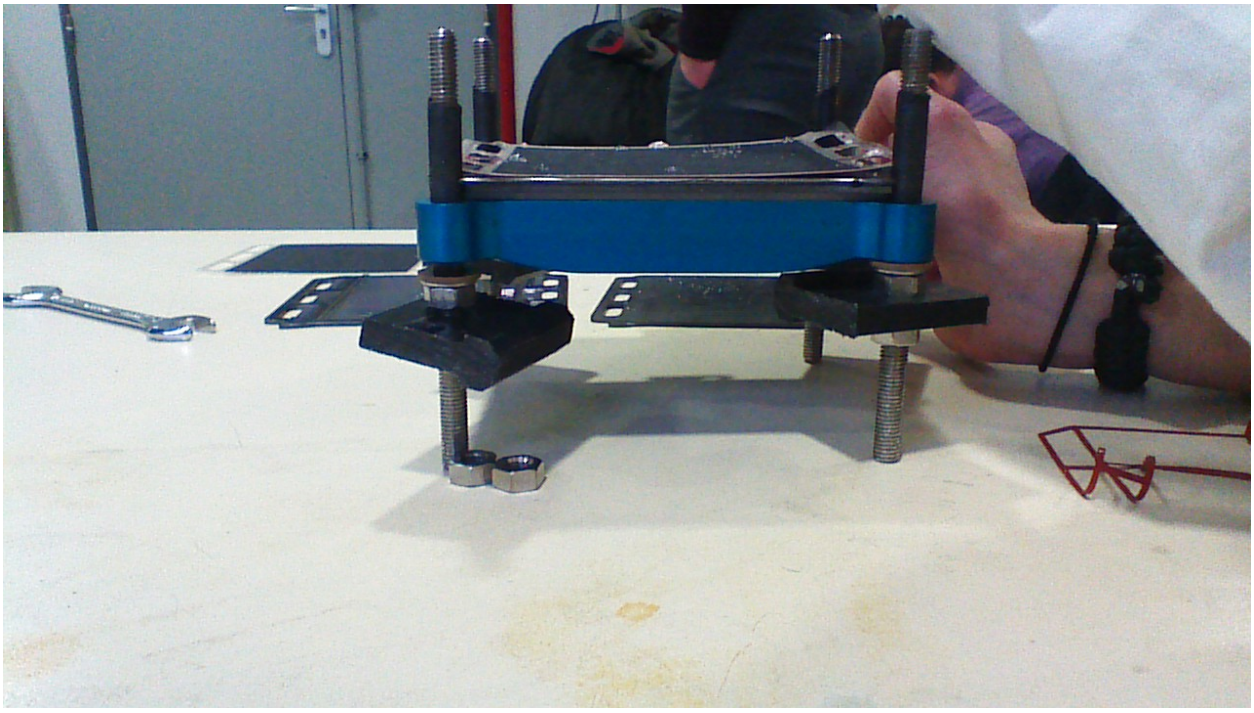

Figure 42: Side view of fuel cell including membrane, bipolar plate, electrode and housing.

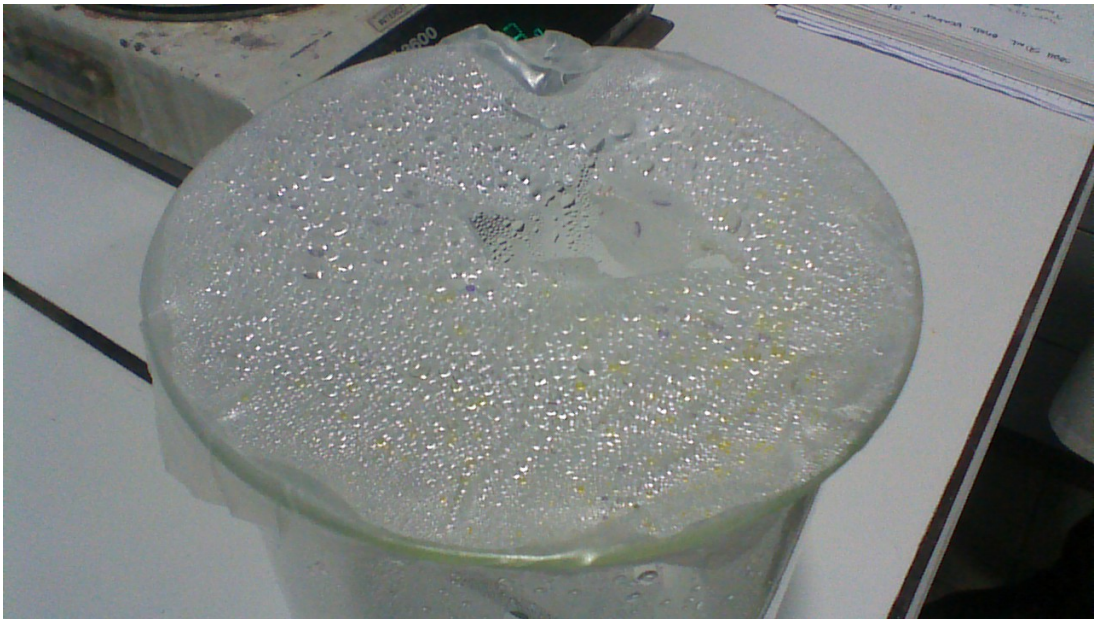

Figure 43: During tests at 50 Amps and 20% Relative Humidity produced purple and yellow spots on the film.

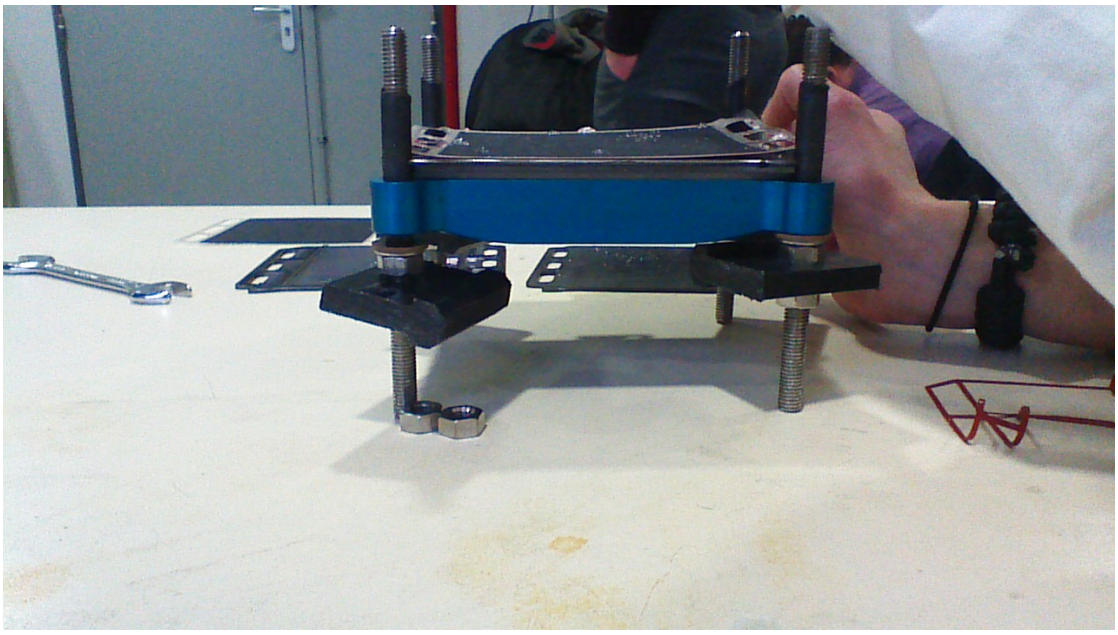

Figure 44: Side view of fuel cell including membrane, bipolar plate, electrode and housing.

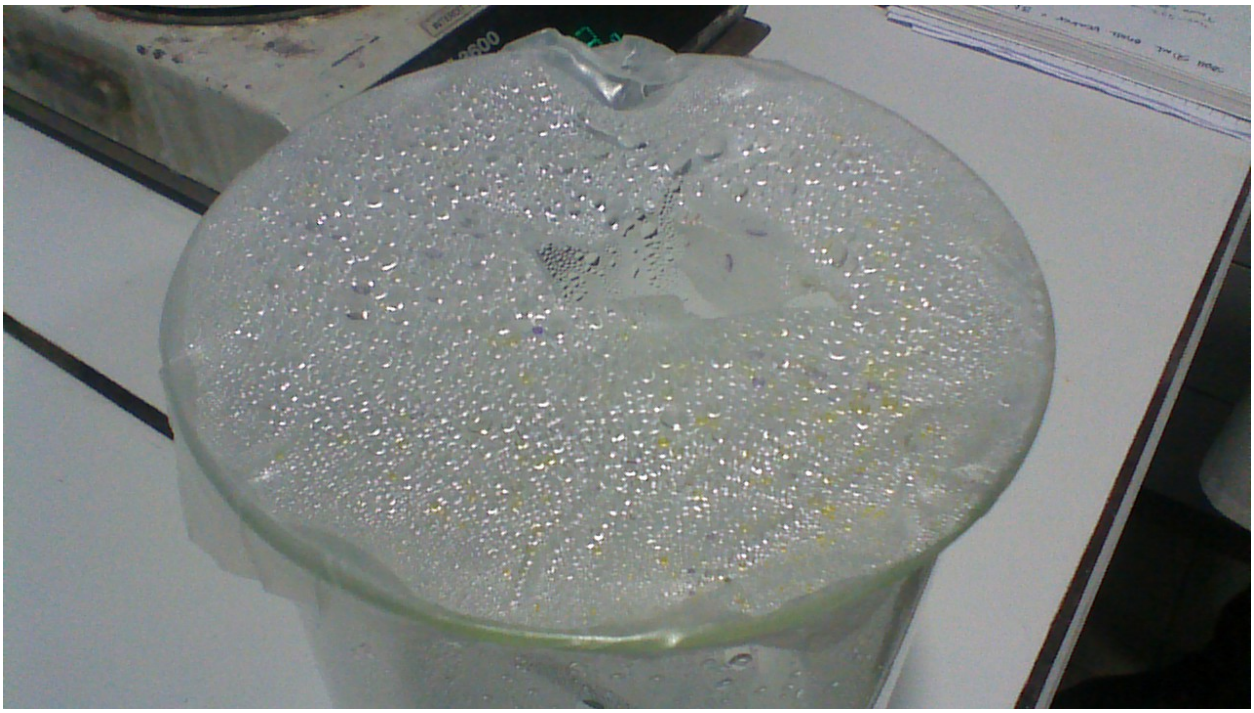

Figure 45: During tests at 50 Amps and 20% Relative Humidity produced purple and yellow spots on the film.

Figure 46: Air and Hydrogen humidifiers